SPATIAL INSTABILITY OF A WALL-BOUNDED FLOW WITH FLUID
INJECTION THROUGH POROUS WALLS

A THESIS SUBMITTED TO
THE GRADUATE SCHOOL OF NATURAL AND APPLIED SCIENCES
OF
MIDDLE EAST TECHNICAL UNIVERSITY

BY

OZAN KÖKEN

IN PARTIAL FULFILLMENT OF THE REQUIREMENTS
FOR
THE DEGREE OF MASTER OF SCIENCE
IN
MECHANICAL ENGINEERING

SEPTEMPER 2019

Approval of the thesis:

SPATIAL INSTABILITY OF A WALL-BOUNDED FLOW WITH FLUID INJECTION THROUGH POROUS WALLS

submitted by **OZAN KÖKEN** in partial fulfillment of the requirements for the degree of **Master of Science in Mechanical Engineering Department, Middle East Technical University** by,

Prof. Dr. Halil Kalıpçılar
Dean, Graduate School of **Natural and Applied Sciences**　　　　　_____

Prof. Dr. Sahir Arıkan
Head of Department, **Mechanical Engineering**　　　　　_____

Prof. Dr. Hakan Işık Tarman
Supervisor, **Mechanical Engineering, METU**　　　　　_____

Examining Committee Members:

Assoc. Prof. Dr. Cüneyt Sert
Mechanical Engineering, METU　　　　　_____

Prof. Dr. Hakan I. Tarman
Mechanical Engineering, METU　　　　　_____

Assoc. Prof. Dr. M. Metin Yavuz
Mechanical Engineering, METU　　　　　_____

Assist. Prof. Dr. Özgür Uğraş Baran
Mechanical Engineering, METU　　　　　_____

Assist. Prof. Dr. Sıtkı Uslu
Mechanical Engineering, TOBB ETÜ　　　　　_____

Date: 13.09.2019

I hereby declare that all information in this document has been obtained and presented in accordance with academic rules and ethical conduct. I also declare that, as required by these rules and conduct, I have fully cited and referenced all material and results that are not original to this work.

Name, Surname: Ozan Köken

Signature:

ABSTRACT

SPATIAL INSTABILITY OF A WALL-BOUNDED FLOW WITH FLUID INJECTION THROUGH POROUS WALLS

Köken, Ozan
Master of Science, Mechanical Engineering
Supervisor: Prof. Dr. Hakan I. Tarman

September 2019, 141 pages

One of the important and yet least understood fields in fluid mechanics research more than a century is hydrodynamic stability. The main objectives in this field are to investigate the breakdown of laminar flows, their subsequent development as the flow evolves along downstream and eventual transition to the fully turbulent flows. The origin of the turbulence and the transition from laminar to turbulent flow is of crucial importance for the whole science of fluid mechanics as well as aviation and marine industries since the flow regime has an impact on the steady operating conditions of many vehicles concerned of those sectors. The focus of the current study is on the stability of an incompressible, homogenous, two-dimensional, planar wall-bounded flow driven by inflow through its porous walls. The non-parallelism of the mean flow and its effect on stability conditions are studied by using two stability approaches, namely, local and nonlocal. Chebyshev collocation method is used to discretize the wall-normal direction, while 1st order-accurate backward difference scheme is used in streamwise marching procedure. Codes for the mean flow calculation, local approach and non-local approach (parabolized stability equations) are written in MATLAB to investigate stability of a non-parallel base flow. Instead of using perturbation of the primitive flow variables, disturbance streamfunction is used in the formulation. The

validation of the codes is performed by comparing the numerical results with the literature.

ÖZ

DUVARLA SINIRLANDIRILMIŞ PORLU AKIŞIN KONUMSAL KARARLILIĞI

Köken, Ozan
Yüksek Lisans, Makina Mühendisliği
Tez Danışmanı: Prof. Dr. Hakan I. Tarman

Eylül 2019, 141 sayfa

Hidrodinamik kararsızlık, yüzyılı aşkın süredir çalışılmakta olan ve hala akışkanlar mekaniği alanında önem verilen çalışma disiplinlerinden biridir. Bu disiplinin temel amacı, laminar akışın yıkılmasını ve yıkılan akışın akış yönünde ilerledikçe gelişimini ve nihai olarak türbülansa geçişini incelemektir. Türbülansın başlangıcı ve akabinde laminar akıştan türbülanslı akışa geçişinin incelenmesi, gerek havacılık gerekse denizcilik sektöründe önemlidir. Bunun sebebi, yapılan endüstriyel ürünlerin sabit durumlu akışlar için tasarlanıyor oluşudur. Bu çalışmanın odağı, sıkıştırılamaz, homojen, iki boyutlu, düzlemsel iki duvarla sınırlandırılmış ve sabit taşınım parametrelerine sahip porlu akışın kararlılığını incelemektir. Temel akışın paralel olmamasının temel akış kararsızlığına etkisi, üç farklı kararlılık yaklaşımıyla çalışılmıştır. Duvar yüzeyine dik yön için Chebyshev düzenleme metodu, adımlama sürecinde ise birinci derece hassasiyetli geriye doğru farklar yöntemi kullanılmıştır. MATLAB ile temel akışın hesaplanması, bölgesel yaklaşım ve bölgesel olmayan yaklaşım (parabolikleştirilmiş kararlılık denklemleri) için üç farklı kod yazılmış ve temel akışın kararsızlılığı incelenmiştir. Yazılan kodların doğrulaması, elde edilen sayısal sonuçların literatürle kıyaslanmasıyla yapılmıştır.

Anahtar Kelimeler: Konumsal Kararsızlık, Hidrodinamik Kararsızlık, Parabolikleştirilmiş Kararlılık Denklemleri, Paralel Olmayan Akış Kararlılığı, Kanal İçi Akış Kararlılığı

To my lovely family, Meral KÖKEN, Necdet KÖKEN and the cutest cat in the world, Karius.

ACKNOWLEDGEMENTS

TABLE OF CONTENTS

LIST OF TABLES

TABLES

LIST OF FIGURES

xvi

LIST OF ABBREVIATIONS

NS	:	Navier-Stokes
TS	:	Tollmien-Schlichting
LST	:	Linear Stability Theory
OSE	:	Orr-Sommerfeld Equation
LNP	:	Local Non-Parallel
PSE	:	Parabolized Stability Equations
DNS	:	Direct Numerical Simulation
PVS	:	Parietal Vortex-Shedding

LIST OF SYMBOLS

U	:	Amplitude of the streamwise velocity component
V	:	Amplitude of the normal velocity component
P	:	Pressure
$\bar{U}$	:	Amplitude of the streamwise velocity component of mean flow
$\bar{V}$	:	Amplitude of the normal velocity component of mean flow
$\bar{P}$	:	Amplitude of pressure of mean flow
u	:	Amplitude of the streamwise velocity component of perturbating flow
v	:	Amplitude of the normal velocity component of perturbating flow
p	:	Amplitude of pressure of perturbating flow
Ψ	:	Streamfunction
φ	:	Amplitude of the streamfunction
α	:	Wavenumber in streamwise direction
β	:	Wavenumber in spanwise direction
ω	:	Disturbance frequency of the wave
f	:	Acoustic wave frequency
k	:	Spatial growth rate vector
ν	:	Kinematic viscosity
Re	:	Reynolds number
t	:	Time
$\mathcal{F}$	:	Dispersion relation
A	:	Amplitude
h	:	Half height of channel
T_n	:	Chebyshev polynomials in degree of n

CHAPTER 1

INTRODUCTION

1.1. Background

Internal recirculating flows generated by the existence of corners and obstacles or just driven purely hydrodynamically within a wall-bounded domain are crucial from a technological perspective and also of a great scientific interest because of their illustration several aspects of fluid mechanics phenomena. A fundamental theoretical tool in studying fluid flow behavior and its mechanisms in various configurations is hydrodynamic stability theory. Before introducing the specifics of this thesis, we will give a short overview of this subject below.

One of the hot topics and yet least understood fields in fluid mechanics research more than a century is hydrodynamic stability. The main objectives of this branch are to investigate the breakdown of laminar flows, their subsequent development as the flow evolves downstream and eventual transition to the fully turbulent flows, or in other words the phenomena of *"The origin of the turbulence"* and accompanying *"Transition from laminar to turbulent flow"* which is fundamentally related with almost whole science of fluid mechanics. Therefore, the first step of understanding the conditions under which a laminar flow becomes turbulent is to study the development of the instabilities in a laminar flow. There are several approaches to this problem and it is well-known that the stability, transition and turbulence characteristics of wall-bounded flows are fundamentally different from those of free shear layer flows in the origin of the disturbances such as the influence of surface geometry and roughness, sound, heat transfer and ablation. Thus, it is not possible to foresee the transition scenario and the nature of the turbulent structures with a general prediction scheme.

1

The origin of the turbulence and the subsequent transition from laminar to turbulent flow is of crucial importance for the whole science of fluid mechanics as well as aviation and marine industries since the flow regime has an impact on the steady operating conditions of many vehicles concerned in these sectors. Although most of the systems are designed to operate under steady or almost steady conditions with a disturbance-free environment, there are some cases that turbulent boundary layer flow may also be desired, especially to increase the efficiency of the combustion process by promoting rapid mixing of fuel and air inside the combustor. The flow in a boundary layer over a solid body also experinces transition from laminar to turbulent flow, a fact which was discovered much later than the transition in internal flows. The phenomenon is affected by many parameters such as pressure distribution in the external flow, wall roughness and the turbulent intensity in the external flow.

A solid body is affected by turbulent boundary layer according to its shape, i.e. blunt bodies and streamlined bodies are affected differently, in the sense of drag force and skin friction. One of the most important diversity between the effects of the turbulent boundary layer on those bodies is their responses to the turbulence in the sense of drag force. The whole physics can be summarized as follows: In a blunt body, pressure drag is dominant over skin-friction drag. When a blunt body undergoes transition, velocities adjacent to the surface and consequently skin-friction drag increases. Nevertheless, the drop in pressure drag is greater than the rise in skin-friction drag. Thus, for a turbulent boundary layer on a blunt body, overall drag force dramatically decreases, and for some cases turbulent boundary layer is desired over such a solid body, like famous golf ball example. This drop in the drag force firstly noticed by Eiffel [29] in relation to spheres. Moreover, due to the ability of turbulent boundary layer to sustain larger adverse pressure gradients in comparison to laminar boundary layer, the point of separation shifts to downstream of the flow that notably decreases the width of the wake. Subsequently, the boundary layer becomes turbulent at a lower Reynolds number.

2

The phenomena of transition process on a flat plate with zero incidence angle is simpler to understand than that on a blunt body. The physics is the same as in a pipe: Near the enterance (or the leading edge), the boundary layer is always laminar, except for the leading edge separation which may occur in a flat plate of finite thickness and the laminar boundary layer becomes turbulent further downstream. Schubauer and Klebanoff [30] demonstrated the changes in the velocity profiles in the transition region in a very low turbulent intensity stream. There is a significant increase in drag force with the transition on a flat plate. In fact, laminar flow over a wing of an airplane may lead to the reduction of the fuel consumption up to 30%, thanks to lower drag force on the solid body surface.

The actual engineering framework of this thesis is to understand the phenomena of transition and its effects on the performance of the solid propellant rocket motor (SPRM). The instability occurring in a solid propellant rocket motor can be defined as the amplification of the pressure oscillations inside the rocket motor spontaneously during firing in the presence of the mean flow and energy released by combustion. Those pressure oscillations can spontaneously grow due to the coupling between the dynamics of propellant combustion and the combustion chamber. Since combustion chambers are intended to operate under steady or almost steady conditions for the kinds of propulsion systems currently used, one should consider if the flow in the combustor is unstable to small disturbances or not.

The main reasons, or mechanisms, of instabilities are possibly the most difficult problem in the field of hydrodynamic stability to identify. Solving the problem requires an accurate representation of the dynamics of the mechanism. The pressure oscillations may result from the complex feedback mechanism fed by vortex shedding and acoustic waves; or coupling between fluid-dynamics instabilities and acoustic modes of a SPRM.

Generation of the oscillations due to the mean flow interactions can be explained briefly by the separation of the flow, followed by instability of the shear layer and

formation of the vortices. Flow separation in small scale solid rocket motors generally occurs at segmented grain, propellant corners and obstacles like inhibitor rings. Each corner with a sharp angle or protruding object can be a point of separation where vorticity production occurs and causes fluid-dynamics instabilities. Vuillot [2] underlines that in the shear layer region with radial mass injection, velocity vector is turned from radial to axial direction of motor, the flow profile becomes unstable and vortical structures can be generated adjacent to the surface. Moreover, those vortices move downsteam in the combustion chamber and interact with the acoustic modes of the motor.

A sketch can be seen in Figure 1.1 that demonstrates the vortex-shedding phenomena with acoustic interactions.
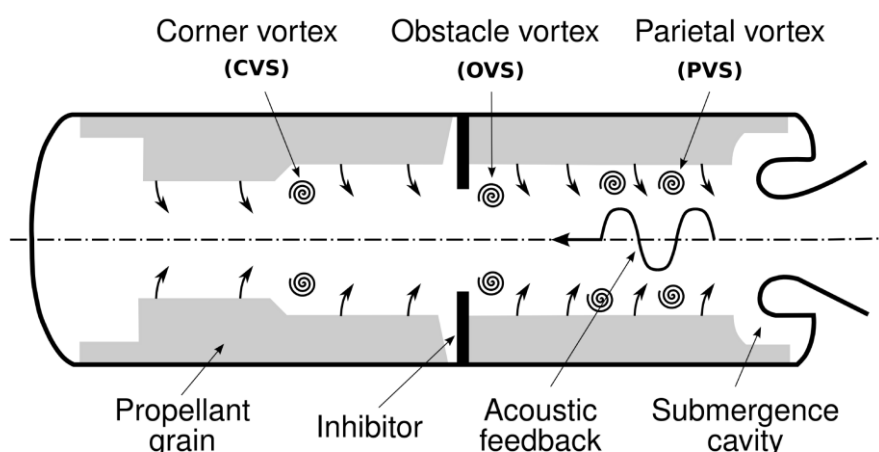
Figure 1.1. Vortex-Shedding – Acoustic Wave Interaction [4]

Although some tools are available in order to predict the frequency of the vortices originating due to presence of corners and obstacles in flow domain of a SPRM, the effects of parietal vortex-shedding phenomena on the instability of a SPRM are difficult to understand. Especially combustion instabilities in large solid rockets where low-frequency oscillations are observed are suffered from the amplification of

pressure oscillations inside the SPRM during operation because of the coupling mechanism of mean flow – acoustic feedback interactions.

In order to drive combustion instability due to the acoustic oscillations in a solid propellant rocket motor, resonant frequency and the characteristic times associated with the combustion process should be compatible i.e. if the most amplified waves do not correspond to the acoustic frequency, a non-linear regime occurs, laminar flow breaks down into fully turbulent flow and amplitude of the acoustic fluctuations will be low. Under all those conditions mentioned before, flow in the SPRMs like Minuteman-II, Ariane-V and Titan-IV may be exposed to large fluctuations at a frequency tuned to that of an acoustic longitudinal mode because of the inevitable disturbances that develop in motor cavities, although those SPRMs are predicted to be stable by means of conventional methods, such as the acoustic balance. Especially for large segmented rocket motors Parietal Vortex-Shedding (PVS) has an impact on pressure oscillations. Moreover, one of the reasons that designers desire laminar flow inside the rocket motor is to reduce propellant surface heating to avoid instantaneous burning rate rise. In other words, transition from laminar to turbulent flow inside the boundary layer of the rocket motor is an important phenomenon concerning internal ballistics. On the grounds of all these information, a rocket motor designer needs to take precautions against the probable flow instabilities and subsequent combustion instabilities due to the interaction of vortex – combustion process adjacent to the burning surface inside the rocket motor when turbulent boundary layer occurs at the surface of the solid propellant.

With the increase in Reynolds number, that represents the relative importance of the inertial forces to the viscous forces, both internal such as flow inside a pipe and external flows such as boundary layers formed over solid bodies undergo a significant transition from laminar to turbulent regime. The existence of turbulence was first recognized for internal flows in straight pipes and channels by feeding a thin thread of liquid dye into the flow to visualize the flow along the channel. In a flow at very low Reynolds number, the flow in a straight pipe with a uniform cross-section is

5

observed to be well-ordered: The fluid moves with a uniform velocity along a straight path and the fluid adjacent to the wall are slowed down by viscous forces. However, this well-ordered flow regime breaks down with the increase in the Reynolds number, the thread diffuses into the flow, the fluid starts to mix dramatically and appears uniformly coloured, and the pattern of streamlines at a fixed point experiences perpetual, irregular and high-frequency velocity and pressure fluctuations which is the most essential feature of turbulent flow causing an exchange of momentum in transverse directions. At a short distance downstream, subsequently, the velocity distribution is observed to be more uniformly distributed across the pipe cross-section in turbulent flow in comparison to the laminar flow. From a historical perspective, these well-known experiments and observations on hydrodynamic stability were performed by Reynolds [22], which are also known as Reynolds's dye experiments. He discovered the law of similarity which states that the transition always occurs at *"almost"* the same Reynolds number, or as commonly known as, *"critical Reynolds number"*. The phrase "almost" is deliberately used in this case, because the critical Reynolds number also depends on the disturbances within the flow before entering the pipe (free-stream conditions). As a pathfinder, Reynolds aimed to understand whether the transition was associated with the stability of laminar flows. That's the reason why such an important dimensionless number is devoted to Reynolds.

The early work in hydrodynamic instability and in particular the studies of Lord Rayleigh [34] emphasized inviscid aspects of the problem. The theoretical investigation of the stability of shear flows starts with the Rayleigh's equation which is a frictionless (inviscid) stability equation:

$$v'' - k^2 v - \frac{U''}{U - c} v = 0 \tag{1.1}$$

where $\overline{U}$ is the streamwise component of the mean flow velocity, v is the fluctuating velocity component in the wall-normal y-direction, k is the resultant growth rate for two-dimensional disturbance wave and $c = \omega/\alpha$ is the disturbance speed.

The concept and types of stability can be summarized in the following illustration of a mechanical system that depicts an object at an equilibrium (base) state in various configurations. The stability of the object (or maintainability of its base state) can be tested by an infinitesimal disturbance. The state in (a) is termed as stable, (b) is unstable and (c) is neutral (indefinite). In (d), the state is stable to small and unstable to large disturbances. This is called conditional stability.
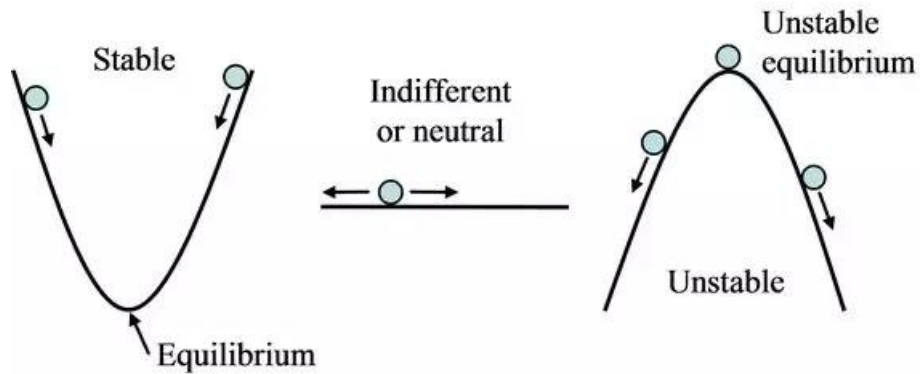
Figure 1.2. The States of Stability

Consider now a basic (laminar) flow characterized by the velocity field $U(x, t)$ that satisfy the Navier-Stokes equations together with some boundary conditions. In order to test the stability of the basic flow, it is disturbed by $u(x, t)$ and its evolution as governed by Navier-Stokes equations is studied. A basic flow is stable (in the sense of Liapounov), if for any $\varepsilon > 0$, there exists some positive number δ (depending upon ε) such that if

$$\text{if } \|u(x, 0) - U(x, 0)\| < \delta, \text{ then } \|u(x, t) - U(x, t)\| < \varepsilon$$

for all $t > 0$.

The inviscid flow stability equation of Rayleigh given in (1.1) is derived based on the normal mode analysis associated with the investigation of the mean flow stability. Normal mode analysis uses infinitesimal perturbations to test the stability of the mean flow. It is based on searching for the normal modes at fixed frequency, position and wavenumber, i.e. a solution that is periodic in x. Consider for example the mean flow U with mean pressure P characterizing the base (mean) flow state. Assume that the mean flow is disturbed by a fully 3D disturbance

$$\boldsymbol{u} = \boldsymbol{U} + \boldsymbol{u}'(x, y, z, t); \qquad p = P + p'$$

and its evolution under the governing incompressible Navier-Stokes equations are sought

$$\nabla \cdot \boldsymbol{u} = 0$$

$$\frac{\partial \boldsymbol{u}}{\partial t} + \underbrace{\boldsymbol{u} \cdot \nabla \boldsymbol{u}}_{N\{u,u\}} = \underbrace{-\nabla p + Re^{-1} \nabla^2 \boldsymbol{u}}_{L\{u,p;Re\}}$$

where $N\{\boldsymbol{u}, \boldsymbol{u}\}$ represents the quadratic nonlinear term and $L\{\boldsymbol{u}, p; Re\}$ represents the linear terms. Substituting the disturbed flow into Navier-Stokes equations yields,

$$\nabla \cdot (\boldsymbol{U} + \boldsymbol{u}') = 0,$$

$$\frac{\partial (\boldsymbol{U} + \boldsymbol{u}')}{\partial t} + N\{\boldsymbol{U} + \boldsymbol{u}', \boldsymbol{U} + \boldsymbol{u}'\} = L\{\boldsymbol{U} + \boldsymbol{u}', P + p'; Re\}.$$

Since the base flow already satisfies the Navier-Stokes equations, it reduces to

$$\nabla \cdot \boldsymbol{u}' = 0,$$

$$\frac{\partial \boldsymbol{u}'}{\partial t} + N\{\boldsymbol{U}, \boldsymbol{u}'\} + N\{\boldsymbol{u}', \boldsymbol{U}\} - L\{\boldsymbol{u}', p'; Re\} = -N\{\boldsymbol{u}', \boldsymbol{u}'\}.$$

These equations are linearized by ignoring $N\{\boldsymbol{u}', \boldsymbol{u}'\}$ term owing to the assumption of infinitesimal disturbances and then used to study the evolution of the infinitesimal disturbances.

Consider a parallel (or almost parallel) flow with the mean

$$\boldsymbol{U} = (U(y), 0, 0)$$

where the mean flow is in x-direction and varies in the y-direction, z is in the transverse direction. In channel flow, for example, x and z range from minus to plus infinity, while y defines the solid boundaries. The linearized disturbance equations involves coefficients as functions of y only due to $U(y)$ appearing in $N\{\boldsymbol{U}, \boldsymbol{u}'\}$ and $N\{\boldsymbol{u}', \boldsymbol{U}\}$ terms. The disturbance can then be Fourier transformed,

$$\widehat{\boldsymbol{u}}'(\alpha, y, \beta, t) = \iint_{-\infty}^{+\infty} \boldsymbol{u}'(x, y, z, t)\exp(i(\alpha x + \beta z))dxdz$$

and similarly for p', where α and β are real transform variables. Since the disturbance equations are linear, it can further be reduced to an ordinary differential equation by applying Laplace transform in time. Classically, however, it is assumed that time dependence can be separated as follows,

$$\widehat{\boldsymbol{u}}'(\alpha, y, \beta, t) = \sum_{n=0}^{\infty} \widetilde{\boldsymbol{u}}'(\alpha, y, \beta)\exp(-i\omega_n t)$$

where ω_n is taken as a complex frequency with its imaginary part rendering the corresponding mode indexed by n as unstable mode when positive. Exponential term models the wavelike form of the disturbances and indicates if those disturbances grow or decay in time. Thus, the definition of such a disturbance form allows one to investigate the flow stability in temporal sense, i.e. the growth or decay or the disturbances in time, but not in space. In spatial stability analysis, however, the initial disturbances are assumed to grow in space in which case α and β are taken as complex numbers while ω as real. The substitution of these representations into the disturbance equations result in a differential eigen problem owing to the homogeneity of the boundary conditions in y as well. The eigenvalues ω_n are now functions of α, β and Re. This is classical normal mode analysis. It should be noted that the mean flow velocity profile may not necessarily be parallel, i.e. it may be a function of the streamwise variable x.

Lord Rayleigh succeeded in deriving several important, general theorems concerning the stability of laminar velocity profiles. It is a second order ordinary differential equation with a regular singular point at $y = y^*$ where $U(y^*) = c$ and y^* is called critical point, therefore, by removing singularity, two analytical solution exists. However, one of the solutions has a logarithmic singularity at $y = y^*$. Thus, in the vicinity of y^*, the approximation breaks down. In order to avoid singularity, the neglected terms such as viscosity and nonlinearity must be included. One can also notice that if $U''(y^*) = 0$ the singularity vanishes. That brings two necessary but not sufficient conditions for transition, which is also known as Rayleigh's criteria:

- The critical point coincides with a inflection point of the mean velocity profile and a regular neutral mode is obtained when c is real and when $U_{min} < c < U_{max}$ and $U_c'' \neq 0$.
- The existence of a point of inflection, i.e. $U''(y) = 0$, constitutes a necessary condition for the occurance of instability.

From the practical point of view, this criterion is important owing to the direct connection between the existence of a point of inflection and the presence of pressure gradient. In the case of convergent channel flow with a favourable pressure gradient velocity profiles possess no point of inflection. On the contrary, in a divergent channel with an adverse pressure gradient, point (or points) of inflection are present.

As an extension of the inflection point criterion of Lord Rayleigh, Fjortoft provided an improved and stronger necessary condition for instability which states that the inequality $(U - U_I)U'' < 0$ over a substantial range of y must be satisfied for all points along streamwise direction. To judge a flow in the sense of stability by only looking mean flow velocity profile, both Lord Rayleigh's and Fjortoft's point of inflection criteria must be satisfied. Even both are satisfied, flow cannot be considered as unstable, but it can be said that flow is likely to be unstable. Those two criteria can be summarized as;

The necessary conditions for an instability of an inviscid shear flow are that;

- D^2U must have a zero at least one point in the flow (Rayleigh's criterion)
- DU, the extremum of vorticity associated with $D^2U = 0$ must be a maximum (Fjortoft's criterion)

Both Reynolds' and Lord Rayleigh's early hypothesis on the mechanism of transition were based on that transition as a consequence of instability due to the disturbances acting on the mean flow.

As an alternative, the energy method of investigating the stability of disturbed flow involves the variation of the energy of the disturbances with time. The theory developed mainly by Lorentz [31], admits an arbitrary form of the superimposed motion and demands only that it should be compatible with the continuity equation. Moreover, Joseph [32] provides the details of the energy method by taking the problem as bulk and approaching the stability problem in terms of bulk kinetic energy, energy production including Reynolds stress and energy dissipation terms:

$$\frac{\partial}{\partial t}\left(\frac{1}{2}\int_{\Omega} u_i u_i d\vec{x}\right) = -\int_{\Omega} u_i u_j \frac{\partial u_i}{\partial x_j} d\vec{x} - \frac{1}{Re}\int_{\Omega} \frac{\partial u_i}{\partial x_j}\frac{\partial u_i}{\partial x_j} d\vec{x} \tag{1.2}$$

where the left-hand side of the equation is the time rate of change of bulk kinetic energy in the whole domain Ω, the first term on the right-hand-side without the minus sign is energy production term, and the second one is the energy dissipation term. The non-linear terms vanish in the process of integration because non-linear terms are responsible for redistribution of energy between scales. Moreover, the second integral on the right-hand-side of the equation is positive-definite. Thus, the viscous term acts to damp the energy in the disturbance field.

An early hypothesis on the mechanism of transition from laminar to turbulent flow is thought as a consequence of instability of the well-ordered mean flow. In 1904, Ludwig Prandtl published a groundbreaking paper and introduced the concept of the boundary layer and its importance on drag. On that paper, he identified the boundary

layer as the thin layer in the neighborhood of the solid surface where the effects of viscosity are important. That paper also covered the effects of viscosity in that thin layer, flow separation due to the existence of boundary layer and clearly explained the concept of stall for the first time, that made Prandtl a pioneer in the science of aerodynamics [19]. Subsequently, the stability theory formulated by Prandtl, was based on the assumption that laminar flows were affected by certain small disturbances. Those disturbances may originate due to irregularities in the free-stream and wall-roughness. He also pointed with Froude and Eiffel that this boundary layer flow is not necessarily laminar but can also be turbulent. Moreover, Prandtl successfully explained the dramatical drop of the skin-friction beyond a critical Reynolds number over a bluff body such as a sphere, while it increases significantly for flat plates, with the ability of the turbulent boundary layers to sustain greater adverse pressure gradient and consequently separation delays [20]. After Prandtl, there have been various successful and unsuccessful theoretical models of transition. In fact, the majority of the models developed are based on Prandtl's hypothesis which states that the process of transition is initiated by the amplification of the infinitesimal oscillations. It should be noted that although Lord Rayleigh takes the instability problem under the generally accepted premise that the effects of the viscosity on the turbulent flow could only be stabilizing (see the right-hand-side of the (1.2)), Prandtl [42] clearly illustrated that viscosity can also be destabilizing and even non-inflected profiles could be unstable. The basic idea is that the distribution of the Reynolds' stress through the shear layer is changed by viscosity in such a way as to destabilize the flow, i.e. Reynolds' stress term in energy consideration analysis is a production term for instabilities. In fluid dynamics, the Reynolds stress is the component of the total stress tensor in a fluid to account for turbulent fluctuations in fluid momentum. By splitting the mean and fluctuating part of the velocity field, the definition of the Reynolds stress for a fluid with constant density can be given as $u_i u_j$, where both u_i and u_j indicate the components of the velocity in different directions. The source of

12

production of the disturbance kinetic energy is the action of Reynolds stresses acting on the mean rate of strain field.

Orr and Sommerfeld derived an equation that takes the viscosity into account and models the amplification of the infinitesimally small two-dimensional waves superimposed over a base flow that is assumed to be streamwise uniform (parallel shear flow). The infinitesimally small disturbances allow neglecting the nonlinear terms. Therefore, this linearization limits the theory to the initial stages of the transition process. This model is called the Orr-Sommerfeld equation:

$$\left(\left(U - \frac{\omega}{\alpha} \right) (D^2 - (\alpha^2 + \beta^2)) - U'' \right) v = i \frac{\nu}{\alpha} (D^2 - (\alpha^2 + \beta^2))^2 v \qquad (1.3)$$

where D denotes the differentiation with respect to y. It is useful to investigate the transition phenomena in uniform (parallel) flows but it gives inconsistent results when nonuniformity (non-parallellity) in the base flow are too significant to be neglected. Strictly speaking, of course, there is no such thing as parallel boundary layer, except under very special circumstances. However, still the parallel flow assumption is important as a first approximation in the study of stability of flow in the boundary layer. This is also called parallel local approach; it neglects the non-parallelism of the mean flow and provides results for a fixed streamwise location.

It is possible to raise the objection that if a complete analysis of the stability of the two-dimensional base flow is to be achieved, the disturbances superimposed on that flow need not be two-dimensional. This objection was removed by Squire [33] who proved that a two-dimensional base flow becomes unstable at a higher Reynolds number when the disturbances are assumed three-dimensional as opposed to two dimensional disturbances, i.e. parallel shear flows become unstable to two-dimensional disturbances at a value of Reynolds number that is smaller than those for three-dimensional disturbances. Therefore, for an incompressible flow, the three-dimensional disturbance equations can be transformed to the completely two-

dimensional Orr-Sommerfeld equation since the base flow is the least stable to two-dimensional disturbances.
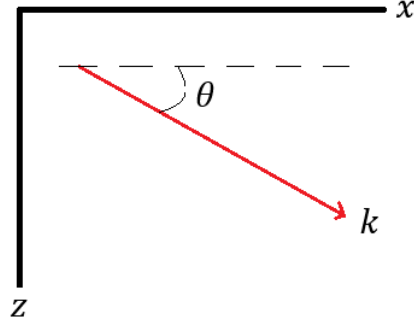
Figure 1.3. Spatial Growth Rate Vector

Let,

$$k = |\tilde{\alpha}| \quad \rightarrow \quad k^2 = \alpha^2 + \beta^2 \tag{1.4a}$$

$$\alpha = k \, cos(\theta) \ , \ \beta = k \, sin(\theta) \ , \ \frac{\tilde{\alpha}}{\alpha} = \frac{1}{cos(\theta)} \ , \ v_{1D} = \frac{v_{2D}}{cos(\theta)} \tag{1.4b}$$

$$Re_{1D} = Re_{2D} \, cos(\theta) \tag{1.4c}$$

$$Re_{cr} = min_{\alpha,\beta} Re_L(\alpha,\beta) = min_\alpha Re_L(\alpha,0) \tag{1.4d}$$

where α and β are the spatial growth rates in x and z direction for two-dimensional wave, respectively, while $\tilde{\alpha}$ is the growth rate in x direction for one-dimensional wave. The plane wave solutions searched by Squire are in the form of,

$$\vec{u} = \big(u(y), v(y), w(y)\big)e^{i(\alpha x + \beta z - \omega t)} \tag{1.5a}$$

$$\vec{w} = \big(\xi(y), \eta(y), \gamma(y)\big)e^{i(\alpha x + \beta z - \omega t)} \tag{1.5b}$$

Almost 20 years later, by advancing Squire's proof, Dunn and Lin [37] demonstrated that when only the leading viscous-conductive effects on the disturbances are considered the equations for three-dimensional disturbances can be transformed to those for two-dimensional disturbances.

Tollmien achieved some progress in stability analysis of a boundary layer flow by solving the Orr-Sommerfeld equation, obtaining critical Reynolds number and plotting neutral stability curve as Reynolds number varied by ignoring the slow growth of the boundary layer, i.e. flow is considered to be fully parallel. Moreover, he identified the wave frequencies at which the flow becomes unstable at some specific Reynolds number. Later, Schlichting extended these results to include growth rates between the points on neutral stability curve. It should be underlined that their approaches to the stability of the boundary layer problem is in the temporal sense, i.e. they obtained temporal growth rates of those two-dimensional waves. The two-dimensional waves obtained in these analysis which are accepted as the initial stages of the transition from laminar to turbulent flow, are called Tollmien-Schlichting waves.

Schubauer and Skramstad [56] provided the first successful experimental results as the verification of the theoretical predictions of Tollmien. Even though the effects of the disturbances such as free-stream turbulence and surface roughness on transition are not well-known, their experimental data showed remarkable agreement with theoretical results. They observed waves grew as they convected downstream. Therefore, they needed to convert the temporal growth predictions by dividing with the wave speed to compare spatial growth of those waves obtained by their experiments.

If the attention is fixed on the boundary layer along a wall, the theoretical critical Reynolds number indicates the point on the wall at which amplification of some individual disturbances begins and proceeds downstream of it. The transformation of those amplified disturbances into fully developed turbulence takes up some time and

distance in the downstream direction. Therefore, it is expected that the observed position of the point of transition will be downstream of the calculated based on the theoretical models, i.e. the experimental critical Reynolds number exceeds the theoretical value. In order to distinguish between these two values, it is usual to call the theoretical critical Reynolds number *"the point of instability"* whereas the experimental critical Reynolds number is called *"the point of transition"*.

Infinitesimal disturbances technique limits the transition analysis with the linear stability theory. The initial growth of these disturbances is assumed to be weak, and occurs over a viscous length scale. However, in the linear limit of those infinitesimal disturbances, the initial disturbance spectrum may be composed of a complete set of orthogonal normal modes in the Fourier sense. As those waves propagate, they will eventually undergo nonlinear interactions and three-dimensional effects as the amplitudes of the unstable modes grow. Growth of the disturbances occurs rapidly, over a convective length scale. Thus, after some point of the transition process, a different kind of approach is needed to investigate the nonlinear behaviour of those waves interacting with the flow characteristics. Landau suggested a general theoretical approach which covers the beyond of the stages limited by linearized theory to study the evolution of the flow and developed a model of conditional temporal stability of the flow in terms of perturbation energy,

$$\frac{d|A|^2}{dt} = \lambda_1 |A|^2 + \lambda_2 |A|^4 \tag{1.6}$$

where A is the perturbation amplitude and $\lambda_{1,2}$ are Landau coefficients. It can be seen that the time evolution of the amplitude is governed by the magnitude of the amplitude itself, with the conjecture being that an initially unstable disturbance at small amplitude does not grow indefinitely in time, but reaches an equilibrium condition at some finite amplitude. The stability regions divided by Landau is given in Figure 1.4.
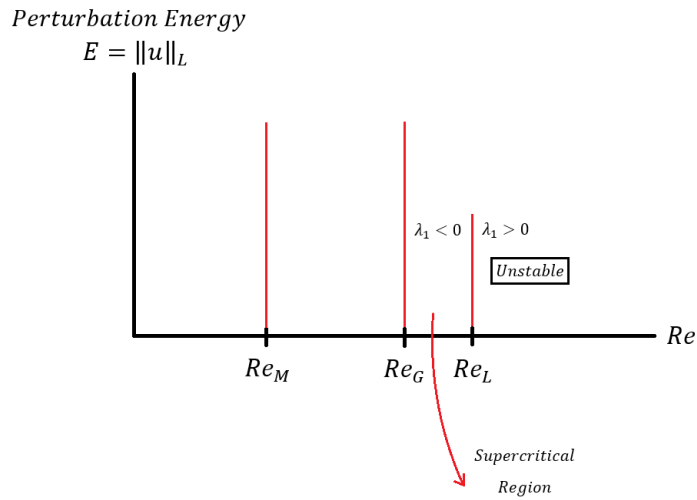
Figure 1.4. Stability Regions in Landau's Approach

Re_M stands for Reynolds number limit of monotonic stability limit of the flow, while Re_G separates the global stability region with supercritical region. In that formulation of Landau's, the flow is considered stable if $\lambda_1 < 0$ and vice versa. It should be mentioned that if only λ_1 is observed, it is called linear hydrodynamic stability. Morovkin [46] explains that there are some cases in which the inital instability is so strong to by-pass the initial stages of the turbulence, turbulent spots occur rapidly and flow becomes turbulent; and transition prediction schemes based on linear stability theory totally fail.

A summary of the transition process in the boundary layer over the flat plate is illustrated in Figure 1.5. As it was mentioned, after some point of transition process, the non-linearity of the flow becomes dominant and linear stability analysis fails.
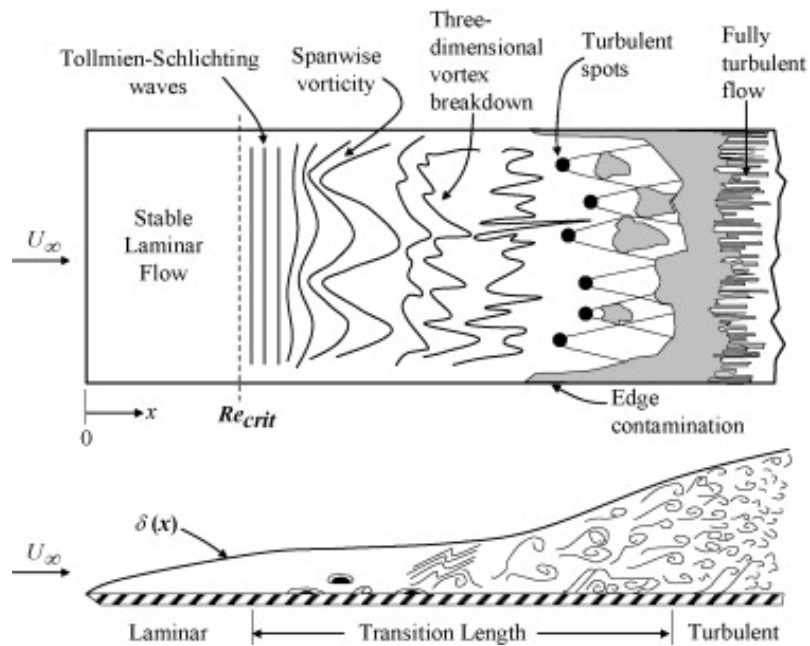
Figure 1.5. Laminar to Turbulent Transition in Boundary Layer [21]

As can be seen in Figure 1.5, the flow goes through the following stages, starting from the leading edge of the plate;

- Stable laminar flow following the leading edge,
- Unstable laminar flow with two-dimensional, sinusoidal Tollmien-Schlichting waves,
- Development of unstable, laminar, three-dimensional waves and vortex formation (hairpin eddies),
- Bursts of turbulence in places of very high vorticity,
- Formation of turbulent spots at locally intense fluctuations,
- Coalescence of turbulent spots into a fully developed turbulent boundary layer.

Herbert [43] had a great impact on understanding the stability problem of those flows by introducing a new definition of the disturbance amplitude by taking into account the non-parallel effects and generalizing the normal mode form. Although most of the

18

works model a temporally growing disturbance and are applicable to cases where the flow evolves in time from one state to another, the idea behind Parabolized Stability Equations (PSE) is to decompose the disturbance into a slowly varying amplitude function and a wave function slowly varying along the streamwise direction, i.e. it is assumed that non-parallel effects are not very large and the streamwise dependency of the amplitude functions are weak. Therefore, the PSE approach allows to neglect secondary spatial derivatives and products of first order derivatives with respect to streamwise direction, i.e. the problem equation becomes parabolic and the method provides the spatial evolution of the modes. The transition is caused by the spatial amplification of waves convected downstream, and does not fall directly into Landau's temporal instability model. In spatial local approach analysis, it is a challenge to solve the eigenvalue problem for a fourth-order spatial wavenumber. However, by a efficient marching in space, PSE allows one to cope with this problem. This is also called non-local non-parallel approach; it takes into account the non-parallelism of the mean flow and unlike local approach, it provides the evolution of the waves along streamwise direction, i.e. it does not provide solution only for a fixed streamwise location.

Bouthier [57][58] put significant effort to incorporate the mean flow nonparallelism (nonuniformity in the streamwise direction) in the linear stability analysis of the boundary layers using multiple scale perturbation technique. However, by using the same perturbation method, Gaster [28] illustrated that non-parallel effects has only minor effects on the stability of boundary layer flows. Saric and Nayfeh [44] repeated those analysis with multiple scale technique using a Cartesian coordinate system. The resulting neutral curve was in better agreement with Schubauer and Skramstad's [56] experimental data than any other theoretical study. Drazin and Reid [45] explained the missing term in Gaster's analysis which should be taken into account to obtain better results for the stability of a non-parallel mean flow.

Orszag [17] obtained the most accurate numerical solution of Orr-Sommerfeld equation given in (1.3) for a planar channel flow by using modal approach with Chebyshev polynomials of the first kind:

$$T_n(\cos\theta) = \cos n\theta$$

$$\varphi(y) = \sum_{n=0}^{\infty} a_n T_n(y)$$

where,

$$a_n = \frac{2}{\pi c_n} \int_{-1}^{1} \varphi(y) T_n(y)(1-y^2)^{-\frac{1}{2}} dy$$

with $c_0 = 2$ and $c_n = 1$ for $n > 0$, and explained why those polynomials are ideal to solve such a problem.

An important review of the numerical methods applied to Orr-Sommerfeld equation for a three-dimensional, compressible boundary layer flow is done by Malik and Hussaini [23] who urged the use of spectral methods and a fourth order finite difference scheme to obtain accurate results using an appropriate mesh. Today, many of the numerical stability analysis are based on these numerical schemes.

The numerical studies of transition using DNS (Direct Numerical Simulation) have yielded considerable results in the 1980's with the increase in the computing power. In such numerical simulations, the full nonlinear disturbance equations are solved directly by employing sophisticated numerical methods. Spatial DNS approach is highly applicable to the transition problems since it is a spatially evolving process and it avoids many of the restrictions that have to be imposed in other models, such as linearization. The basic idea of the spatial DNS is to disturb a known mean flow by time-dependent perturbations. Then the stability of the mean flow against those perturbations is determined by the numerical solution of the full perturbation equations derived from the Navier-Stokes equations. The spatial simulation of two-

dimensional incompressible boundary layer flow was first accomplished by Fasel [60] who used second-order-accurate finite difference scheme in both streamwise and wall-normal directions. There are also several successful works on spatial DNS by using higher order finite difference schemes and spectral methods ([61] to [73]). However, since the full numerical simulation requires to resolve all of the scales up to Kolmogorov dissipative scales, it requires large amount of CPU and memory. Thus, DNS is still not completely feasible yet for realistic engineering problems.

Casalis *et. al.* [11], Boyer *et. al.* [48], Majdalani *et. al.* [49], Flandro [8] and Griffond *et. al.* [47] applied the stability analysis developed for the investigation of transition process in a laminar boundary layer to a wall bounded flow with porous walls. Both local approach developed by Orr and Sommerfeld and non-local approach developed by Herbert [12] and Bertolotti [43] are applied to a simplified two dimensional (both planar and axisymmetric) model of a rocket motor by including non-parallelism of induced by the flow through the porous walls. They superposed and perturbed the primitive flow varibles, such as velocity components and pressure, for an incompressible flow. The numerical discretization scheme they used is the fourth-order accurate two-point finite difference scheme introduced by Malik and Hussaini [23]. In contrast, in this thesis, it is aimed to resolve the variation in the wall-normal direction by using Chebyshev Gauss-Lobatto collocation approximation, while the streamwise direction is discretized by 1st order accurate backward differencing scheme which allows an efficient marching procedure.

In this thesis, the focus is on the stability of an incompressible, homogenous, isothermal, two-dimensional, planar wall-bounded flow with flow through its porous walls. Our motivation in focusing on such a problem is to study the stability of flow in a simplified rocket motor by assuming it has fully cylindrical grain with uniform fluid injection speed. After the numerical models are developed for the planar case that provide an accurate prediction of the linear stability, the axisymmetrical case will be studied in a future work.

CHAPTER 2

LINEAR STABILITY THEORY I: LOCAL APPROACH

2.1. Linear Stability Theory

The main aim of hydrodynamic stability studies is to answer the decisive question: Do the disturbances increase or die out in time and/or in space? If those disturbances decay, the flow is considered stable; on the other hand, if the disturbances grow in time and/or in space, the flow is said to be unstable, and then there exists the possibility of transition to a turbulent pattern. To answer that crucial question, theory of stability is developed, and its main objective is to predict the value of critical flow control parameters such as Reynolds number for the loss of stability of the flow under consideration. Since disturbances at early stages of the instability are pretty weak, nonlinear terms can be neglected. This linearization assumption limits the theory to the initial stages of the instability. The study of stability of laminar flows begins with decomposing the fluid motion into its mean (basic) flow and intodisturbances superimposed on it. For a two-dimensional flow, primitive flow variables, such as velocity components and pressure, can be decomposed as;

$$U(x, y, t) = \bar{U}(x, y) + u(x, y, t) \tag{2.1a}$$

$$V(x, y, t) = \bar{V}(x, y) + v(x, y, t) \tag{2.1b}$$

$$P(x, y, t) = \bar{P}(x, y) + p(x, y, t) \tag{2.1c}$$

This decomposition allows one to solve for the mean flow and the evolution of the disturbances separately. This thesis is about the stability of a viscous and incompressible flow developed in a 2D planar channel having porous walls with

uniform fluid injection and with a bounding head wall . The geometry of the problem is in fact a simplified SPRM with porous injection given in Figure 2.1.
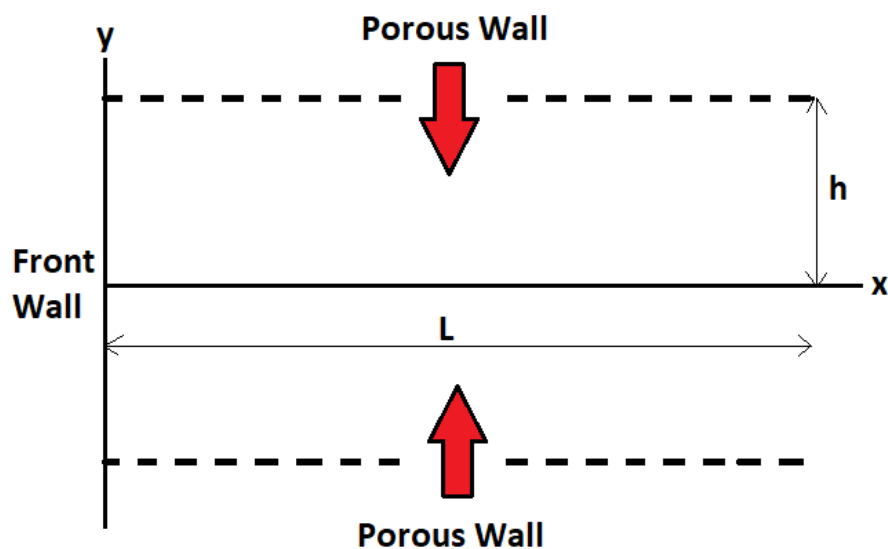
Figure 2.1. General Cartesian Geometry

Here, h represents the half channel height while L stands for the channel length. The dimensional form of the governing equations are the following 2D Navier-Stokes equations;

$$\frac{\partial U}{\partial x} + \frac{\partial V}{\partial y} = 0 \tag{2.2a}$$

$$\frac{\partial U}{\partial t} + U\frac{\partial U}{\partial x} + V\frac{\partial U}{\partial y} = -\frac{1}{\rho}\frac{\partial p}{\partial x} + \nu\left(\frac{\partial^2 U}{\partial x^2} + \frac{\partial^2 U}{\partial y^2}\right) \tag{2.2b}$$

$$\frac{\partial V}{\partial t} + U\frac{\partial V}{\partial x} + V\frac{\partial V}{\partial y} = -\frac{1}{\rho}\frac{\partial p}{\partial y} + \nu\left(\frac{\partial^2 V}{\partial x^2} + \frac{\partial^2 V}{\partial y^2}\right) \tag{2.2c}$$

between two parallel porous walls with boundary conditions;

$$\forall x, \forall t, \quad \begin{cases} U(x, y = h, t) = U(x, y = -h, t) = 0 \\ V(x, y = h, t) = -V(x, y = -h, t) = -V_{inj} \end{cases} \tag{2.3}$$

where V_{inj} is the injection speed of the fluid through porous walls, U and V are the streamwise and normal components of the flow, respectively, and p is the pressure. It should be highlighten that the left and right boundary conditions do not exist, i.e. the problem is taken as semi-infinite planar channel flow. Moreover, there is no fluid injection through those boundaries. In order to derive stability equations from Navier-Stokes equations, the following block diagram given may be used.
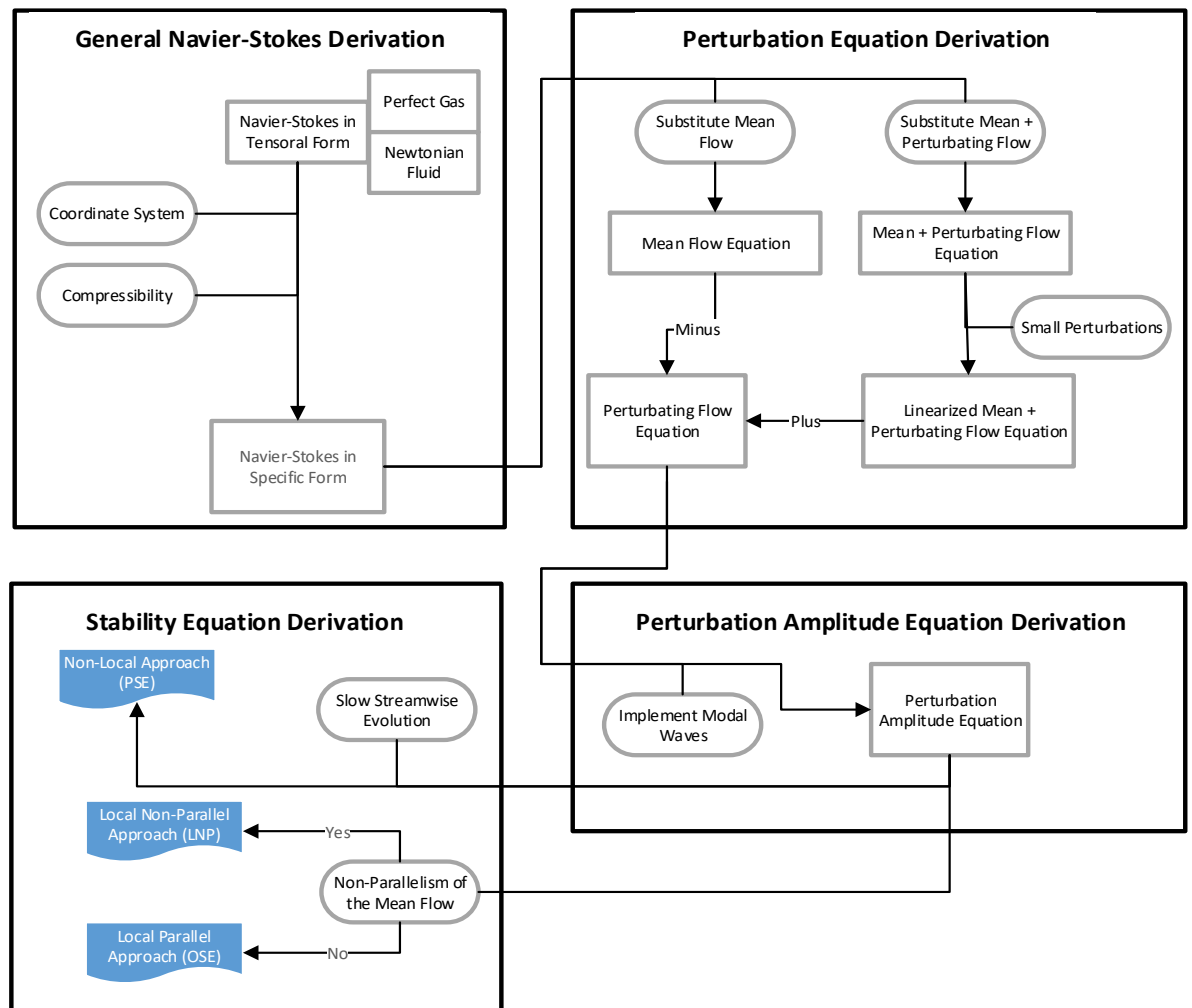
Figure 2.2. Block Diagram of the Derivation of Stability Equations

First, the flow configuration is considered as a parallel flow, i.e. the streamlines are everywhere parallel to any bounding surface and the mean flow is independent of the streamwise variable x. In the case of a boundary layer over a flat plate, for example, this assumption would mean that the boundary layer thickness does not change downstream. Under this assumption, mean wall-normal velocity ($\bar{V}$) and derivatives of mean flow quantities with respect to the streamwise variable x are omitted. It should be mentioned that, here, we are considering 2D flow only.

2.2. Mean Flow

The mean flow is considered to be viscous and incompressible along a 2D channel with parallel walls with uniform fluid injection through the walls. It can be shown that the flow can be described in the form [50] ;

$$\bar{U} = xF'(y), \quad \bar{V} = -F(y) \tag{2.4}$$

in terms of an auxiliary function $F(y)$ that satisfies the nonlinear ordinary differential equation,

$$F'F'' - FF''' = \frac{1}{Re}F^{(IV)} \tag{2.5a}$$

reduced from the Navier-Stokes equations, subject to the boundary conditions

$$F(1) = 1, \quad F'(1) = 0, \quad F(-1) = -1, \quad F'(-1) = 0 \tag{2.5b}$$

while Reynolds number, Re, is defined as,

$$Re = \frac{V_{inj}\,h}{\nu} \tag{2.6}$$

26

It should be noted that all of the variables given in (2.4) to (2.6) are non-dimensionalized. However, for simplicity, asteriks is removed in the governing equations for fluid motion written for both mean and perturbating flow. The mean flow equations (2.5) are solved using Chebyshev approximation in this thesis for its high accuracy and resolution power resulting in lower degrees of freedom N as opposed to the fourth order accurate compact finite difference scheme used in literature [23].

However, an approximate analytical solution form also exists for 2D inviscid flows, which is also be known as Taylor's mean flow profile.

$$\bar{U} = \frac{\pi}{2} x \cos\left(\frac{\pi y}{2}\right), \quad \bar{V} = -\sin\left(\frac{\pi y}{2}\right) \tag{2.7}$$

It is pointed by Casalis *et. al.* [11] that for small Reynolds numbers, Taylor's analytic mean flow solution for inviscid flow slightly differs from the solution of (2.5), while they are almost match perfectly as Reynolds number inceases. Therefore, that analytical solution given in (2.7) can be directly used if it is preferred.

For the numerical approximation, Chebyshev Gauss-Lobatto grid points and associated differentiation matrices are used as constructed in [14] and boundary conditions are applied directly by modifying the differentiation matrices. An advantage of this approach is the accurate treatment of the boundary conditions due to the grid crowding near the boundaries and global approximation of the derivatives such as in the Neumann conditions (2.5b) without the need to use ghost cells (or nodes). The details of the solution procedure of Chebyshev collocation method is given in Appendix A together with the code written in MATLAB to solve mean flow for a given Reynolds number defined in (2.6) and L/h ratio (or non-dimensionalized channel length) is shared in Appendix B.

27

Numerical mean flow with auxiliary function F as obtained for Re=900, and $L/h = 20$ is shown in Figure 2.3 -Figure 2.5. The number of the degree of freedem is choosen as $N = 120$ (see below for details).
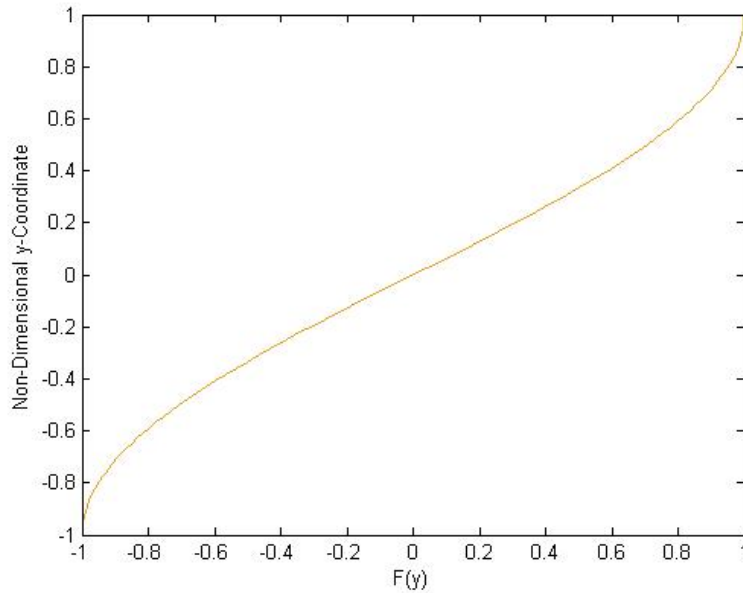
Figure 2.3. Mean Flow Solution for $L/h = 20$

Since $F(y)$ has no physical meaning, the magnitude and the vector plots of the mean flow are shown in Figure 2.4 and Figure 2.5, respectively.
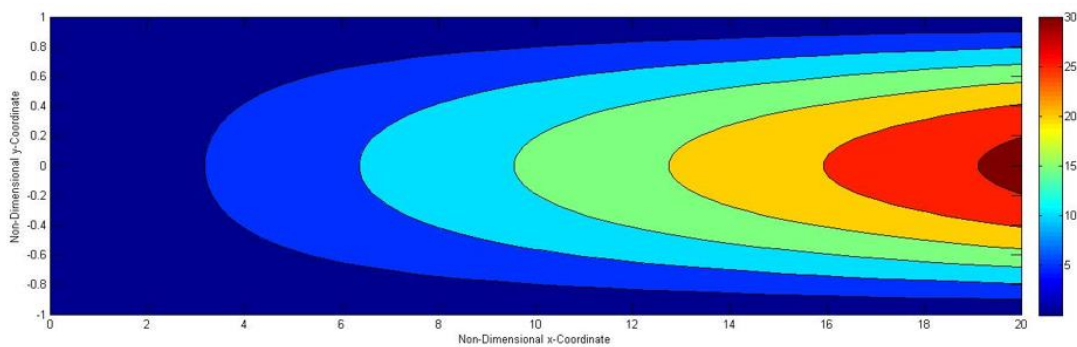
Figure 2.4. Mean Velocity Magnitude Contours for L/h = 20
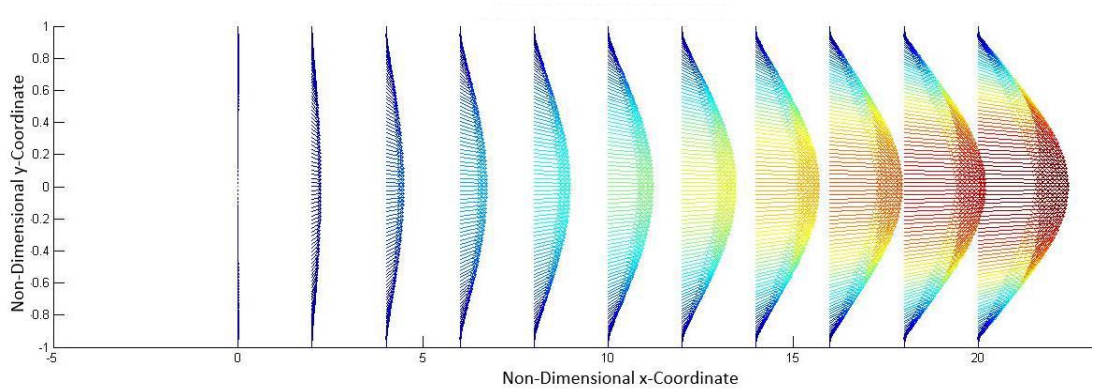
Figure 2.5. Mean Velocity Vectors for $L/h = 20$

As it can be seen from the vector plots in Figure 2.5 that there is a strong non-parallelism in the base flow. In other words, conventional normal-modes analysis used to investgate hydrodynamic stability that, for example, leads to Orr-Sommerfeld equation, in which the mean wall-normal velocity component and the variation of the mean axial velocity component along the sreamwise direction are neglected, do not give accurate results on such a mean flow, since the non-parallelism has an impact on cross-flow vortices. Thus, it is needed to derive a stability equation that takes non-parallelism into account.

It can seen in Figure 2.6-Figure 2.9 that Taylor's mean flow profile (2.7) can be directly used since the terms $\bar{U}^*$, $\partial^2 \bar{U}^*/\partial y^{*2}$, $\partial^2 \bar{U}^*/\partial x^* \partial y^*$ and $\bar{V}^*$ do not differ with the solution found using Chebyshev Collocation method for $N = 120$ and for a given Reynolds number, $Re = 900$, where $\bar{U}^*$ and $\bar{V}^*$ represent the non-dimensional velocity components of the mean flow in streamwise and normal direction, respectively. The reason of choosing those variables for comparison is going to be mentioned in the following section. Here, for $Re = 900$ this is true, as Casalis *et. al.* [11] stated, while for lower Reynolds numbers this may not be true.

29
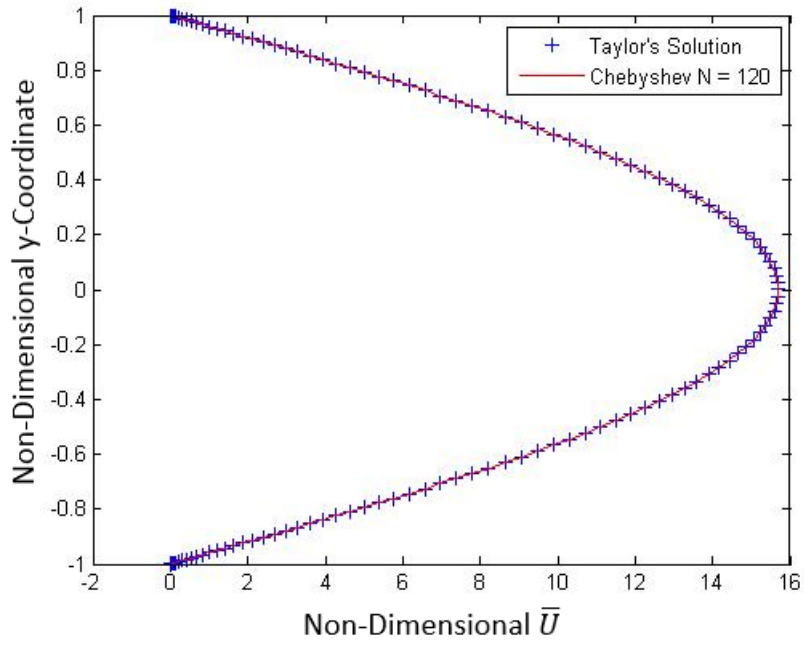
Figure 2.6. $\bar{U}^*$ Comparison at $x/h = 10$
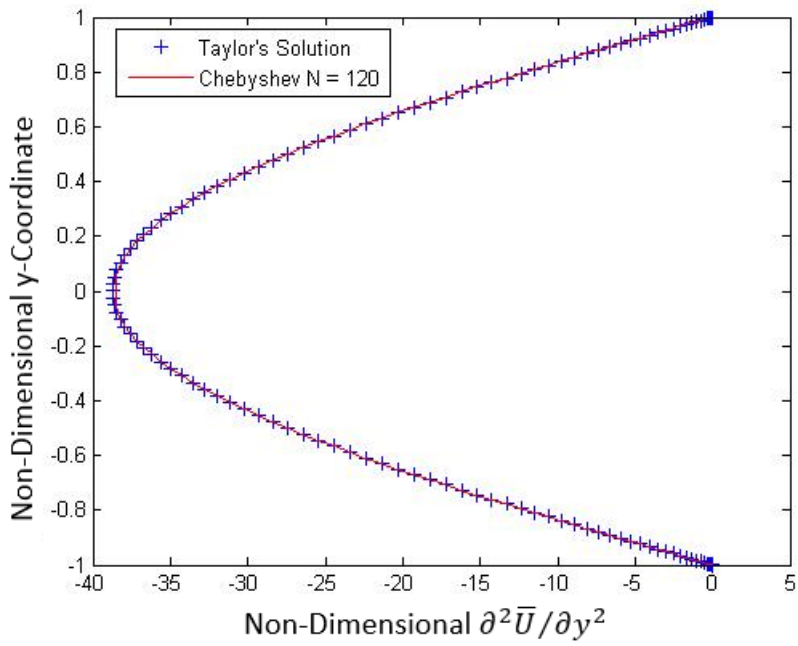
Figure 2.7. $\partial^2 \bar{U}^* / \partial y^{*2}$ Comparison at $x/h = 10$

30
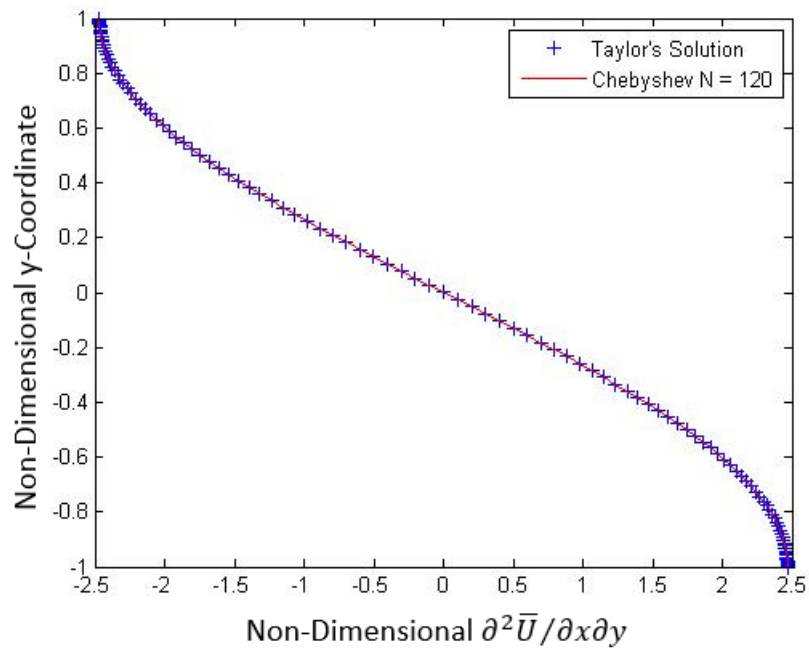
Figure 2.8. $\partial^2 \overline{U}^* / \partial x^* \partial y^*$ Comparison (Independent of x-Direction)
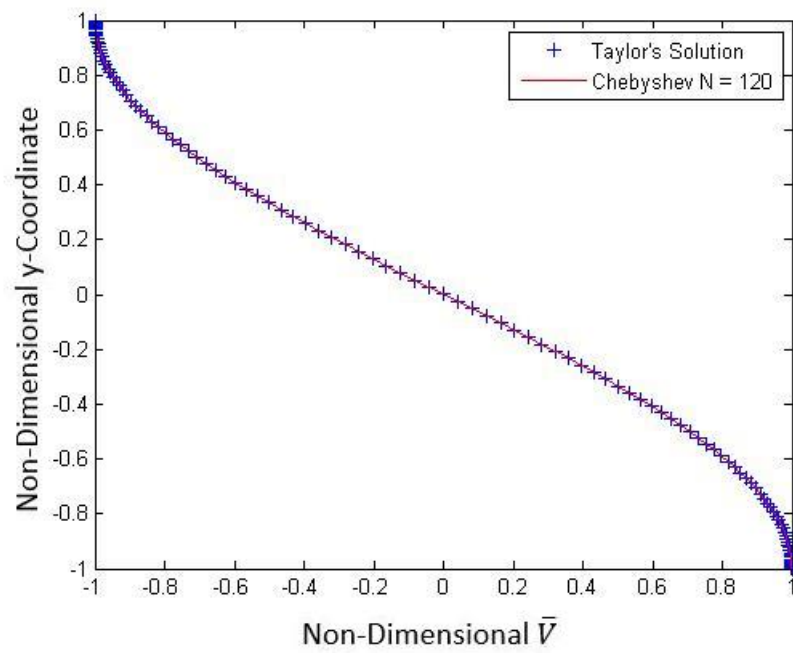
Figure 2.9. $\overline{V}^*$ Comparison (Independent of x-Direction)

31

2.3. Local Approach

In the local approach, the perturbation variables are written in the form of normal modes that are normally used in those cases where the mean flow is independent of the streamwise variable x. The assumption of *small disturbances* leads to a linear problem,

$$U = \bar{U}(x, y) + u(y)e^{i(\alpha x - \omega t)} \tag{2.8a}$$

$$V = \bar{V}(x, y) + v(y)e^{i(\alpha x - \omega t)} \tag{2.8b}$$

$$P = \bar{P}(x, y) + p(y)e^{i(\alpha x - \omega t)} \tag{2.8c}$$

where ω stands for the frequency and α represents streamwise wavenumber. For simplicity, asterisk is removed from each non-dimensional quantity.

The exponential term $e^{i(\alpha x - \omega t)}$ in the normal-modes analysis models the wavelike nature of the disturbance while its amplitude is restricted to be only y-dependent terms as if the mean flow does not depend on the streamwise variable x. Since spatial stability is studied in this thesis, the perturbation frequency, ω, is taken as a real quantity, while the wavenumber $\alpha = \alpha_r + i\alpha_i$ is taken as a complex quantity in the normal-modes formulation. Therefore, for that wavelike perturbation form, it can be clearly seen that to obtain a stable flow, imaginary part of the complex streamwise wavenumber, α, must be positive, and to have a marginally stable flow, imaginary part must be zero. In that case, the real part of α represents the wavenumber, while the imaginary part stands for the growth rate.

These forms are directly substituted into the Navier-Stokes equations (2.2) and (2.3), and linearized. The linear perturbation equations are then obtained by taking into account that the mean flow already is a solution of the associated Navier-Stokes equations (or that the solutions given in (2.7) are directly used). The detailed derivations of the stability equations are given in Appendix C, Appendix D and Appendix E, for continuity, x-momentum and y-momentum equations, respectively.

The resulting set of perturbation equations represents the local approach and takes the non-dimensional form,

$$i\alpha^* \hat{u}^* + \frac{\partial \hat{v}^*}{\partial y^*} = 0 \tag{2.9a}$$

$$-i\omega^* \hat{u}^* + i\alpha^* \bar{U}^* \hat{u}^* + \hat{u}^* \frac{\partial \bar{U}^*}{\partial x^*} + \bar{V}^* \frac{\partial \hat{u}^*}{\partial y^*} + \hat{v}^* \frac{\partial \bar{U}^*}{\partial y^*} \tag{2.9b}$$

$$= -i\alpha^* \hat{p}^* + \frac{1}{Re} \left(\frac{\partial^2 \hat{u}^*}{\partial y^{*2}} - \alpha^{*2} \hat{u}^* \right)$$

$$-i\omega^* \hat{v}^* + i\alpha^* \bar{U}^* \hat{v}^* + \bar{V}^* \frac{\partial \hat{v}^*}{\partial y^*} + \hat{v}^* \frac{\partial \bar{V}^*}{\partial y^*} \tag{2.9c}$$

$$= -\frac{\partial \hat{p}^*}{\partial y^*} + \frac{1}{Re} \left(\frac{\partial^2 \hat{v}^*}{\partial y^{*2}} - \alpha^{*2} \hat{v}^* \right)$$

with the boundary conditions ,

$$\hat{u}^*(-1) = \hat{u}^*(1) = \hat{v}^*(-1) = \hat{v}^*(1) = 0 \tag{2.10}$$

leads to a fourth order differential eigenvalue problem (see Appendix F for the derivation) and the search for the nontrivial solution leads to the dispersion relation .

$$F(\alpha, \omega, x, Re) = 0 \tag{2.11}$$

where α is the eigenvalue. According to the expansion of the primitive variables given in (2.7), a solution to the system of equations given in (2.9) and (2.10) with $Im(\alpha) < 0$ is an unstable linear eigenmode, in the sense that the amplitude of the disturbance grows exponentially in the streamwise direction. It should be known that these

boundary conditions are not related to a force response due to some fluctuations coming through the porous wall; the perturbation is searched as the eigenmode of the corresponding mean flow. In other words, an auxiliary disturbance with a certain frequency is not imposed to the mean flow by the fluid injection through porous walls, but the eigenmodes which makes the mean flow unstable are sought. By fixing two of those parameters in (2.11), namely, the real ω and Reynolds number, problem can be solved for complex α at each x location. The growth rate, $\alpha_i(x)$, defines the amplitude of the perturbation.

$$A(x) = A_0 e^{\int_{x_0}^{x} -\alpha_i(\xi)d\xi} \tag{2.12}$$

where A_0 is the perturbation at the position x_0 which is usually taken as the x-position where the steady flow is marginally stable or vicinity of that position.

Local approach can be divided into two procedures;

- Orr-Sommerfeld Equation (OSE): Streamwise variation and normal velocities of the steady flow are neglected, i.e. non-parallel term of the steady flow, $\bar{V}$, is considered as zero. Therefore, for consistency according to continuity equation, $\partial \bar{U}/\partial x$ terms is also dropped. In this case, $\bar{U} = 1 - y^2, \bar{V} = 0$ and thus, the simplified set of equations become completely equivalent to the Orr-Sommerfeld equation:

$$i\varphi''(\alpha\bar{U} - \omega) + i\varphi\left(-\alpha\frac{\partial^2\bar{U}}{\partial y^2} + \alpha^2\omega - \alpha^3\bar{U}\right) \tag{2.13}$$
$$= \nu\left[\varphi^{(IV)} - 2\alpha^2\varphi'' + \alpha^4\varphi\right]$$

or using non-dimensional form of the variables,

$$\omega^* = \frac{\omega}{1/t} = \frac{\omega h}{V_{inj}} \quad , \quad \alpha^* = \frac{\alpha}{1/h} = \alpha h \quad , \quad \varphi^* = \frac{\varphi}{V_{inj}} \quad , \quad \overline{U}^* = \frac{\overline{U}}{V_{inj}} \quad ,$$

$$\overline{V}^* = \frac{\overline{V}}{V_{inj}} \quad , \quad x^* = \frac{x}{h} \quad , \quad y^* = \frac{y}{h}$$

$$i\varphi^{*\prime\prime}(\alpha^* \overline{U}^* - \omega^*) + i\varphi^*\left(-\alpha\frac{\partial^2 \overline{U}^*}{\partial y^{*2}} + \alpha^{*2}\omega^* - \alpha^{*3}\overline{U}^*\right) \tag{2.14}$$

$$= \frac{1}{Re}\left[\varphi^{*(IV)} - 2\alpha^{*2}\varphi^{*\prime\prime} + \alpha^{*4}\varphi^*\right]$$

with boundary conditions,

$$\varphi^*(\pm1) = \varphi^{*\prime}(\pm1) = 0 \tag{2.15}$$

For simplicity, asterisk can be removed from (2.14) and (2.15), which are together indicate non-dimensionalized OSE approach formula for a wall-bounded flow with fluid injection written in the form of perturbation streamfunction $\psi(x, y, t)$ in terms of which the physical variables, u and v, are computed as :

$$\psi(x, y, t) = \varphi(y). e^{i(\alpha x - \omega t)} \tag{2.16a}$$

$$\frac{\partial \psi}{\partial y} = \varphi'(y). e^{i(\alpha x - \omega t)} \quad \rightarrow \quad u(y) = \varphi'(y) \tag{2.16b}$$

$$-\frac{\partial \psi}{\partial x} = -i\alpha\varphi(y). e^{i(\alpha x - \omega t)} \quad \rightarrow \quad v(y) = -i\alpha\varphi(y) \tag{2.16c}$$

The transformation of this set to a fourth order differential eigen-system in terms of disturbance streamfunction is detailed in Appendix F. However, for such a problem to include the porous inflow, $\overline{V}$ cannot be taken as zero and $\overline{U}$

is dependent on streamwise variable x. To obtain consistent and accurate results, those terms are needed to be taken into account. Thus, OSE approach does not give satisfactory results for this problem.

- Local Non-Parallel Approach (LNP): The non-parallel terms are not neglected. However, the fluctuations are taken still in the normal mode form as in (2.8). Therefore, the mean flow equation (2.5) is needed to be solved simultaneosly with (2.9) (or Taylor's mean flow profile (2.7) may be used) to calculate primitive variables of the perturbation, u, v and p. Another possibility, as in the case of Orr-Sommerfeld equation, is to reduce the system into a fourth order differential eigen problem:

$$i\varphi''(\alpha\bar{U} - \omega) + i\varphi\left(-\alpha\frac{\partial^2\bar{U}}{\partial y^2} + \alpha^2\omega - \alpha^3\bar{U}\right) \tag{2.17}$$

$$+\varphi'\left(\frac{\partial^2\bar{U}}{\partial x\,\partial y} - \alpha^2\bar{V}\right) + \bar{V}\varphi''' = \nu\left[\varphi^{(IV)} - 2\alpha^2\varphi'' + \alpha^4\varphi\right]$$

The details of the derivation for the LNP approach are given in Appendix F. It should be noted that these two approaches, namely OSE and LNP, differ by three extra terms which are the contributions of non-parallelism of the mean flow, i.e. $\bar{V} \neq 0$ and $\partial\bar{U}/\partial x \neq 0$.

By using non-dimensional form of the variables, the non-dimensionalized perturbation equations for LNP approach can be obtained as :

$$\omega^* = \frac{\omega}{1/t} = \frac{\omega h}{V_{inj}} \quad , \quad \alpha^* = \frac{\alpha}{1/h} = \alpha h \quad , \quad \varphi^* = \frac{\varphi}{V_{inj}} \quad , \quad \bar{U}^* = \frac{\bar{U}}{V_{inj}} \quad ,$$

$$\bar{V}^* = \frac{\bar{V}}{V_{inj}} \quad , \quad x^* = \frac{x}{h} \quad , \quad y^* = \frac{y}{h}$$

$$i\varphi^{*''}(\alpha^*\bar{U}^* - \omega^*) + i\varphi^*\left(-\alpha^*\frac{\partial^2\bar{U}^*}{\partial y^{*2}} + \alpha^{*2}\omega^* - \alpha^{*3}\bar{U}^*\right) \tag{2.18}$$

$$+\varphi^{*'}\left(\frac{\partial^2 \overline{U}^*}{\partial x^* \partial y^*} - \alpha^{*2}\overline{V}^*\right) + \overline{V}^*\varphi^{*'''} = \frac{1}{Re}\left[\varphi^{*(IV)} - 2\alpha^{*2}\varphi^{*''} + \alpha^{*4}\varphi^*\right]$$

For simplicity, asterisks can be removed from (2.18) and the boundary conditions are given as in (2.15). This is the non-dimensional LNP differential eigenproblem for a wall-bounded flow with fluid injection through porous channel wall boundaries written in terms of perturbation streamfunction. It should be noted that as in the OSE approach that the shape-functions and the streamwise wavenumbers of the disturbances are taken both independent of the streamwise location (see 2.8).

After reduction of the stability equations to a fourth order equation, the problem is treated as an eigenvalue problem solved at each x coordinate of the channel for given ω and Re. MATLAB's eigenvalue solver, *eig.m*, function is used to calculate eigenpairs at each x coordinate. The discretization in the wall-normal direction y is performed by Chebyshev Gauss-Lobatto collocation method with $N = 120$ and the associated differentiation matrices are constructed using the function *chebdif.m* given in [14], due to the accuracy and resolving power considerations mentioned earlier for the mean flow computation. The reason to choose Chebyshev polynomial approximation as the numerical scheme is that to have infinitely differentiable mean velocity components and therefore, eigenfunctions of (2.14) and (2.18), φ^*, is also infinitely differentiable for the interval $-1 \leq y \leq 1$, with one-sided derivatives at the boundaries. This statement can ve proved as follows. Let $T_n(x)$ denote the n-th degree Chebyshev polynomial of the first kind defined as

$$T_n(x) = P^{(-1/2)}(x) = cos(n \arccos x) = cos(n\theta) \text{ where } x = cos\theta \qquad (2.19)$$

for all non-negative integers n. It is possible to expand $\varphi^*(y)$ in the interval,

$-1 \leq y \leq 1$ as,

$$\varphi^*(y) = \sum_{n=0}^{\infty} a_n T_n(y) \tag{2.20}$$

where

$$a_n = \frac{2}{\pi c_n} \int_{-1}^{1} \varphi^*(y) T_n(y)(1-y^2)^{-1/2} dy \tag{2.21}$$

with $c_0 = 2$ and $c_{n \neq 0} = 1$.

The promptness of the convergence of $\varphi^*(y)$ given in (2.20) for $-1 \leq y \leq 1$ can be easily illustrated by observing that

$$g(\theta) = \varphi^*(cos\theta)$$

is an infinitely differentiable and periodic function of θ. Therefore, the theory of Fourier series guarantees that Fourier cosine expansion of $g(\theta)$ exists,

$$g(\theta) = \sum_{n=0}^{\infty} a_n (cosn\theta) \tag{2.22}$$

with the property that the error after N terms decreases much more dramatically than any power of $1/N$ as $N \rightarrow \infty$. The same result can be obtained by using any other orthogonal polynomials. However, in most cases, although expansion of $\varphi(y)$ are made in terms of orthogonal functions that seem to bear much closer relation to the eigenfunctions which are interested than do the orthogonal polynomials, only finite-order rates of convergence are obtained.

2.4. Validation Studies

The validity of the code is simply tested by comparing the computed results against the cases:

- The classical Orr-Sommerfeld problem for plane Poiseuille flow solved by Orszag [17] using Chebyshev polynomials (modal approach),

- The porous flow case solved by Casalis *et. al.* [11] by using fourth-order accurate finite difference scheme at $Re = 900, x = 10$ and $\omega = 30$.

The first validation of the code written in MATLAB is for the classical Orr-Sommerfeld problem for plane Poiseuille flow with the mean flow profile taken as,

$$\bar{U} = 1 - y^2 \quad , \quad \bar{V} = 0$$

to the Local approach code which is the exact solution for the plane Poiseuille flow without any fluid injection through walls (boundaries). The value of the critical Reynolds number, critical growth rate and critical disturbance frequency that satisfy the dispersion relation (2.11) and make $-\alpha_i \cong 0$ is calculated for $N = 120$ as;

$$Re_c = 5772.22768 \quad , \quad \alpha_c = 1.020742 \quad , \quad \omega_{cr} = 0.26950617$$

which is in good agreement with Orzsag [17] who used a modal expansion involving 50 Chebyshev polynomials,

$$Re_c = 5772.22 \quad , \quad \alpha_c = 1.02056 \quad , \quad \omega_{cr} = 0.26400174$$

.
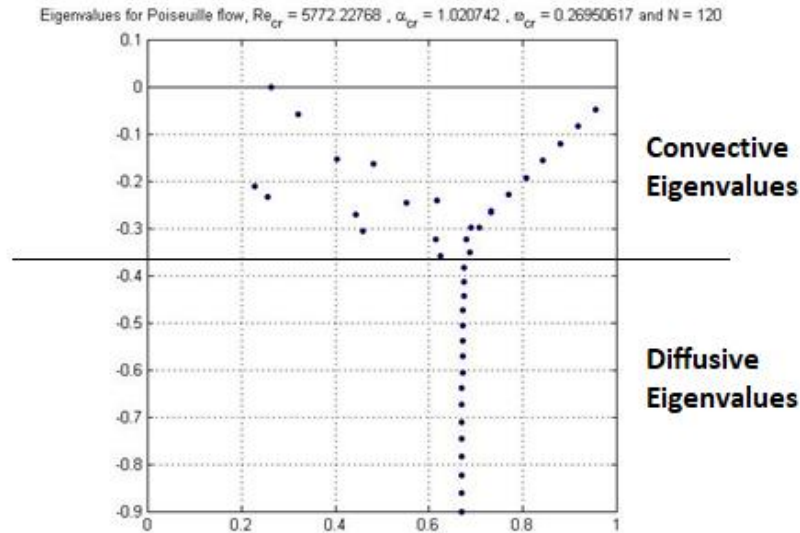
Figure 2.10. Temporal Stability Spectrum for Plane Poiseuille Flow at Critical Conditions Re_c and α_c

If the eigenvalue $-\alpha_i$ closest to the real axis contacts this axis, the flow becomes marginally stable, while once it exceeds that border the flow is considered to be unstable, or in other words *"transition begins"*.

Deciding on the degree of Chebyshev polynomials or the number of Chebyshev grid points along y-direction is not an easy task that usually requires some numerical experimentation. In spectral methods, the accuracy is expected to get poorer after some point of reolution N due to the deterioration in the conditioning of the numerical approximation. Moreover, because of the nature of the eigenvalue solvers, accuracy of the intermediate eigenvalues and corresponding eigenfunctions gets worse with the decline in the resolution. In order to assess the necessary numerical resolution in the computation of the stability spectrum, we temporarily switch to computing the time stability in OSE case by computing ω as the complex eigenvalue for given real α and Re, because more results are available in the literature. We computed the spectrum for selected resolution values $N = 40, 60, 80, 100$ and 120 in sequence as shown in Appendix G. The time spectrum of the OSE case for $N = 120$ is given in Figure 2.10. The foreseen critical Reynolds number, growth rate, disturbance frequency and all those convective and diffusive eigenvalues adjacent to the imaginary axis are given in Appendix G. On the grounds that mesh independence study, it can be clearly seen that both convective and diffusive eigenvalues cannot be calculated accurately for $N = 40, 60$ cases, while convective eigenvalues do not change by the increase of number of Chebyshev grid points after $N = 80$ case. However, even in that case, diffusive eigenvalues cannot be computed accurately, thus, number of grid points is still needed to be increased. After $N = 100$, it can be said by comparing the distribution of the eigenvalues adjacent to the imaginary axis with $N = 120$ case that results do not change significantly. Therefore, for the OSE case, the resolution needs to be at least $N = 100$ along y-direction for accurate numerical calculation of the eigenvalues at the critical conditions.

The second trial for the validation of the code is done for the LNP case and compared with [11], at $Re = 900, x = 10, \omega = 30$ with fluid injection through the porous

boundaries of the wall-bounded region where $\bar{V} \neq 0$ and $\partial \bar{U}/\partial x \neq 0$. Therefore, velocity profile found in section 2.2 is used to calculate critical Reynolds number for given conditions. The dispersion relation given in (2.11) is satisfied for at least two different α values at given conditions, i.e. for given values of Reynolds number, x-position and disturbance frequency, at least 2 wavenumbers have been found with negative imaginary parts, so the mean flow is unstable. The comparison of the two unstable modes for given Re, x and ω that satisfies the dispersion relation given in (2.11) as found by Casalis *et. al.* [11] and by the Chebyshev Collocation code written in MATLAB is given in Table 2.1.

Table 2.1. Comparison Of The Results for $Re = 900, \omega = 30$ and $x = 10$

	Casalis *et. al.* [11]		$N = 120$	
	α_r	α_i	α_r	α_i
Mode-1	3.6739	-0.39791	3.6712975	-0.3920295
Mode-2	3.6511	-0.38398	3.6485435	-0.3785782

The features of the complex physical amplitude functions u and v are as follows:

➤ Mode-1: Real part of u is antisymmetric and real part of v is symmetric in $y = 0$ axis

➤ Mode-2: Real part of u is symmetric and real part of v is antisymmetric in $y = 0$ axis

The perturbating pressure disappears in the process of deriving LNP equations, after taking the curl of the momentum equations. Therefore, after solving (2.18) for φ^* and calculating the corresponding physical functions u and v, x-momentum equation for perturbating flow $(2.9b)$ may be used to calculate the amplitude of the perturbating pressure, $p(y)$ by imposing a condition, say, p(-1) = 1.

The general idea behind the spatial instability analysis is that the frequency, ω, is taken as a real quantity, while the wavenumber, α, is complex. Because the eigenvalue of the local approach is $\lambda = \omega/\alpha$, then the following statement can be written.

$$(\lambda_r + i \, \lambda_i) \, (\alpha_r + i\alpha_i) = \omega$$

➤ $\lambda_r \, \alpha_r - \lambda_i \, \alpha_i = \omega$
➤ $\lambda_r \, \alpha_i + \lambda_i \, \alpha_r = 0$

Thus, the code given in Appendix.K uses these two equations with some specified error to calculate the wavenumber, α, that satisfies dispersion relation given in (2.11). The solution procedure is based on scanning the possible solution space and bracketing the root, α, for smaller specified error at each iteration. This iteration is manually done in the code to make debugging easy, however, it can be automated .

The real parts of the amplitude functions of velocity components calculated at given conditions, $Re = 900, x = 10, \omega = 30$, for both Mode-1 and Mode-2 are given in Figure 2.11 and Figure 2.12, respectively, to illustrate the symmetry and antisymmetry of components of the perturbating flow velocity. For the magnitudes of the complex perturbation velocity amplitudes corresponding to the wavenumber solutions given in Table 2.1, are presented in Figure 2.13 and Figure 2.14, for Mode-1 and Mode-2, respectively. The computed magnitudes of complex perturbation pressure amplitude areshown in Figure 2.15 and Figure 2.16, for Mode-1 and Mode-2, respectively. Unfortunately, because Casalis et. al. [11] did not share their results for the real parts of the perturbating velocities, the comparison of the results for those real parts is not applicable. However, since the rest of the results are found compatible, it may be easily claimed that the real parts of the perturbating velocity components are also expected to be calculated the same. It should be mentioned that the demonstration of the real parts of the perturbating velocity components is only shared for to clarify the difference between Mode-1 and Mode-2, they have no physical meaning. These profiles are in good agreement with [11].
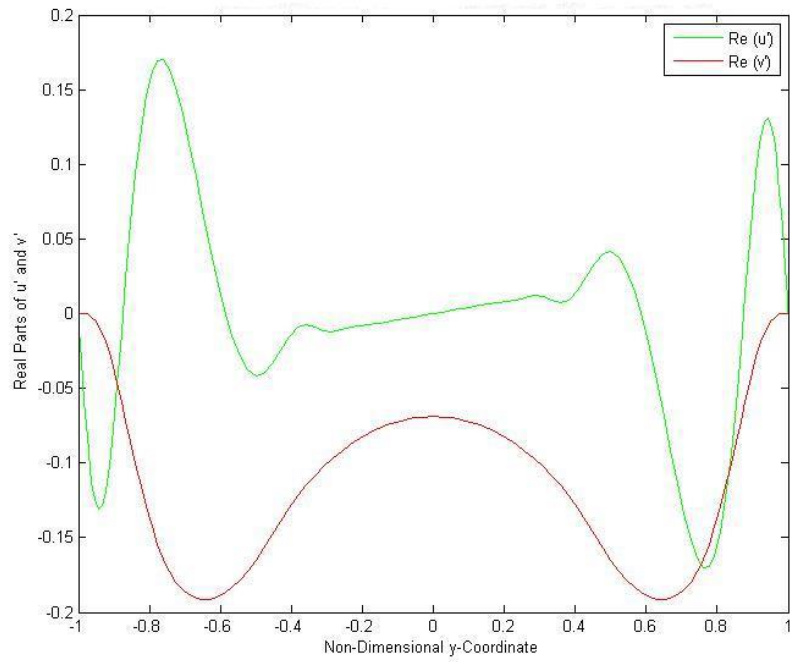
Figure 2.11. Real Parts of Perturbating Velocity Components for $Re = 900, x = 10, \omega = 30$ – Mode-1
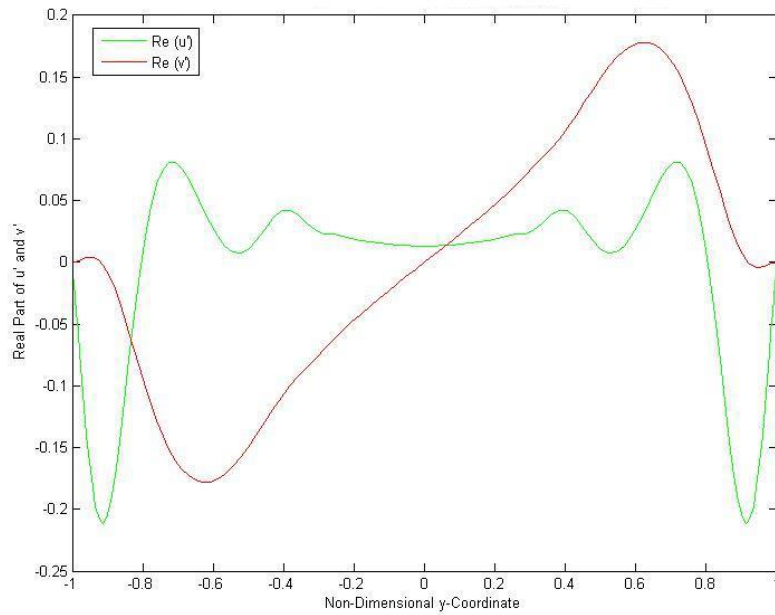
Figure 2.12. Real Parts of Perturbating Velocity Components, $Re = 900, x = 10, \omega = 30$ – Mode-2
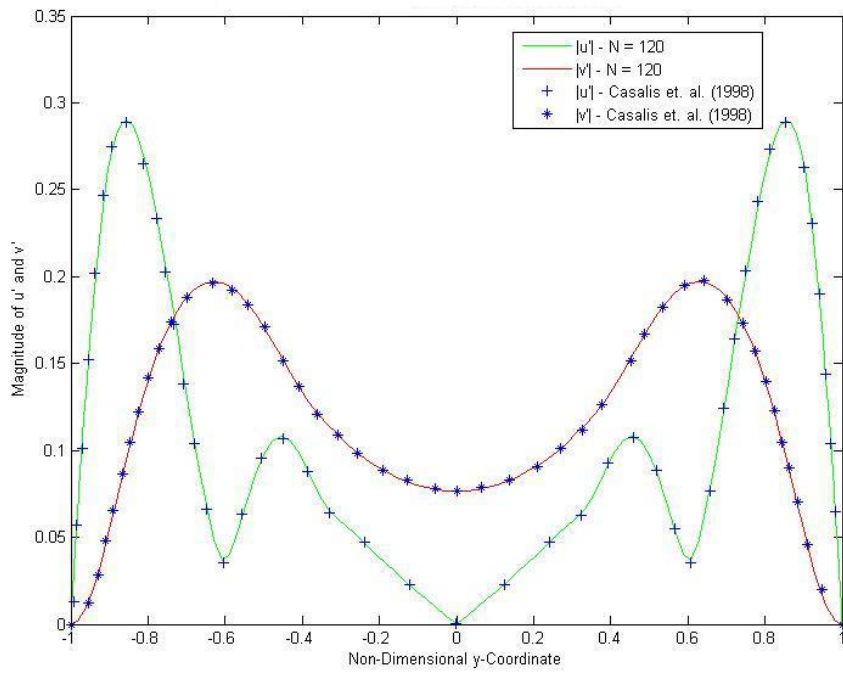
Figure 2.13. Magnitude of Perturbation Velocity Components, $Re = 900, x = 10, \omega = 30 -$ Mode-1
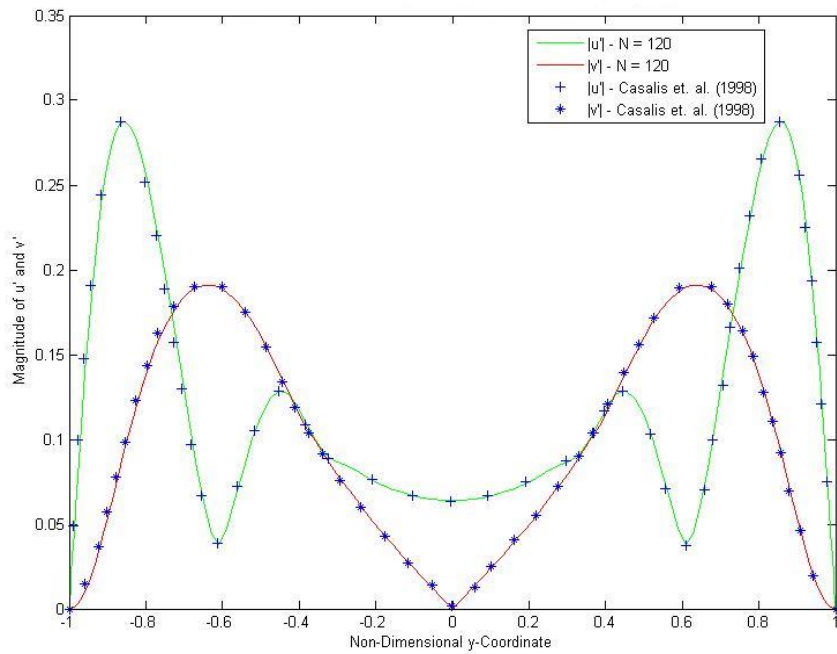
Figure 2.14. Magnitude of Perturbation Velocity Components, $Re = 900, x = 10, \omega = 30 -$ Mode-2
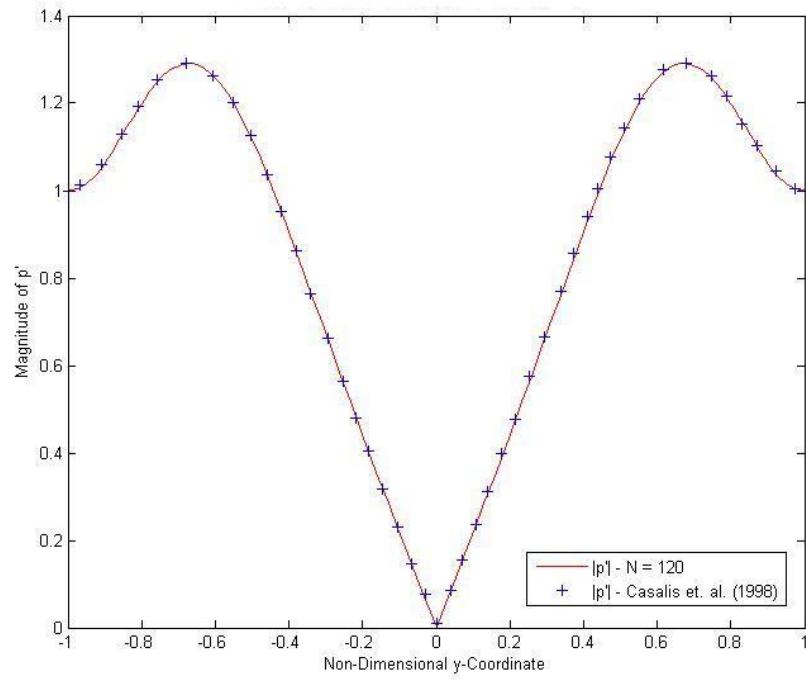
Figure 2.15. Magnitude of Perturbation Pressure for $Re = 900, x = 10, \omega = 30$ – Mode-1
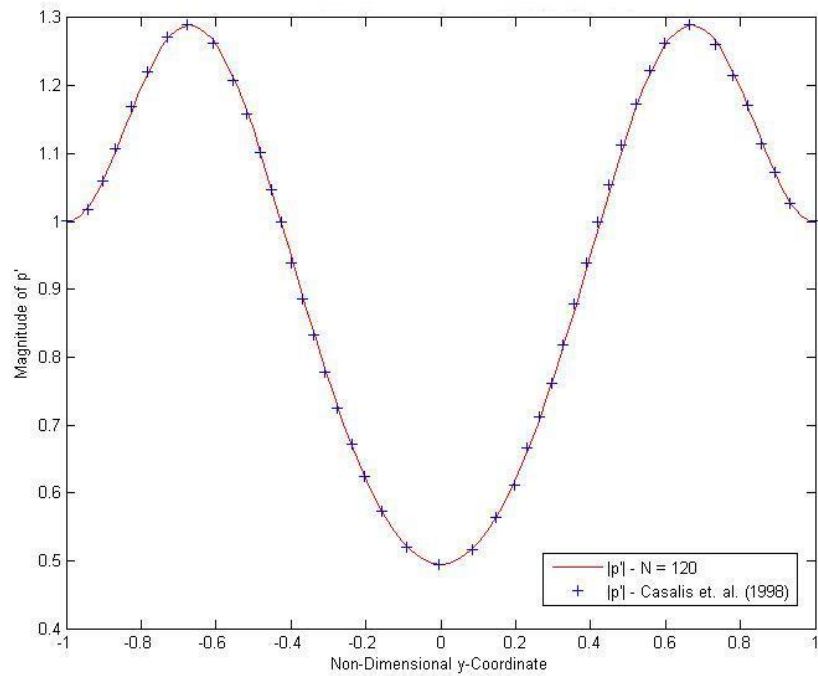
Figure 2.16. Magnitude of Perturbation Pressure for $Re = 900, x = 10, \omega = 30$ – Mode-2

The good agreement with the results in literature verifies that the Matlab code for local approach to study the stability of non-parallel flows is working satisfactorily.

2.5. Neutral Curves

From a practical point of view, the neutral curve for given parameters specifies and separates the stable and unstable regions, i.e. the region is stable for ($\alpha_i > 0$), while unstable for ($\alpha_i < 0$). On neutral curve, the flow is accepted to be marginally stable, i.e. for a spatial instability study, $\alpha_i = 0$ on that curve.

In the construction of the neutral curve, first, a mesh independence study is performed involving frequencies and corresponding wavenumbers for given Re=900. This comparison is given with tables for Mode-1 and Mode-2, in Appendix I and Appendix J, respectively. The new code written in MATLAB is presented in Appendix H that contructs the neutral curve where $\alpha_i = 0$ It can be observed from those tables that $N = 120$, the number of Chebyshev grid points in the wall-normal y-direction, still gives good results. Moreover, the results obtained from the code is compared with the neutral curve obtained by Casalis *et. al.* [11]. The neutral curves for given Reynolds number, $Re = 900$ and (α, ω) pair are simply formed by solving (2.18) with the boundary conditions (2.15) at different x-positions corresponding velocity profiles that define Mode-1 and Mode-2.
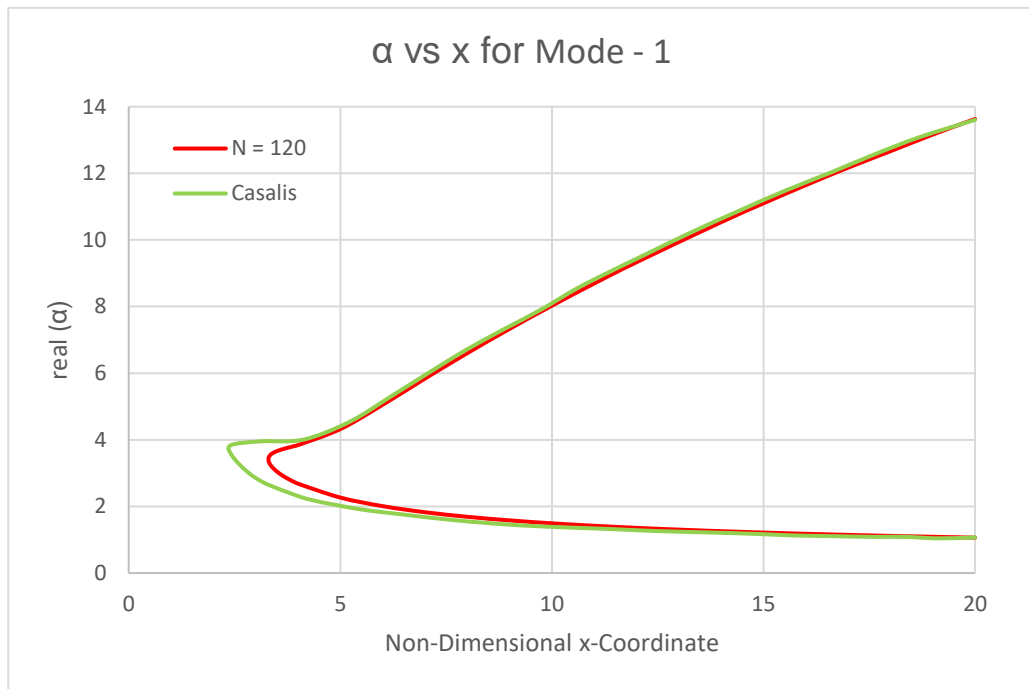
Figure 2.17. Comparison Of The Neutral Curves For Wavenumber – Mode-1
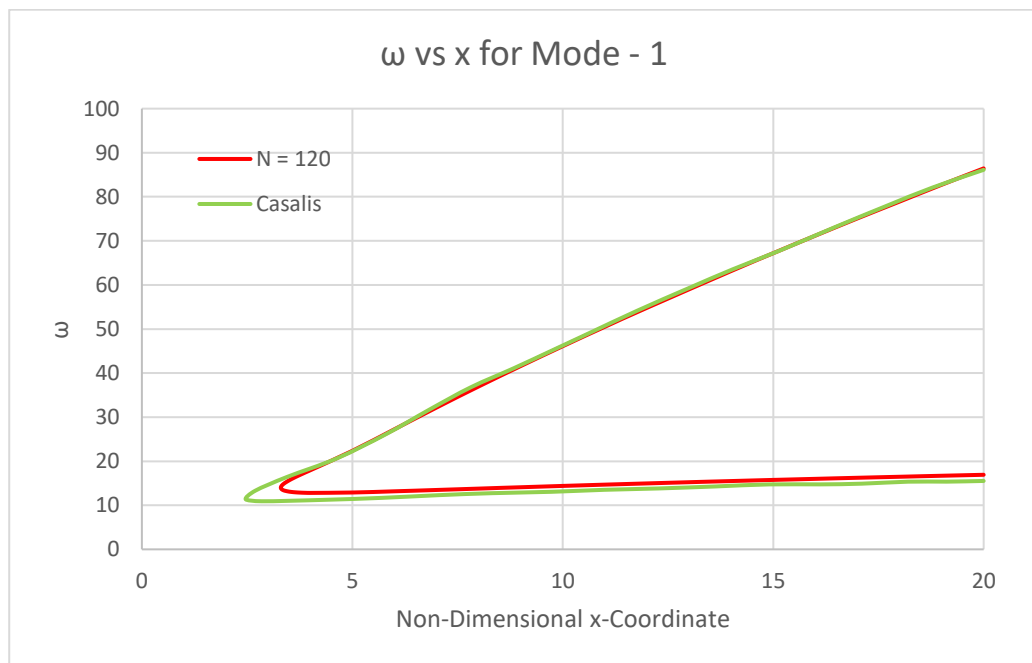
Figure 2.18. Comparison Of The Neutral Curves For Disturbance Frequency – Mode-1
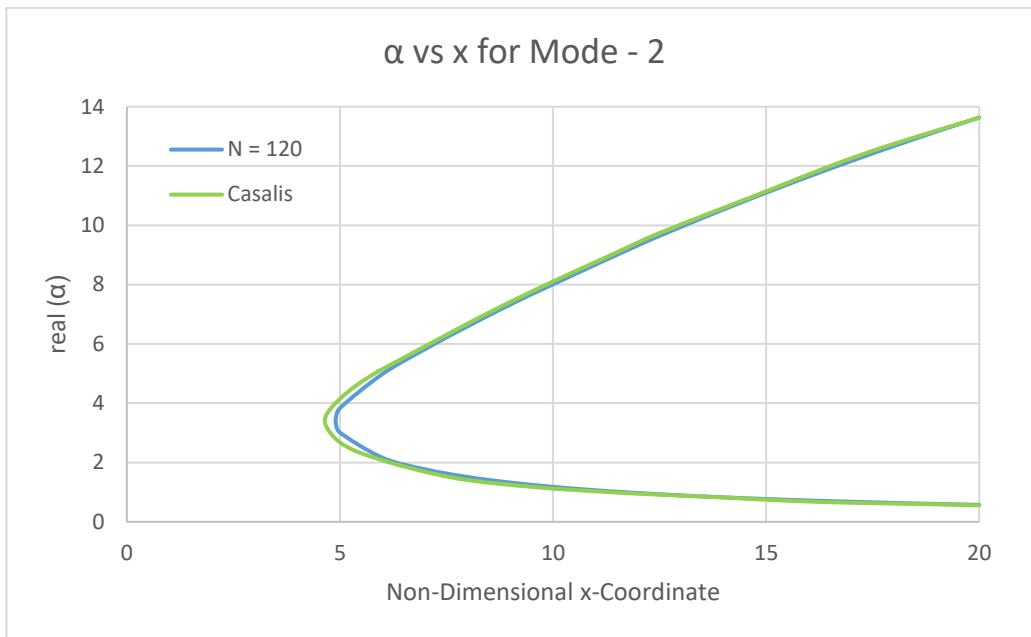
Figure 2.19. Comparison Of The Neutral Curves For Wavenumber – Mode-2
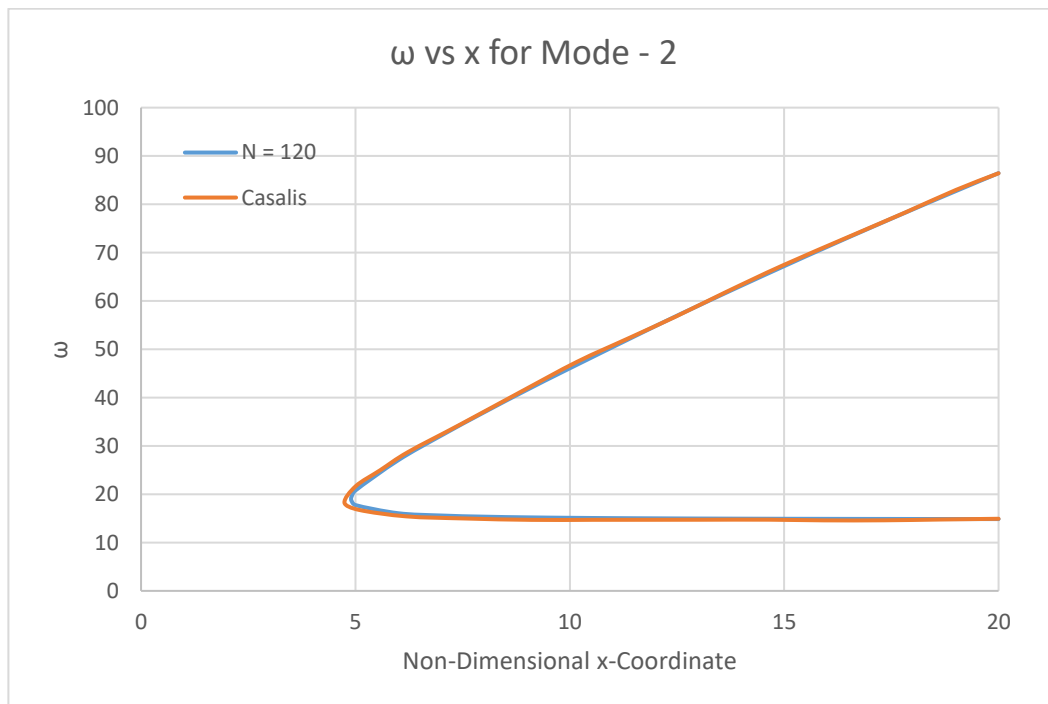
Figure 2.20. Comparison Of The Neutral Curves For Disturbance Frequency – Mode-2

48

By comparing the neutral curves drawn for (α, ω) pair at $Re = 900$ computed by the Matlab code and presented by Casalis *et. al.* [11] in Figure 2.17 Figure 2.20, it can be stated that Mode-2 results are almost the same, while there is a discrepancy at the tip of the neutral curves drawn for Mode-1. This may be caused by the difference in the numerical scheme used, the fourth-order compact scheme in [11] versus our Chebyshev Pseudospectral method.

2.6. The Effect Of Reynolds Number on Dispersion Relation

The purpose of the present paragraph is to assess the effect of the Reynolds number on the stability results. The first comparison is performed for the effect of Reynolds number on neutral curves. In section 2.4, neutral curves of (α, ω) pair for $Re = 900$ are demonstrated. In this section, the main aim is to illustrate the change of the shape of neutral curve for different Reynolds numbers. For this purpose, Reynolds number is changed from 50 to 2000 with non-uniform intervals. For Mode-1, the curves as wavenumber varied versus x for those Reynolds numbers are given in Figure 2.21, while the results as disturbance frequency varied versus x are presented in Figure 2.22. The same results for Mode-2 are demonstrated in Figure 2.23 and Figure 2.24.
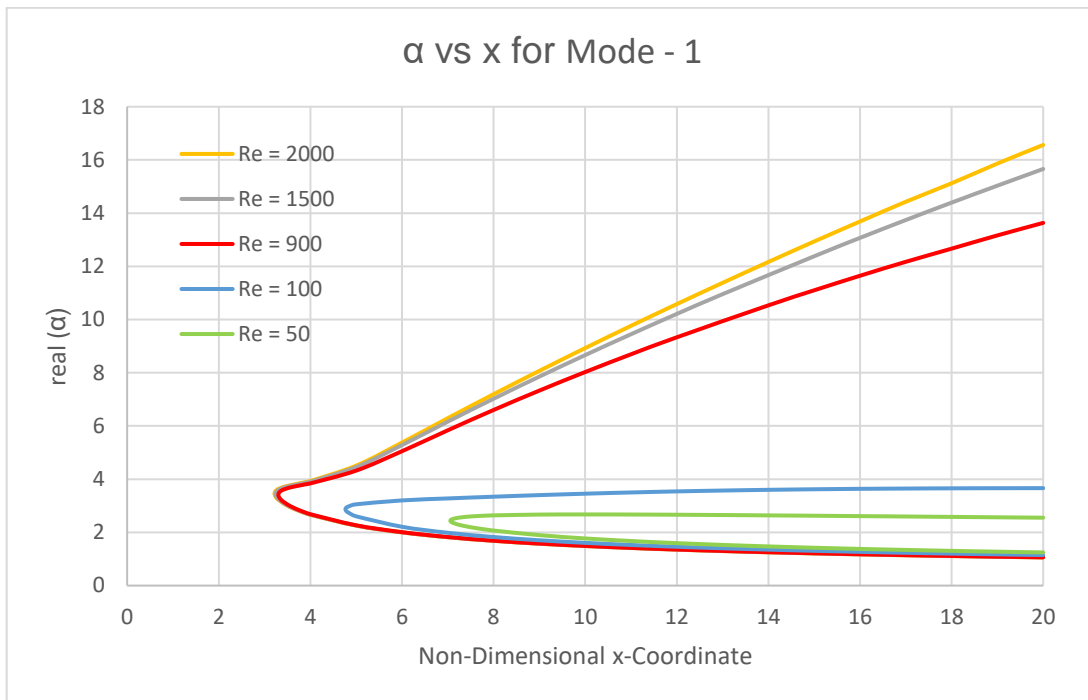
Figure 2.21. Neutral Curves of Wavenumber for Different Reynolds Numbers – Mode-1
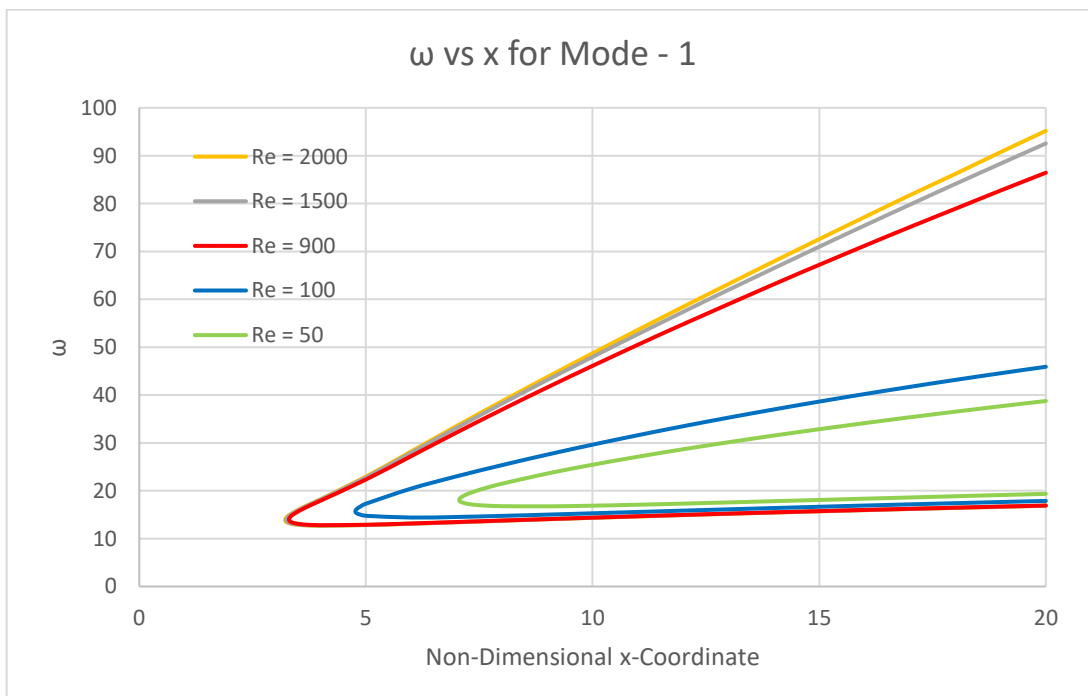
Figure 2.22. Natural Curves of Disturbance Frequency for Different Reynolds Numbers – Mode-1
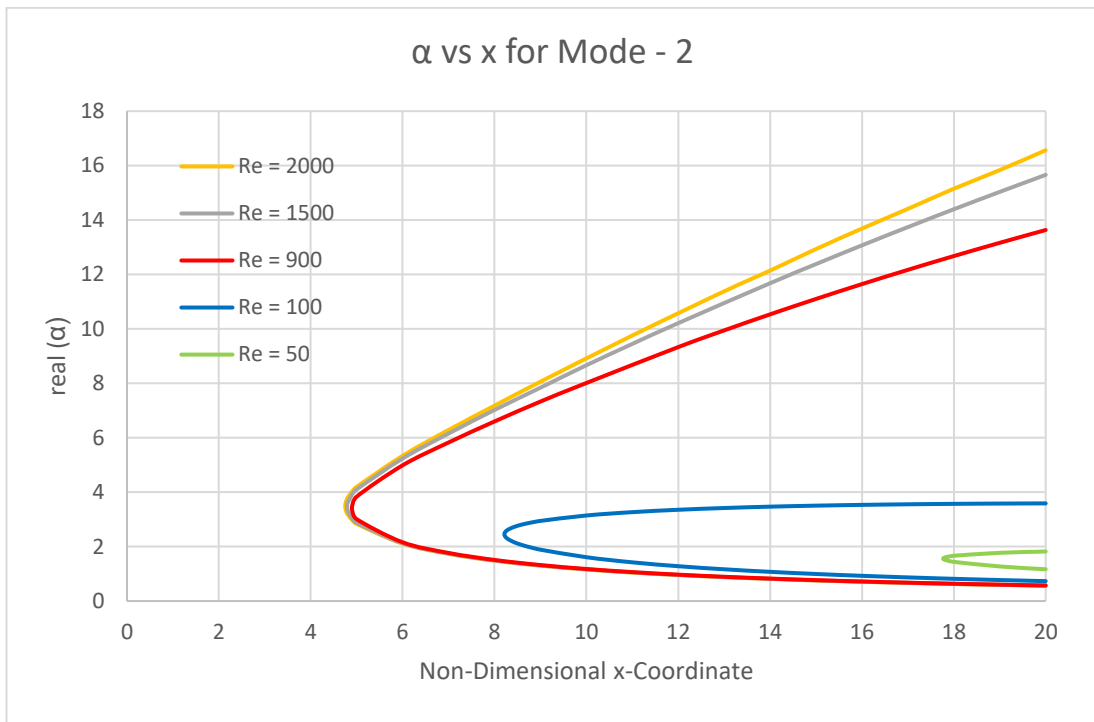
Figure 2.23. Natural Curves of Wavenumber for Different Reynolds Numbers – Mode-2
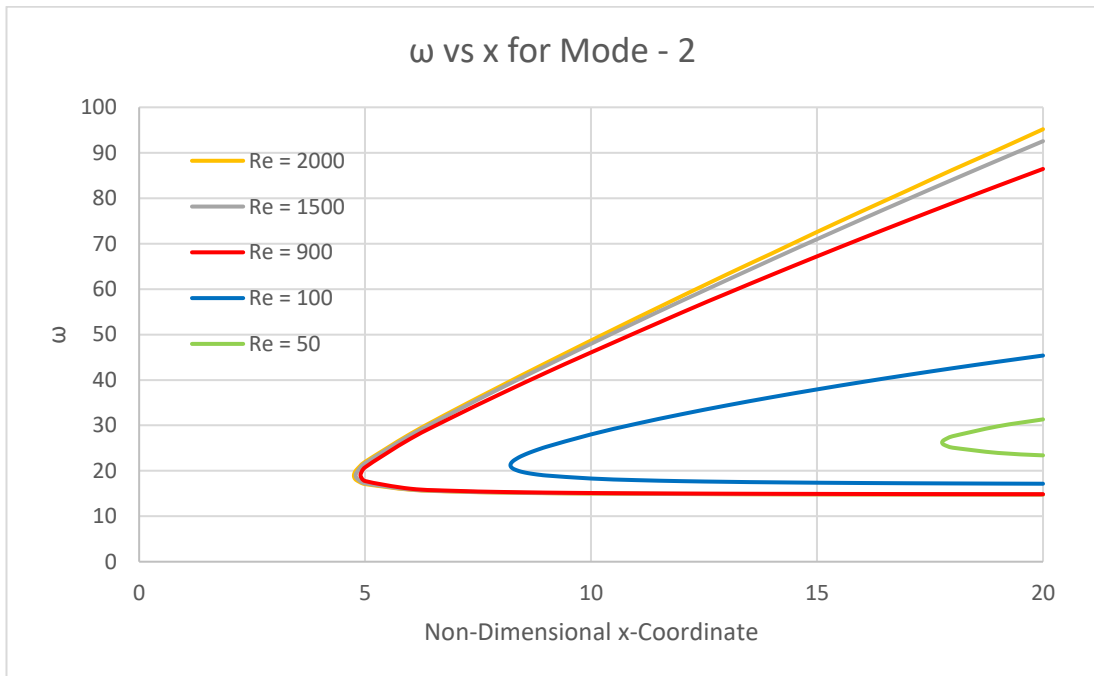
Figure 2.24. Natural Curves of Disturbance Frequency for Different Reynolds Numbers – Mode-2

It is clear that beyond a certain Reynolds number, the tip of the neutral curve does not change, i.e. critical position in x, critical wavenumber and corresponding critical disturbance frequency do not change significantly. As Reynolds number increases, it is observed that flow becomes unstable for a wider range of wavenumbers and frequencies where most of this enlargement occurs near the upper branch. The decrease in Reynolds number has a huge effect on the neutral curves by shifting of the tip point to further right and tightening the range of the wavenumber and frequency at which the mean flow becomes unstable. Moreover, no matter what Reynolds number is, Mode-1 becomes unstable earlier in comparison to Mode-2, in the sense of streamwise position. Further, for a fixed point in streamwise position $x = 10$ and fixed disturbance frequency $\omega = 30$, the change of wavenumber with respect to Reynolds number is studied. Considering the results given in Figure 2.25 and Figure 2.26, it is observed that after some value of Reynolds number, the real part of the complex wavenumber does not change at all, while the imaginary part changes slightly as Reynolds number increases.
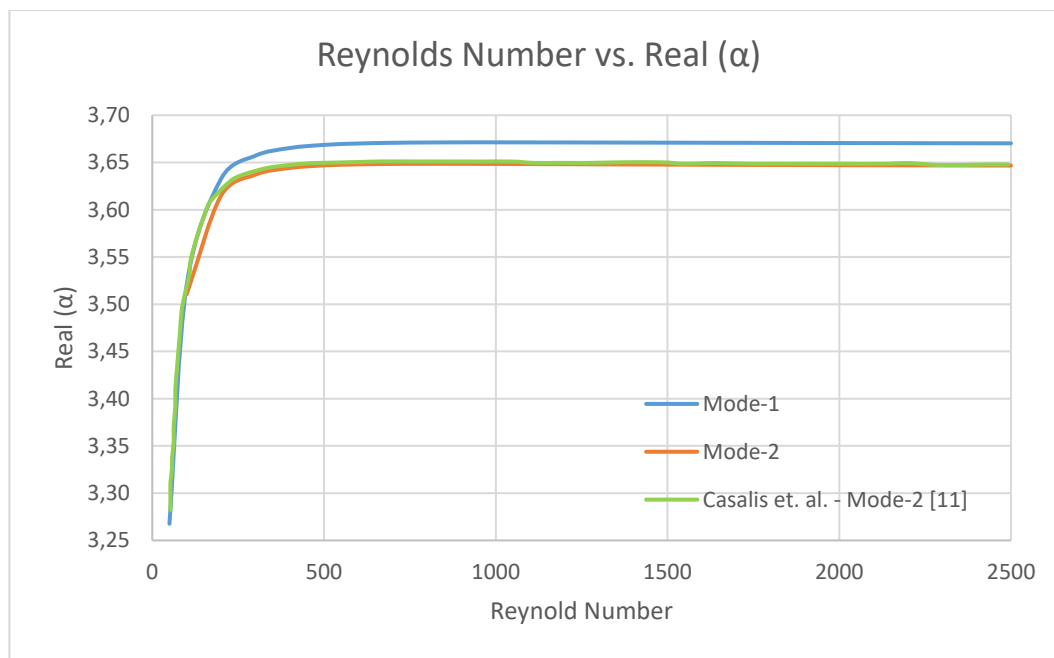
Figure 2.25. Change of Real Part of Complex Wavenumber
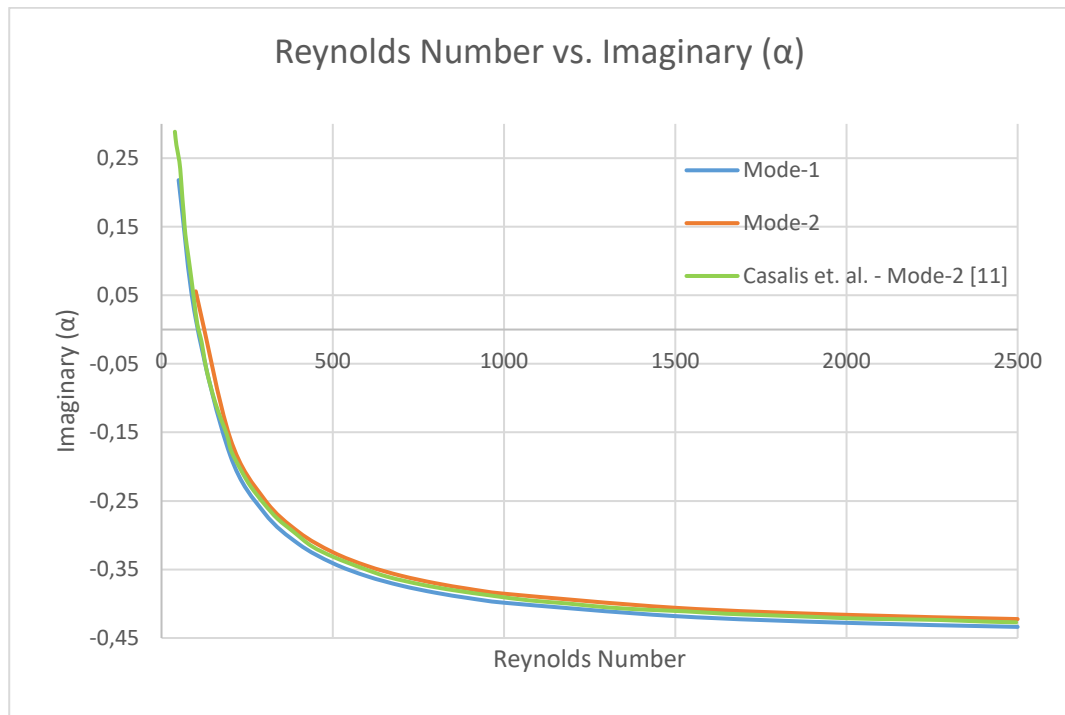
Figure 2.26. Change of Imaginary Part of Complex Wavenumber

The change in the tip of the neutral curve as Reynolds number is varied, in terms of the cirtical streamwise position, critical wavenumber and critical disturbance frequency is tracked. Those results can be seen in Figure 2.27-Figure 2.29. The tip of the neutral curve defined by the critical values of all three parameters one-by-one up to $Re \cong 300$, shows significant change while its effect decreases beyond $Re \cong 300$.
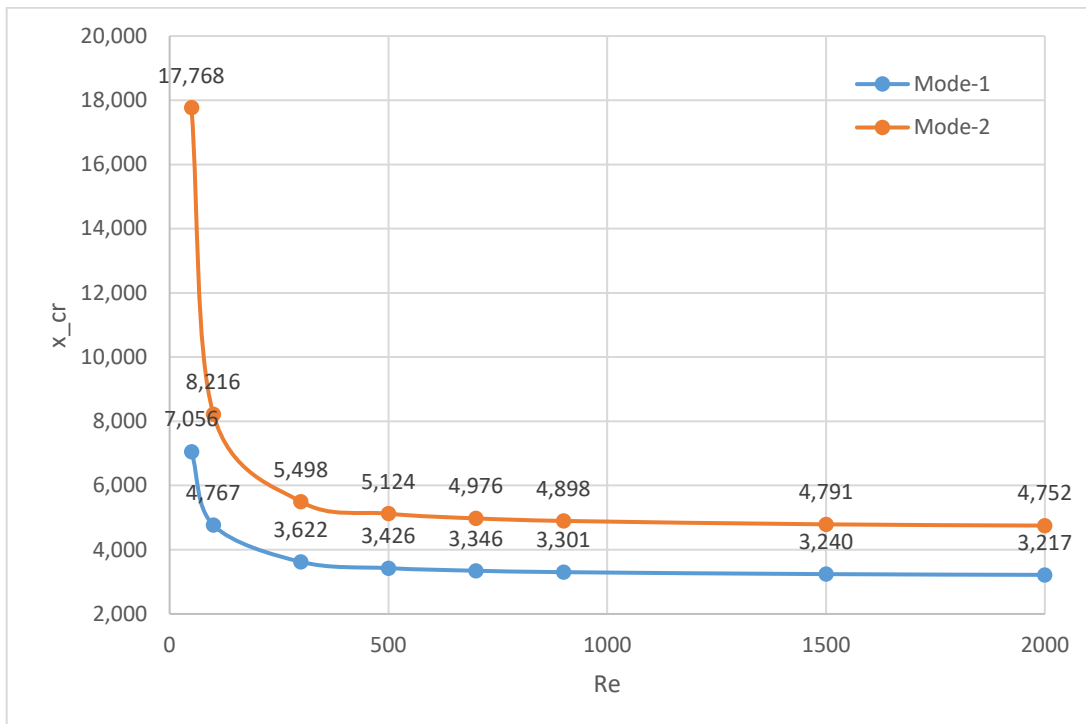
Figure 2.27. Change of the Tip of The Neutral Curve with Reynolds Number
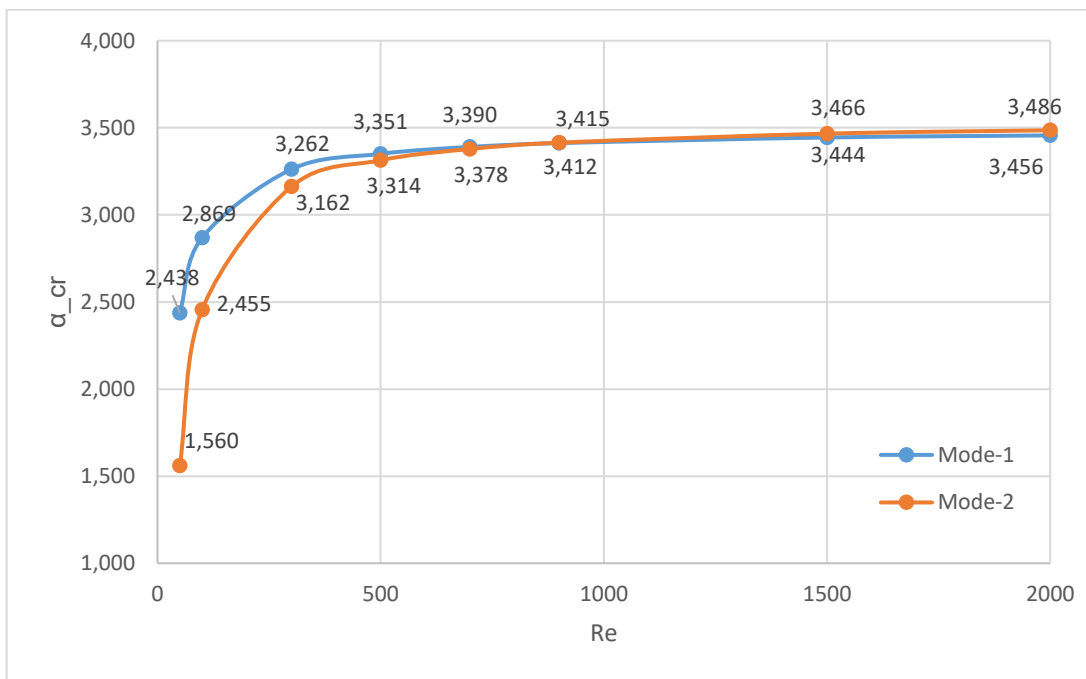
Figure 2.28. Change of the Critical Wavenumber with Reynolds Number

54
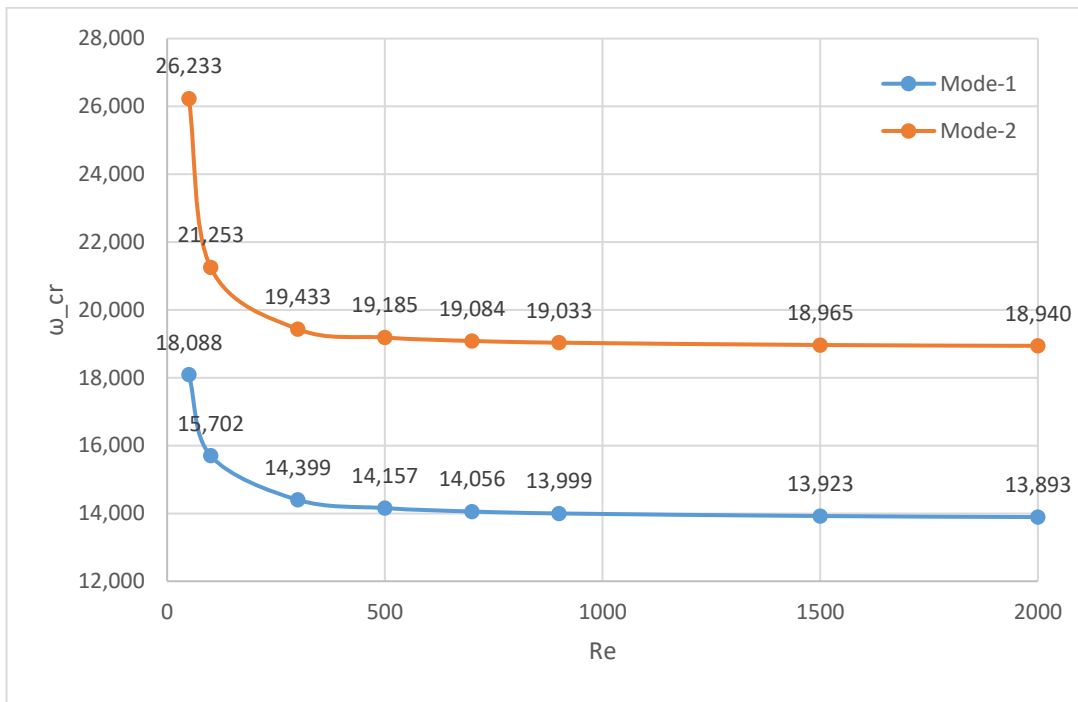
Figure 2.29. Change of the Critical Disturbance Frequency with Reynolds Number

CHAPTER 3

LINEAR STABILITY THEORY II: NON-LOCAL APPROACH

3.1. Parabolized Stability Equations

The parabolic stability equations (PSE) approach, takes into account the nonparallellity by assuming slow variation in the sreamwise direction x, thus eliminating second derivatives in x and ending up with parabolic equations to numerically solve them using an efficient marching scheme in the streamwise direction. PSE approach is relatively new that produces some satisfactory results concerning the stability analysis of weakly non-parallel flows such as boundary layers. In contrast to the local approach, PSE assumes the perturbation amplitudes are slowly varying functions of x while the main x-dependence is in the wavenumber in the exponential form that provides a proper spatial evolution of the modes as follows:

$$U = \bar{U}(x,y) + \hat{u}(x,y)e^{i\left[\int_{x_0}^{x} \alpha(X)dX - \omega t\right]} \tag{3.1a}$$

$$V = \bar{V}(x,y) + \hat{v}(x,y)e^{i\left[\int_{x_0}^{x} \alpha(X)dX - \omega t\right]} \tag{3.1b}$$

$$P = \bar{P}(x,y) + \hat{p}(x,y)e^{i\left[\int_{x_0}^{x} \alpha(X)dX - \omega t\right]} \tag{3.1c}$$

where x_0 is taken as the first x position where the mean flow is marginally stable, i.e. x_0 is the position at $\alpha_i \cong 0$. This decomposition is directly substituted into the Navier-Stokes equations with the boundary conditions as in (2.2) and (2.3).Then the resulting equations are simplified by linearization, the removal of the second derivatives of the perturbation amplitude functions and cancelling those terms associated with the equations that the mean flow satisfies. The derivations of the linear stability equations are given in Appendices.L, M and N, for continuity, x-momentum and y-momentum

equations, respectively. The resulting linear stability equations in the non-dimensional form are:

$$\frac{\partial \hat{u}^*}{\partial x^*} + i\alpha^* \hat{u}^* + \frac{\partial \hat{v}^*}{\partial y^*} = 0 \tag{3.2a}$$

$$-i\omega^* \hat{u}^* + \bar{U}^* \frac{\partial \hat{u}^*}{\partial x^*} + i\alpha^* \bar{U}^* \hat{u}^* + \hat{u}^* \frac{\partial \bar{U}^*}{\partial x^*} + \bar{V}^* \frac{\partial \hat{u}^*}{\partial y^*} + \hat{v}^* \frac{\partial \bar{U}^*}{\partial y^*} \tag{3.2b}$$

$$= -\left(\frac{\partial \hat{p}^*}{\partial x^*} + i\alpha^* \hat{p}^*\right) + \frac{1}{Re}\left(2i\alpha^* \frac{\partial \hat{u}^*}{\partial x^*} + i\hat{u}^* \frac{\partial \alpha^*}{\partial x} + \frac{\partial^2 \hat{u}^*}{\partial y^{*2}} - \alpha^{*2} \hat{u}^*\right)$$

$$-i\omega^* \hat{v}^* + \bar{U}^* \frac{\partial \hat{v}^*}{\partial x^*} + i\alpha^* \bar{U}^* \hat{v}^* + \bar{V}^* \frac{\partial \hat{v}^*}{\partial y^*} + \hat{v}^* \frac{\partial \bar{V}^*}{\partial y^*} \tag{3.2c}$$

$$= -\frac{\partial \hat{p}^*}{\partial y^*} + \frac{1}{Re}\left(2i\alpha^* \frac{\partial \hat{v}^*}{\partial x^*} + i\hat{v}^* \frac{\partial \alpha^*}{\partial x^*} - \alpha^{*2} \hat{v}^* + \frac{\partial^2 \hat{v}^*}{\partial y^{*2}}\right)$$

with the boundary conditions ,

$$\hat{u}^*(-1) = \hat{u}^*(1) = \hat{v}^*(-1) = \hat{v}^*(1) = 0 \tag{3.3}$$

As it was done earlier for the local approach, the similar reduction of equations (3.2) into a fourth order system is performed by introducing the streamfunction

$$\psi(x, y, t) = \varphi(x, y).\, e^{i\left(\int_{x_0}^{x} \alpha(X)dX - \omega t\right)} \tag{3.4a}$$

with the details in Appendix O yields the Parabolic Stability Equations: PSE. The non-dimensional form of the equation is written by removing asterisk for simplicity below.

$$\left\{\left[-i\omega \frac{\partial^2 \varphi}{\partial y^2} + i\alpha \bar{U} \frac{\partial^2 \varphi}{\partial y^2} + \frac{\partial \varphi}{\partial y}\frac{\partial^2 \bar{U}}{\partial x\,\partial y} + \bar{V}\frac{\partial^3 \varphi}{\partial y^3} - i\alpha\varphi \frac{\partial^2 \bar{U}}{\partial y^2}\right.\right. \tag{3.4b}$$

$$\left.\left. + i\omega\alpha^2\varphi - i\bar{U}\varphi\alpha^3 - \alpha^2\bar{V}\frac{\partial \varphi}{\partial y}\right] - \nu\left[-2\alpha^2 \frac{\partial^2 \varphi}{\partial y^2} + \frac{\partial^4 \varphi}{\partial y^4} + \varphi\alpha^4\right]\right\} + \left\{\left[\bar{U}\frac{\partial^3 \varphi}{\partial x\partial y^2}\right.\right.$$

$$-\frac{\partial^2 \bar{U}}{\partial y^2}\frac{\partial \varphi}{\partial x} + 2\alpha\omega\frac{\partial \varphi}{\partial x} - 3\alpha^2\bar{U}\frac{\partial \varphi}{\partial x} + 2i\bar{V}\alpha\frac{\partial^2 \varphi}{\partial x \partial y}\bigg] - v\bigg[4i\alpha\frac{\partial^3 \varphi}{\partial x \partial y^2} - 4i\alpha^3\frac{\partial \varphi}{\partial x}\bigg]\bigg\}$$

$$+\bigg\{\bigg[\omega\alpha'\varphi - 3\bar{U}\varphi\alpha\alpha' + i\alpha'\bar{V}\frac{\partial \varphi}{\partial y}\bigg] - v\bigg[i\alpha'\frac{\partial^2 \varphi}{\partial y^2} - 6i\varphi\alpha^2\alpha' + i\alpha'\frac{\partial^2 \varphi}{\partial y^2}\bigg]\bigg\}$$

or, written in operator form after non-dimensionalization process using the conversions given in section 2.3;

$$(L_0 + L_1)\varphi + L_2\frac{\partial \varphi}{\partial x} + \frac{d\alpha}{dx}L_3\varphi = 0 \tag{3.5}$$

where the operators L_i's that operate only on the wall-normal y variable are given by,

$$L_0 = -\frac{1}{Re}(D^2 - \alpha^2)^2 + (i\alpha\bar{U} - i\omega)(D^2 - \alpha^2) - i\alpha\frac{\partial^2 \bar{U}}{\partial y^2} \tag{3.6a}$$

$$L_1 = \frac{\partial^2 \bar{U}}{\partial x\, \partial y}D + \bar{V}(D^2 - \alpha^2)D \tag{3.6b}$$

$$L_2 = -\frac{4i\alpha}{Re}(D^2 - \alpha^2) + \bar{U}(D^2 - 3\alpha^2) + 2\alpha\omega - \frac{\partial^2 \bar{U}}{\partial y^2} + 2i\alpha\bar{V}D \tag{3.6c}$$

$$L_3 = -\frac{2i}{Re}(D^2 - 3\alpha^2) + \omega - 3\bar{U}\alpha + i\bar{V}D \tag{3.6d}$$

Here D denotes the differentiation in the y-variable and for simplicity, asterisk are removed from all of the variables.

It should be noted that the operator L_0 is in fact the Orr-Sommerfeld operator, while L_1 is the contribution of non-parallelism of the mean flow to the local approach, i.e. $L_0 + L_1$ is the operator associated with the Local-Nonparallel Approach (LNP). This is verified, because only this term survives under the LNP assumption that $\partial\varphi/\partial x = d\alpha/dx = 0$. At first sight, the equation (3.5) appears to be a linear initial-boundary-value problem to be solved for the amplitude φ, however, the existence of $d\alpha/dx$ term with α being unknown and appearing nonlinearly together with the operators,

59

$L_{0,1,2,3}$, is disturbing. The parabolic character of closely related equations has been mentioned by Gaster [28].

3.2. Normalization Condition

In order to resolve the ambiguity in x dependence of the streamfunction ψ that is partitioned between φ and α in (3.4a), and to maintain slow variation of the amplitude function φ, some additional normalization conditions are needed.

Herbert [51] suggested an integral norm that is both physically and mathematically meaningful. It is based on the equation

$$-i(ln\psi)_x = \alpha - i\frac{\varphi_x}{\varphi} \tag{3.7}$$

that can be obtained from (3.4a). In order to remove the dependence of (3.7) on y variable, it is multiplied with the weight $|\varphi|^2$ and integrated over the domain Ω in y to obtain

$$-i\frac{\int_\Omega |\varphi|^2 (ln\,\psi)_x\, dy}{\int_\Omega |\varphi|^2\, dy} = \alpha - i\frac{\int_\Omega \varphi^\dagger \varphi_x\, dy}{\int_\Omega |\varphi|^2\, dy} \tag{3.8}$$

where the superscript † denotes the complex conjugate. Then it is chosen to normalize φ,

$$\int_\Omega \varphi^\dagger \varphi_x\, dy = 0 \tag{3.9}$$

and (3.8) gives the definition of $\alpha(x)$ that will provide a numerical scheme to compute the wavenumber α iteratively in the next section. It should be noted that the normalization condition (3.9) minimizes the streamwise change in a weighted sense across the wall-normal direction y.

3.3. Marching Procedure

The procedure starts with a 1st order-accurate backward difference formula

$$(\varphi_x)_{j+1} \approx \frac{\varphi_{j+1} - \varphi_j}{\Delta x_j} \tag{3.10}$$

where j is the step index and $\varphi_j = \varphi_j(y) = \varphi(x_j, y)$ as recommended by Herbert [51] and Bertolotti [12] for the discretization in the x-direction. They also mention that 2nd order-accurate central differencing does not provide any better results. Due to the equation (3.5) being nonlinear in α, a predictor-corrector type approach is employed to get

$$\left[\Delta x_j \left(L_{0\,j+1}^n + L_{1\,j+1}^n \right) + L_{2\,j+1}^n + \left(\alpha_{j+1}^n - \alpha_j \right) L_{3\,j+1}^n \right] \varphi_{j+1}^n = L_{2\,j+1}^n \varphi_j \tag{3.11}$$

starting with $\varphi_j^0 = \varphi_j$ and $\alpha_j^0 = \alpha_j$ where $(\alpha_x)_{j+1}^n = \alpha_{j+1}^n - \alpha_j$ and superscript n counts the inner iteration while subscript j indicates the location on the x axis. Further, (3.9) and (3.10) are exploited to obtain an updated wavenumber using

$$\alpha_{j+1}^{n+1} = \alpha_{j+1}^n - \frac{2i}{\Delta x_j} \frac{\int_\Omega \left(\varphi_{j+1}^n \right)^\dagger \left(\varphi_{j+1}^n - \varphi_j \right) dy}{\int_\Omega \left| \varphi_{j+1}^n \right|^2 dy} \tag{3.12}$$

Equations (3.11) and (3.12) are solved simultaneously and the integration-update cycle is repeated until equation (3.9) is satisfied within a given error tolerance as a stopping criterion. After convergence to $\varphi_{j+1}(y)$ and α_{j+1} is obtained, we proceed to the next step in x where estimates are now available to continue the marching procedure.

3.4. Results

As it can be seen in (3.11) that Δx multiplies the operator associated with the LNP approach that is used to generate the initial guess. Therefore, as $\Delta x \to 0$, the contribution of this term to the resulting matrix gets smaller. The associated code written in MATLAB for the PSE is given in Appendix.P. It was observed after a few trials that for a smaller step size Δx results in solution that is not smooth. In selecting large Δx, however, the accuracy is expected to be poor. The trials showed that $\Delta x \cong 0.2$ provided satisfactory results in that sense.
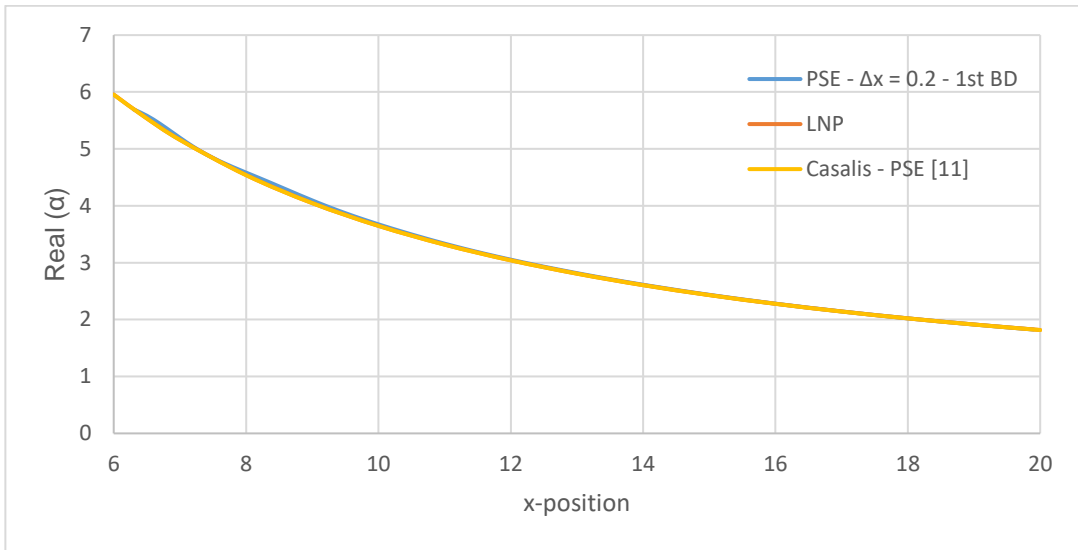
Figure 3.1. Change of Real Part of Wavenumber Along x
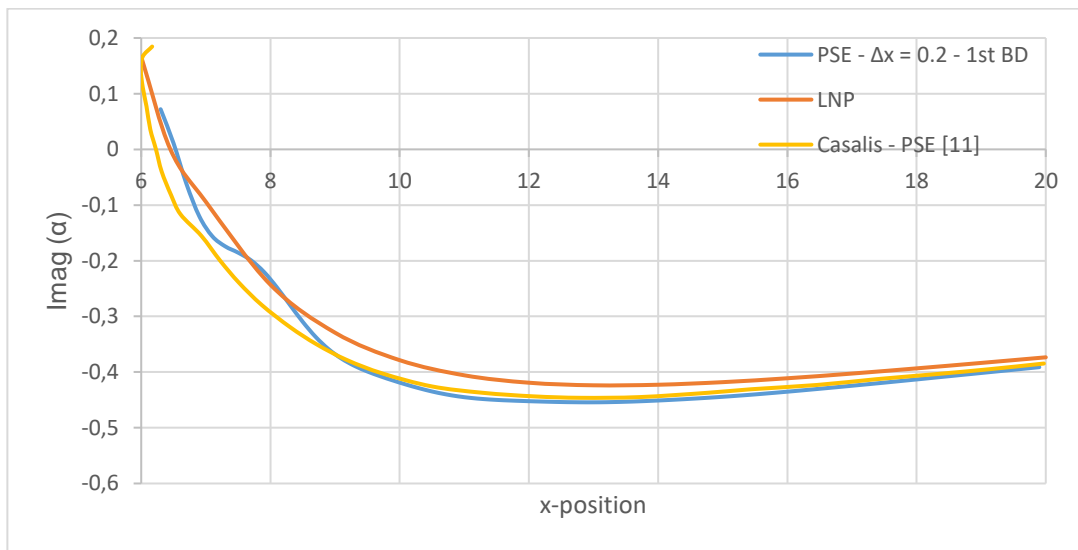
Figure 3.2. Change of Imaginary Part of Wavenumber Along x

As it can be seen from Figure 3.1, there is almost no difference between the solutions of LNP and PSE formulations in comparison to that of Casalis *et. al.* [11] , in the x-variation of the real part of the complex wavenumber. However, from Figure 3.2, it is

clear that there is a difference between the two formulations in the x-variation of the imaginary part of complex wavenumber. However, our solutions for imaginary part of complex wavenumber slightly differs from that in [11]. The possible reason again may be the discretization scheme in y-direction, namely, our Chebyshev collocation method versus the fourth-order finite difference scheme of [11].

Nevertheless, the trend in the x-variation of the real and imaginary parts of the complex wavenumber is captured satisfactorily. It should be noted that the streamwise position where imaginary part of the complex wavenumber crosses the axis and becomes negative signals the growth of the disturbances superimposed on the mean flow.

3.5. Comparison With The Experimental Data Provided By VECLA

VECLA is a half-channel experimental setup has been carried out at ONERA-Palaiseau. The main aim of it to provide velocity fluctuations for different frequencies at different streamwise locations. It has a length $L = 581\ mm$, a width $l = 60\ mm$, and an adjustable height h. The sketch of the experimental setup is given in Figure 3.3.
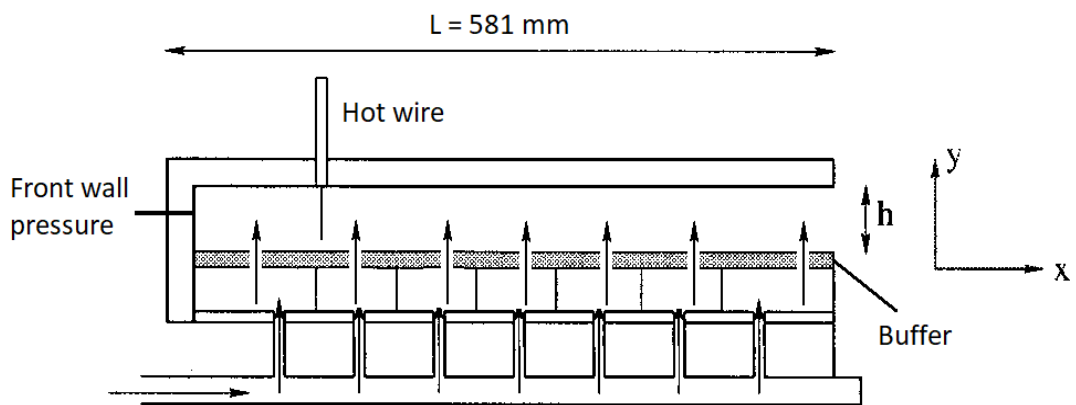
Figure 3.3. Set-up of VECLA Facility [11]

As it can be seen, VECLA facility has only one porous wall which is located at $y^* = -1$, while the top wall at $y^* = 0$ is assumed to correspond to a symmetry plane for the full channel represented in this thesis. This mean, the effect of top wall to the stability of the channel flow is neglected.

Casalis *et. al.* [11] compared their findings using the LNP approach for Mode-2 with the experimental measurements, and found proper initial disturbance amplitude, A_0, for different cases by considering the experimental results up to the threshold of the non-linear regime. The reason of the selection of Mode-2 is the symmetry considerations of u and the assumption that only Mode-2 takes place in this channel setup. In (2.12), the amplitude A of the disturbance relative to the initial disturbance A_0 at a streamwise position x is given by the *n factor* that is defined by:

$$n = -\int_{x_0}^{x} \alpha_i \, d\xi \qquad (3.13)$$

The initial amplitude of the disturbance, A_0, is assumed to be independent of the disturbance frequency and the half channel height, h, but dependent on the fluid injection speed, V_{inj}. Two of the cases studied in VECLA experimental setup are given below.

- **Case-1**
  Half channel height $(h) = 10$ mm , Injection speed $(V_{inj}) = 1.36 \; {}^{m}/_{s}$
  Reynolds number $(Re) = 900$, Acoustic wave frequency $(f) = 690$ Hz

- **Case-2**
  Half channel height $(h) = 10$ mm , Injection speed $(V_{inj}) = 1.70 \; {}^{m}/_{s}$
  Reynolds number $(Re) = 1125$, Acoustic wave frequency $(f) = 690$ Hz

The acoustic wave frequency of those cases are choosen because it is the most amplified one according to the stability theory and the experimental results of VECLA for the channel heights used.

3.5.1. Case-1

The comparisons are done for both local and non-local approaches using the MATLAB code developed. It was expected that as the unstable waves move downstream, the non-linear terms gain importance and the validity of the linear stability analysis is lost. Since, the current LNP and PSE approaches can model only the initial linear stages of transition , in order to find the initial disturbance amplitude, the results provided by VECLA test setup at $x = 8.1$ is used by simply dividing with the e^n value, obtained by local and non-local approaches. Integration process to find the *n factor* defined in (3.13) is performed manually for the LNP approach, while it is done automatically by the code for the PSE approach. The x-variation of the imaginary part of the complex wavenumber computed by using the LNP approach for Case-1 is shown in Figure 3.4.
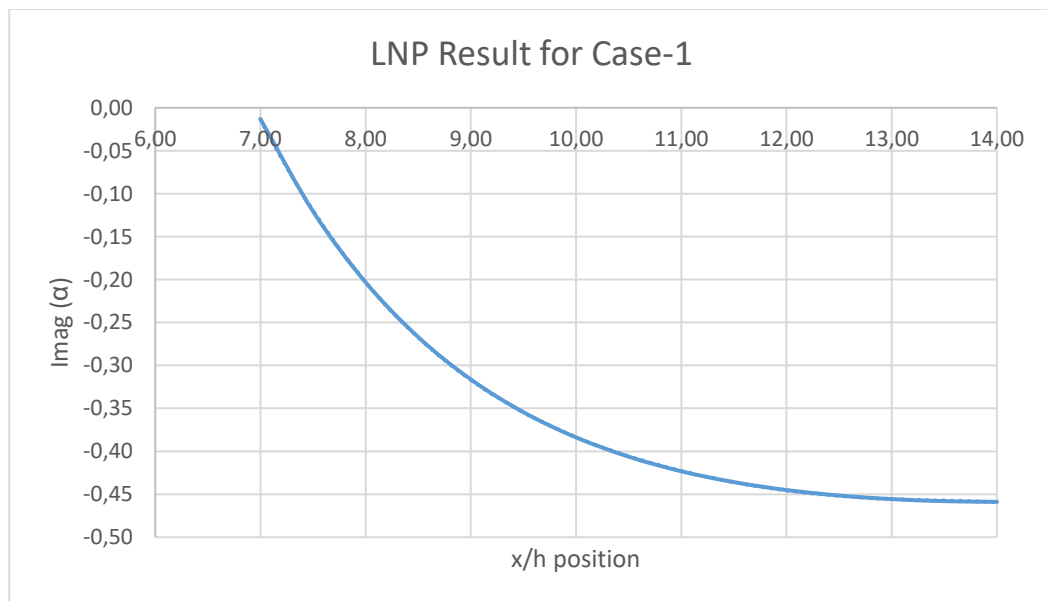
Figure 3.4. Change of Imaginary Part of Complex Wavenumber for Case-1

The x-variation of the imaginary part of the wavenumber is fitted by the polynomial:

$$\alpha_i \cong -0.873.\,10^{-5}\,x^6 + 0.5227.\,10^{-3}\,x^5 - 0.12581.\,10^{-1}\,x^4 \qquad (3.14)$$

$$+0.152522\,x^3 - 0.93174\,x^2 + 2.25355\,x$$

It should be noted that a numerical integration process for computing n-factor can be also preferred instead of using algebraic integration as performed in this thesis. After the integration process, the amplitude of the disturbance at each streamwise position can be found by multiplying it with initial disturbance amplitude. The initial disturbance amplitudes that satisfy the results of VECLA at $x = 8.1$ for LNP and PSE cases are shown below:

$$A_{0_{LNP}} \cong 1/500 \ m/s$$

$$A_{0_{PSE}} \cong 1/450 \ m/s$$

Fortunately, Casalis *et. al.* [11] found the initial disturbance amplitude for LNP approach to be approximately $1/500 \ m/s$, and used it to calculate all disturbance amplitudes along the streamwise direction, i.e. the change of fluctuating streamwise velocity is foreseen. The comparison of the numerical and the experimental test results are shown in Figure 3.5.
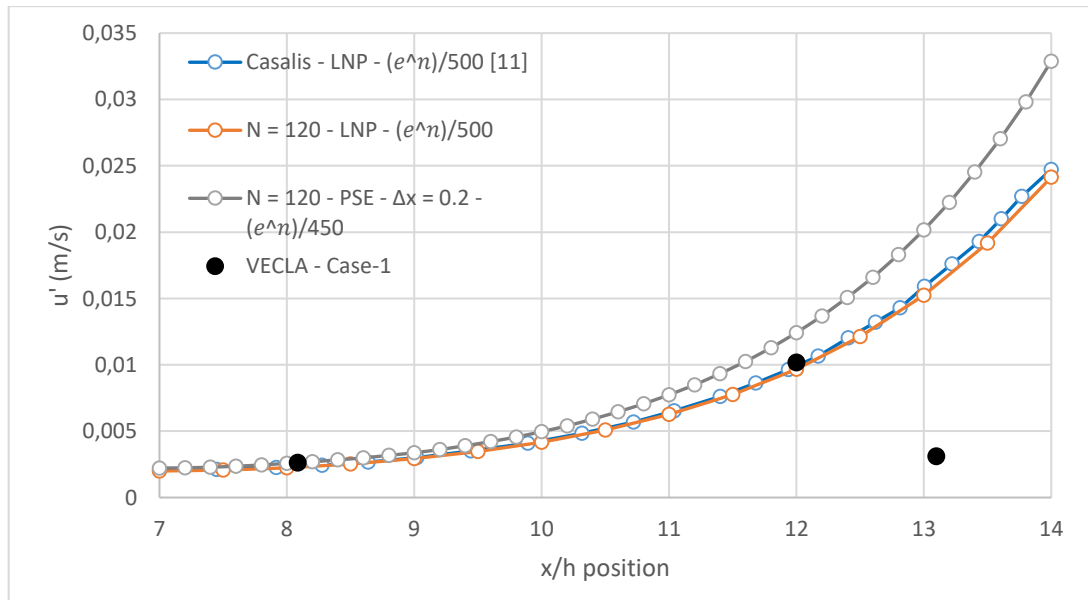
Figure 3.5. Fluctuating Streamwise Velocity – Case-1

3.5.2. Case-2

Similarly for Case-2, and both LNP and PSE results are compared with the experimental data. For the given channel height, injection speed, Reynolds number and acoustic disturbances frequency, the imaginary part of the complex wavenumber that indicates the growth of disturbances in streamwise x-direction is computed using the local approach (LNP).
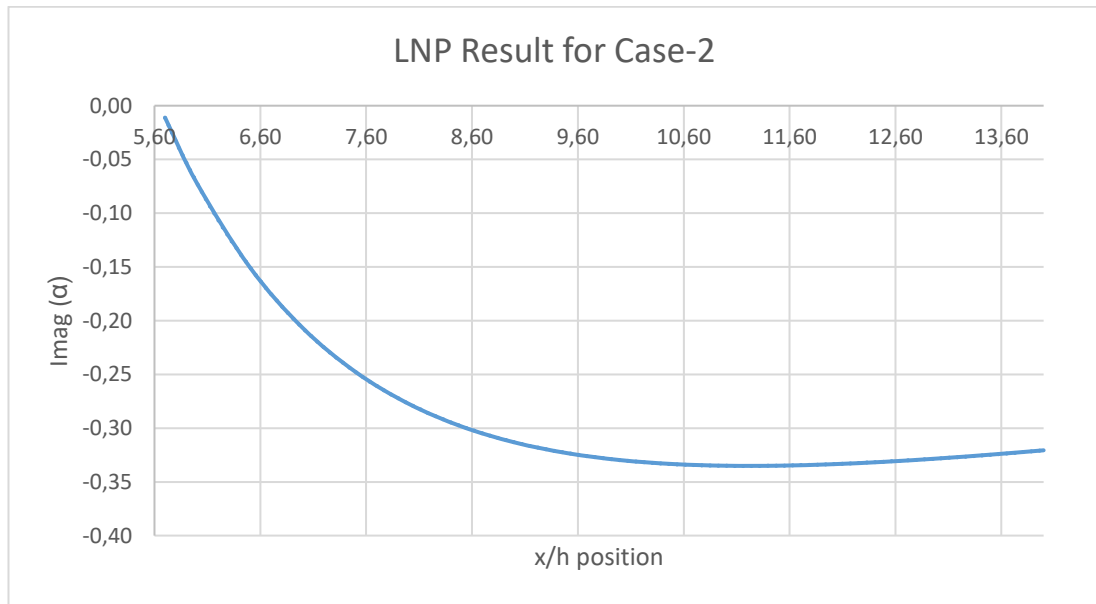
Figure 3.6. Change of Imaginary Part of Complex Wavenumber for Case-2

The x-variation of the imaginary part of the wavenumber is again fitted by a polynomial to obtain:

$$\alpha_i \cong 0.36.\,10^{-5}\,x^6 - 0.2426.\,10^{-3}\,x^5 + \, 0.68424.\,10^{-2}\,x^4 \qquad (3.15)$$

$$-0.104044\,x^3 + 0.906941\,x^2 - 4.33768\,x + 8.628442$$

After the integration process, the amplitude of the disturbance at each streamwise position can be found by multiplying it with initial disturbance amplitude. As mentioned before, the initial disturbance amplitude, A_0, is assumed to be only the function of the injection velocity. Therefore, the initial disturbance amplitudes of

Case-1 and Case-2 are different from each other. The initial disturbance amplitude that satisfies the results of VECLA at $x = 8.1$ for LNP and PSE cases are shown below:

$$A_{0_{LNP}} \cong 1/200 \ m/s$$

$$A_{0_{PSE}} \cong 1/180 \ m/s$$
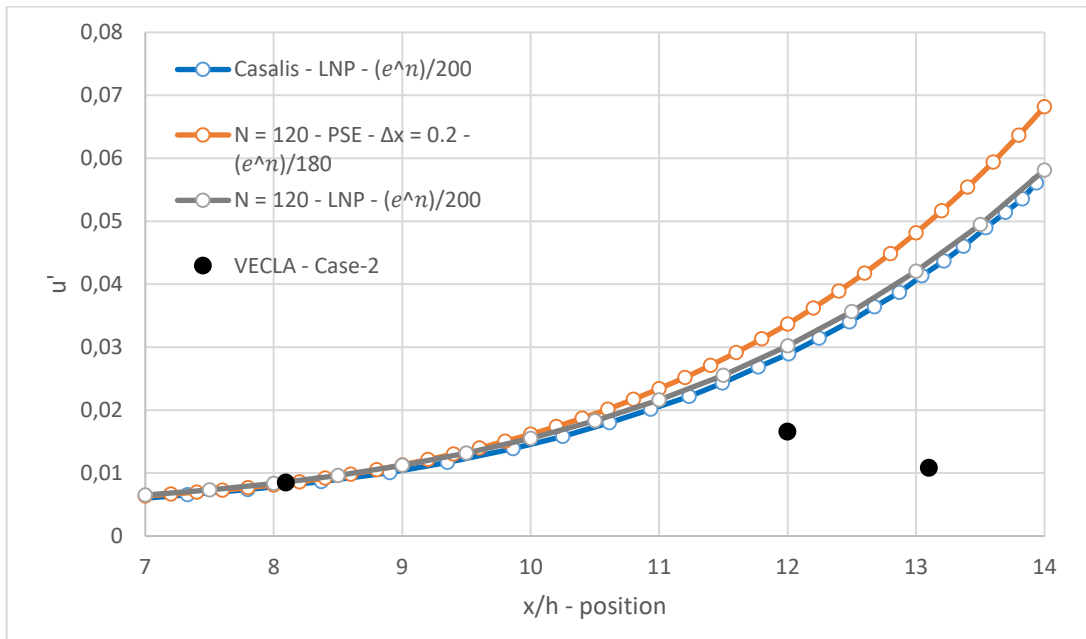
Figure 3.7. Fluctuating Streamwise Velocity – Case-2

It should be noted that both LNP and PSE are linear models, thus, the dominant non-linear effects beyond a certain streamwise position cannot be predicted. According to the results given in Figure 3.5 and Figure 3.7, $x/h \cong 12$ distance from the front wall situated at $x = 0$, seems to correspond more or less to the appearance of the non-linear behavior of the disturbances.

The typical picture in the nonlinear regime then develops as follows: If the frequency of the most amplified wave does not correspond to the acoustic frequency, the flow becomes three-dimensional, turbulent spots occur and then break down into

68

turbulence. Consequently, the amplitude of the acoustic fluctuations falls. On the other hand, if the frequency of the most amplified wave coincides with the acoustic frequency of any mode, then the pressure fluctuations will grow to form coherent large structures that will eventually lead SPRM to become unstable and fail [11]. It should be underlined that the effect of the top wall on the stability of the steady mean flow is negleglected, which can be deceiving for the judgement on a flow stability.

CHAPTER 4

CONCLUSIONS

Instability developing in a boundary layer is one of the least understood topic in fluid mechanics research. To foresee the possible instabilities and provide satisfactory remedies are crucial for industrial flows, especially in the design process of airplanes, ships, rocket motors, submarines, etc. In order to make some predictions on the transition from laminar to turbulent flow, it is crucial to start with studying the instabilities of a boundary layer, since it is a common feature in all wall-bounded flows. Even though there are many approaches and models geared towards predicting the transition phenomena, such as energy considerations, Reynolds stress models and Direct Numerical Simulation, hydrodynamic stability theory is considered to be the most sophisticated and efficient, in terms of insight, accuracy and computation power requirements.

- In the current study, the main aim is to investigate linear stability of a wall-bounded planar flow with porous injection through the bounding walls. It is intended to be a simple representation of a solid propellant rocket motor (SPRM). The complicating influences such as surface geometry, wall roughness, environment sound, heat transfer, ablation and compressibility are not taken into account. The source of the initial disturbance is thought to be the acoustic modes of the geometry, which is the function of channel length, channel height and speed of sound inside the channel. In oder to predict the instabilities until the non-linear regime dominates , the following steps are followed:

- The mean flow is computed for a planar channel flow with porous flow injection,

- Local stability approach is formulated and coded to investigate the spatial stability of the flow,

- Local stability analysis is used as *a priori* for the non-local approach. Parabolized stability equations (PSE) are derived, discretized and numerically solved by a code developed .

In order to validate the code written in MATLAB, Orr-Sommerfeld problem solved by Orszag [17] using a spectral method is taken as the benchmark solution and our code is validated to work correctly for OSE approach. However, for the flow configuration in focus, Orr-Sommerfeld approach is known to give unsatisfactory results in the sense of predicting the instability of the flow, since non-parallel effects play important role in the prediction.

Mesh independency study is performed for both OSE and LNP approaches. Although Chebyshev collocation method used to obtain the numerical solution is a high-order method providing exponential order of accuracy, it is known to introduce ill-conditioning with increasing resolution. Moreover, the eigenvalue solvers are known to produce poor accuracy for the intermediate eigenvalues as the degrees of freedom increases. Therefore, a careful mesh independence study is required to be performed in validating the stability spectrum computations.

The other local approach that takes non-parallelism of the basic flow into account, namely, LNP approach is performed next. The results obtained using our Chebyshev collocation code are validated against those from the literature that uses a fourth-order accurate finite difference scheme. We have found two unstable modes for given some parameter values that are classified in accordance with the inherent symmetries as Mode-1 and Mode-2. These results are in agreement with the literature, however, some discrepancies are observed in the tip of the neutral curve that is interpreted likely to be caused as a result of the differences in the numerical schemes used. The effect of Reynolds number on various critical parameter values, such as the complex

wavenumber and disturbance frequency, is shown to be negligible after a certain value of Reynolds number .

The assumption that disturbances are slowly varying in the streamwise direction x due to the slow variation of the mean flow justifies neglecting second order derivatives and the products of the first order derivatives in x, leads to parabolic stability equations (PSE), and allows an efficient marching scheme for numerical solution in the streamwise direction as developed by Herbert [43].

In order to ensure that the amplitude of the disturbances exhibit slow variation in the streamwise direction , an additional normalization condition is required. There have been various suggestions in literature on a proper normalization condition [11], however, the integral norm suggested by Bertolotti [12] and Herbert [51] as physically and mathematically meaningful is used in this work. They also suggested that using higher order-accurate differencing for marching in the streamwise direction is unnecessary. Thus, 1st order-accurate backward differencing method is used in the discretization in the streamwise direction in this work.

PSE is derived for the disturbance streamfunction can be organized into four operators, as expected, the two of the operators are those from the local approach, i.e. those two operators together constitute the LNP approach, which provides the initial guess for the PSE approach. After discretization for the marching procedure, the marching step size appears as a multiplier in front of those local operators. After a few numerical trials, it is observed that as marching step size decreases, the solution becomes wiggly lacking smoothness. The same phenomena is also observed for 2nd order-accurate backward difference scheme as a test case, with even greater lack of smoothness in the numerical solution curves for x-variation of the imaginary part of the complex wavenumber. After some experimentation to obtain smoother curves, the marching step size, $\Delta x = 0.2$, is observed to provide more satisfactory results .

It was observed that the local and non-local approaches do not produce any significant difference as far as the x-variation of the real part of the wavenumber is

73

concerned, however the imaginary part is slightly affected by the two approaches in agreement with the literature.

Furthermore, the streamwise component of the disturbance velocity is compared with the experimental results obtained using the VECLA test setup in literature. It is observed that for a given disturbance (acoustic) frequency, nonlinearity becomes dominant beyond a streamwise position and the results beyond that position are not reliable because of the current linear stability approach. As a typical picture in the nonlinear regime, if the most amplified waves do not correspond to the acoustic frequency, the flow may become three-dimensional, turbulent spots occur and then break down into turbulence. In this case, amplitude of the acoustic fluctuations fall. On the other hand, if the frequency of the most amplified wave coincides with acoustic frequency of any mode, then the pressure fluctuations will be higher leading to catastrophic failure.

4.1. Recommendation for Improvement and Future Work

Recommendations for improvement and possible future work are given below:

- For a more realistic investigation of the stability of an SPRM, it may be better to use an axisymmetric geometry.
- Linear stability theory gives reliable results only up to the non-linearities become important. In order to investigate the nonlinear transition processes and obtain more reliable results, nonlinear stability analysis, utilizing, for example, non-linear parabolized stability equations (NPSE) approach should be used.
- A graphical user interface (GUI) may be developed to make the codes more user-friendly.
- Reynolds number range studied in this thesis is considerably low. However, combustion products with low viscosity results with higher Reynolds numbers.
- In a subsonic combustion chamber, let's say inside a SPRM, temperatures can reach up to 4000 K and flow can be considered isothermal. Density, which is

a function of temperature, can be assumed constant in a combustion chamber of a SPRM. Therefore, compressibility is not necessarily taken into account.

- Compressibility of the flow is not needed to be taken into consideration for an SPRM combustion chamber since Mach number in the chamber is below 0.3. However, heat transfer, ablation and roughness of the solid propellant surface should be taken into consideration that may make a difference.

REFERENCES

[1]Culick, F.E.C. 2002. Combustion Instabilities in Solid Rocket Motors, Notes for Two-Lectures given as part of the special course "Internal Aerodynamics in Solid Rocket Propulsion" - Von Karman Institute

[2] Vuillot, F. Vortex-Shedding Phenomena in Solid Rocket Motors, Journal of Propulsion and Power

[3] Rossiter, J.E. 1962. The Effect of Cavities on the Buffeting of Aircraft, Royal Aircraft Establishment – Technical Memo

[4] Ferretti, V. Numerical Simulation of Acoustic Resonance of Solid Rocket Motor, Sapienza, University of Rome, Ph.D Thesis

[5] Blomshield, F. S. 2006. Lessons Learned In Solid Rocket Combustion Instability, AIAA-Missile Sciences Conference

[6] Sirignano, W. A. 2015. Driving Mechanisms for Combustion Instability, Taylor & Francis- Combustion Science and Technology

[7] Malhotra, S. and Flandro, G.A. 1997. The Origin of the DC Shifts, AIAA

[8] Flandro, G.A. 1995. Effects of Vorticity on Rocket Combustion Stability, AIAA-Journal of Propulsion and Power

[9] Groot, K. 2013. Error Free Derivation of Parabolized Stability Equations, Von Karman Institute – Technical Internship Report

[10] Schlichting, H. 1951. Boundary Layer Theory, McGraw-Hill

[11] Casalis, G., Avalon, G. and Pineau, J.-P. 1998. Spatial Instability of Planar Channel Flow With Fluid Injection Through Porous Walls, Physics Of Fluids – Vol.10, No.10

[12] Bertolotti, F.P. 1991. Linear and Nonlinear Stability of Boundary Layers With Streamwise Varying Properties, Ph.D Thesis - Ohio State University

[13] Reshotko, E. 1969. Boundary Layer Stability and Transition, Conference on Boundary Layer Concepts in Fluid Mechanics – University of Massachusetts

[14] Weideman, J.A.C. and Reddy, S.C. 2000. A MATLAB Differentiation Matrix Suite, ACM Transactions on Mathematical Software, Vol. 26, No. 4

[15] Özgen, S. 1999. Two-Layer Flow Stability in Newtonian and Non-Newtonian Fluids, Ph.D Thesis, Von Karman Institute for Fluid Dynamics and Universite Libre de Bruxelles

[16] Higgins, B. G. and Binous, H. 2014. Derivation of the Linear Stability Equations for Rectilinear Flow in a 2-D Channel using Mathematica

[17] Orszag, S.A. 1971. Accurate Solution of the Orr-Sommerfeld stability equation, J. Fluid Mechanics, 50, pp. 689-703

[18] Drazin, P.G. and Reid, W.H. 1981. Hydrodynamic Stability, Cambridge University Press

[19] Prandtl, L. 1904. Über Flüssigkeitsbewegung bei sehr kleiner Reibung, Verhandl, 3rd Intern. Math. Kongr., Heidelberg, 484-491

[20] Prandtl, L. 1914. Über den Luftwiderstand von Kugeln, Göttingen Nachrichten, 177

[21] White, F.M. 2006. Viscous Fluid Flow, *3rd Edition*, McGraw-Hill

[22] Reynolds, O. 1895. On the experimental investigation of the circumstances which determine whether the motion of water shall be direct or sinuous, and the law of resistance in parallel channels, Phil. Trans. Roy. Soc. A 186, 123-164; see also Coll. Papers *II*.

[23] Malik, M.R. and Hussaini, M.Y. 1992. "Accurate numerical solution of compressible, linear stability equations", J. Appl. Math. Phys. 33, 189

[24] Grosch, C.E. and Salwen, H. 1968. The stability of steady and time-dependent plane Poiseuille flow, J. Fluid Mech. 34, 177-205

[25] Gallagher, A.P. and Mercer, A. McD. 1962. On the behaviour of small disturbances in plane Couette flow, J. Fluid Mech. 13, 91-100

[26] Dolph, C.L. and Lewis, D.C. 1958. On the application of infinite systems of ordinary differential equations to perturbations of plane Poiseuille flow, Quart. Appl. Math. 16, 97-110

[27] Rotta, J. 1956. Experimenteller Beitrag zur Entstehung turbulenter Strömmung im Rohr -Ing. Arch. 24, 258-281

[28] Gaster, M. 1974. On the effects of boundary-layer growth on flow stability, J. Fluid Mech., Vol. 66, pp. 465-480

[29] Eiffel, G. 1912. Sur la resistance des spheres dans l'air en monvement, Comptes Rendus 155, 1597 – 1599

[30] Schubauer, G.B. and Klebanoff, P.S. 1955. Contributions on the mechanisms of boundary layer transition, NACA TN 3489 and NACA Rep. 1289 (1956); see also Proc. Symposium on Boundary Layer Theory, NPL, England, 1955

[31] Lorentz, H.A. 1907. "Abhandlung über theoretische Physik I", 43-71, Leibzig; new version of earlier paper: Akad. v. Wet. Amsterdam 6, 28 (1897); see also Prandtl, L. The mechanisms of viscous fluids, in Durand, W.F. 1935. Aerodynamic Theory III. 34-208

[32] Joseph, D.D. 1976. Stability of Fluid Motions Vol. I-II, Springer Tracts in Natural Philosophy

[33] Squire, H.B. 1933. On the stability of three-dimensional distribution of viscous fluid between parallel walls, Proc. Roy. Soc. London A 142, 621-628

[34] Lord Rayleigh, 1880. On the stability of certain fluid motions, Proc. Math. Soc. London 11, 57 and 19, 67 (1887); Scientific Papers I, 474-487 and III, 17; see also Scientific Papers IV, 203 (1895) and VI, 197 (1913)

[35] Gaster, M. 1962. A note on a relation between temporally increasing and spatially increasing disturbances in hydrodynamic stability, J. Fluid Mech., 14, 222-224

[36] Reshotko, E. 1969. Boundary layer stability and transition, Conference on Boundary Layer Concepts in Fluid Mechanics

[37] Dunn, D.W. and Lin, C.C. 1955. "On the stability of the laminar boundary layer in a compressible fluid", J. Aero. Sci., 22, 455-477

[38] Owen, P.R. and Randall, D.G. 1953 Boundary layer transition on a swept back wing: a further investigation, Rep. Aero 330, British Rae.

[39] Gregory, N., Stuart, J.T. and Walker, W.S. 1955. On the stability of three dimensional boundary layers with application to the flow due to a rotating disk, Phil. Trans. Roy. Soc., London, Ser. A, 248, 155-159

[40] Moore, F.K. 1956. Three-dimensional boundary layer theory, In Kuerti, C. ed.: Advances in applied mechanics, IV, 159-228

[41] Reshotko, E. 1962. Stability of three-dimensional compressible boundary layers, NASA TN D-1220

[42] Prandtl, L. 1921. Bemerkungen Über die Entstehung der Turbulenz, Z.A.M.M., 1, 431-436

[43] Herbert, T. 1980. Nonlinear stability of parallel flows by high-order amplitude expansions, AIAA J., 18, 3

[44] Saric, W.S. and Nayfeh, A.H. 1975. Nonparallel stability of boundary-layer flows, Phys. Fluids, 18

[45] Drazin, A.P. and Reid, A.W. 1981. Hydrodynamic Stability, Cambridge University Press

[46] Morovkin, M.V. 1969. On the many faces of transition, Viscous Drag Reduction, ed: C.S. Wells, Plenum

[47] Griffond, J., Casalis, G. and Pineau, J.-P. 2000. Spatial instability of flow in a semiinfinite cylinder with fluid injection through its porous walls, Eur. J. Mech. B – Fluids 19, 69-87

[48] Boyer, G., Casalis, G. and Estivalezes, J.-L. 2013. Stability analysis and numerical simulation of simplified solid rocket motors, Phys. Fluids 25

[49] Majdalani, J. and Flandro, G. 2002. Oscillatory pipe flow with arbitrary wall injection, Proc. R. Soc. Lond. A. 458

[50] Varapaev, V.N. and Yagodkin, V.I. 1969. Flow stability in a channel with porous wall, Izv. Akad. Nauk SSSR, Mekh. Zhidk. Gaza 4 (5), 91

[51] Herbert, T. 1993. Parabolized stability equations, AGARD-VKI Special Course on 'Progress in Transition Modeling

[52] Saric, W.S. 1993. Physical description of boundary-layer transition: Experimental evidence, AGARD-VKI Special Course on 'Progress in Transition Modeling

[53] Arnal, D. 1993. Boundary layer transition: Predictions based on linear theory, AGARD-VKI Special Course on 'Progress in Transition Modeling'

[54] Cowley, S.J. and Wu, X. 1993. Asymptotic approaches to transition modelling, AGARD-VKI Special Course on 'Progress in Transition Modeling

[55] Reed, H.L. 1993. Direct numerical simulation of transition: The spatial approach, AGARD-VKI Special Course on 'Progress in Transition Modeling'

[56] Schubauer, G.B. and Skramstad H.K. 1947. Laminar boundary-layer oscillations and transition on a flat plate, J. Res. Nat. Bur. Stand., 38.

[57] Bouthier, M. 1972. Stabilite lineaire des ecoulements Presque paralelles. J. Mecanieque, 11.

[58] Bouthier, M. 1973. Stabilite lineaire des ecoulements Presque paralelles: Partie ii. la couche limite de Blasius . J. Mecanieque, 12.

[59] Tarman, H.I., Hydrodynamic instability, vortex dynamics and turbulence, Lecture Notes

[60] Fasel, H.F. 1976. Investigation of the stability of boundary layers by a finite difference model of the Navier-Stokes equations, J. Fluid. Mech., 78,355

[61] Patera, A.T. 1984. Spectral methods for spatially evolving hydrodynamic flows, in Spectral Methods for Partial Differential Equations, 239-256, SIAM

[62] Patera, A.T. 1984. A spectral element method for fluid dynamics; laminar flow in a channel expansion, J. Comp. Phys., 54, 468

[63] Karniadakis, G.E., Bullister, E.T. and Patera, A.T. 1985. A spectral element method for solution of two and three dimensional time dependent Navier-Stokes equations, Proceedings of the Europe-U.S. Conference on Finite Element Methods for Nonlinear Problems, 803

[64] Maday, Y. and Patera, A.T. 1987. Spectral element methods for the Navier-Stokes equations, State-of-the-Art Surveys in Computational Mechanics

[65] Karniadakis, G.E. 1989. Spectral element simulations of laminar and turbulent flows in complex geometries, Applied Numerical Mathematics 6, 85

[66] Karniadakis, G.E. 1990. Spectral element-Fourier methods for incompressible turbulent flows, Computer Methods in Applied Mechanics and Engineering 80, 367.

[67] Fischer, P.F. and Patera, A.T. 1991. Parallel spectral element solution of the Stokes problem, J. Comp. Phys 92, 2, 380

[68] Danabasoglu, G. 1992. Spatial simulation of transition in wall-bounded shear flows: active control and effects of surface roughness. Ph.D Thesis, Aerospace Engineering Sciences, University of Colorado Bounder

[69] Danabasoglu, G., Biringen, S. and Streett, C.L. 1990. Numerical simulation of spatially-evolving instability, Instability and Transition I & II, Springer-Verlag

[70] Danabasoglu, G., Biringen, S. and Streett, C.L. 1991. Numerical simulation of spatially evolving instability in plane channel flow, AIAA-91-0234

[71] Danabasoglu, G., Biringen, S. and Streett, C.L. 1991. Spatial simulation of instability control by periodic suction blowing, Phys. Fluids A 3, 2183

[72] Danabasoglu, G., Biringen, S. and Streett, C.L. 1992. Application of spectral multidomain method to Navier-Stokes equations, Submitted for publication

[73] Danabasoglu, G., Biringen, S. and Streett, C.L. 1993. Spatial simulation of boundary layer instability: effects of surface roughness, AIAA-93-0075

84

[74] Singer, B.A. 1993. Modeling the transition region, AGARD-VKI Special Course on 'Progress in Transition Modeling

APPENDICES

A. Chebyshev Collocation Method for Chebyshev Gauss-Lobatto Grid in Barycentric Form

Chebyshev-Gauss-Lobatto grid points for $y \in [-1, 1]$ are calculated for as;

$$x_j = cos\left(\frac{\pi.j}{N}\right) \quad , \quad j = 0,1,2, \dots, N$$

where N is the number of degrees of freedom in the expansion.

Associated differentiation matrices are obtained using the barycentric form in chebdif.m in [14] that is known to be a more stable algorithm;

Barycentric interpolation is obtained by modifying the Lagrange interpolation algorithm toward more efficient implementation as follows:

$$L_j(x) = L(x)\frac{w_j}{x - x_j}$$

where

$$L(x) = (x - x_0)(x - x_1) \dots (x - x_N)$$

and the barycentric weights which are precomputed

$$w_j = \left[\prod_{k=0,k\neq j}^{N} (x_j - x_k)\right]^{-1} = (-1)^j \alpha_j$$

for Chebyshev - Gauss – Lobatto grid where

$$\alpha_j = \begin{cases} 1/2 & j = 0, N \\ 1 & otherwise \end{cases}$$

Interpolation for the barycentric form can be written as follows;

$$I_N u(x) = L(x) \sum_{j=0}^{N} \frac{w_j}{x - x_j} u(x_j) = \left[\sum_{j=0}^{N} \frac{w_j}{x - x_j} u(x_j) \right] \Bigg/ \left[\sum_{j=0}^{N} \frac{w_j}{x - x_j} \right]$$

$$\approx u_N(x)$$

The elements of nodal differentiation matrix can be computed as follows

$$D_{k,j\,,k \ne j} = \frac{w_j}{w_k} \frac{1}{x_k - x_j} \quad , \quad D_{k,k} = -\sum_{j=0,j \ne k}^{N} D_{k,j}$$

The differentiation matrices for higher order derivatives, m, is calculated using a recursive procedure in chebdif.m.

B. Calculation of Mean (Base) Flow

```matlab
% -------------------------- MEAN FLOW SOLVER --------------------------
% ------------ Solves the 1D equation F'F'' - FF''' = (1/Re)F'''' ---------
% ---------- with BCs ; F(-1) = -1 , F(1) = 1 , F'(-1) = F'(1) = 0 -------

clear all
clc
close all

global DM1 DM2 DM3 DM4 N Re

Nspan = 120;          % Degree of Chebyshev polinomials
M = 4;                % Maximum degree of the derivative in the equation

options = optimset('MaxFunEvals', 1e10, 'TolFun', 1e-15, 'MaxIter', 1000);
x = 0:0.001:20;
xx = 0:2:20;              % Introduced only for plotting purposes

%Re = H*Vinj/Nu;
Re= 900;                  % Reynolds Number

for i = 1:length(Nspan)

  N = Nspan(i)
  [D,y] = cheb(N);        % Function that generates Chebyshev polynomial
                          basis, differentiation matrices and Chebyshev
                          Collocation grids

  DM = barycdiffm(y,M);   % Barycentric form of the differentiation matrices
                          with respect to Chebyshev Collocation grid points

  DM1 = DM(:,:,1);        % First differentiation matrix (D)
  DM2 = DM(:,:,2);        % Second differentiation matrix (D^2)
  DM3 = DM(:,:,3);        % Third differentiation matrix (D^3)
  DM4 = DM(:,:,4);        % Fourth differentiation matrix (D^4)

% f is initialized according to Taylor's mean flow profile for inviscid flows

  f_init = sin(pi * y / 2);
  f_new = fsolve(@meanflow2d, f_init, options);    % Details of @meanflow2d
                                                   is given in the very end
                                                   of Appendix.B

  f_prime = DM1 * f_new;
  for j = 1:length(x)
      u_mean(:,j) = x(j) * f_prime(:);        % U = x * f'
      v_mean(:,j) = - f_new;                  % V = -f
  end
    for j = 1:length(xx)
      ux_mean(:,j) = xx(j) * f_prime(:);      % Introduced only for plotting
                                              purposes
      vx_mean(:,j) = - f_new;                 % Introduced only for plotting
                                              purposes
```

89

```matlab
    end

    ux_mean(:,j) = xx(j) * f_prime(:);
    vel_mean = sqrt(u_mean.^2 + v_mean.^2) * Vinj;
    velx_mean = sqrt(ux_mean.^2 + vx_mean.^2);
    scale = 1.5;


    [X,Y] = meshgrid(x,y*H/2);
    [XX,Y] = meshgrid(xx,y*H/2);
    Error(i) = norm(f_new - f_init,inf);
    figure(1)
    plot(f_new,y*H/2,'color',rand(1,3))
    hold on


    figure(2*i)
    title(' Mean Velocity Contours')
    contourf (XX,Y,velx_mean)

    figure(2*i + 1)
    title(' Mean Velocity Vectors')
    quiverc(XX,Y,ux_mean * Vinj, vx_mean * Vinj,scale)

    clear u_mean v_mean vel_mean
% Saving necessary data for local and non-local approach
    NStr = num2str(N);
    FileName = strcat(NStr, 'CASE_NAME_MEAN_FLOW');
    fileID = fopen(FileName, 'w');
    fprintf(fileID, '%f\n', f_new);
    fclose(fileID);

    save(FileName, 'f_new', 'N', 'Re', 'H', 'x', 'DM', 'y');

end
```

```matlab
function F = meanflow2d(f)

  global DM1 DM2 DM3 DM4 Re


   F = [f(1) - 1;  f(end) + 1;
        f(2) + (sum(DM1(1,3:end) * f(3:end)) / DM1(1,2)) + DM1(1,1) * f(1) /
DM1(1,2) - 0;
        f(end-1) + (sum(DM1(end,1:end-2) * f(1:end-2)) / DM1(end,end-1)) +
DM1(end,end) * f(end) / DM1(end,end-1) - 0;
       (DM1(3:end-2,:) * f(:)) .* (DM2(3:end-2,:) * f(:)) - ...
       (DM3(3:end-2,:) * f(:)) .* f(3:end-2) - ((1/Re) * DM4(3:end-2,:) *
f(:)) - 0];


end
```

C. Derivation of 2D Non-Dimensional Continuity Stability Equation for Local Approach

$$\frac{\partial U}{\partial x} + \frac{\partial V}{\partial y} = 0$$

$$\frac{\partial}{\partial x}\left[\bar{U}(x,y) + \hat{u}(y)e^{i(\alpha x - \omega t)}\right] + \frac{\partial}{\partial y}\left[\bar{V}(x,y) + \hat{v}(y)e^{i(\alpha x - \omega t)}\right] = 0$$

$$\frac{\partial \bar{U}}{\partial x} + i\alpha\hat{u}.\,e^{i(\alpha x - \omega t)} + \frac{\partial \bar{V}}{\partial y} + \frac{\partial \hat{v}}{\partial y}.\,e^{i(\alpha x - \omega t)} = 0$$

$$i\alpha\hat{u}.\,e^{i(\alpha x - \omega t)} + \frac{\partial \hat{v}}{\partial y}.\,e^{i(\alpha x - \omega t)} = 0 \quad \rightarrow \quad i\alpha\hat{u} + \frac{\partial \hat{v}}{\partial y} = 0$$

By writing terms α, $\hat{u}$, $\hat{v}$ and y in non-dimensional form;

$$\alpha^* = \frac{\alpha}{1/h} = \alpha h \quad, \quad \hat{u}^* = \frac{\hat{u}}{V_{inj}} \quad, \quad \hat{v}^* = \frac{\hat{v}}{V_{inj}} \quad, \quad y^* = \frac{y}{h}$$

$$i\alpha^*\hat{u}^* + \frac{\partial \hat{v}^*}{\partial y^*} = 0$$

D. Derivation of 2D Non-Dimensional x-Momentum Stability Equation for Local Approach

$$\frac{\partial U}{\partial t} + U\frac{\partial U}{\partial x} + V\frac{\partial U}{\partial y} = -\frac{1}{\rho}\frac{\partial P}{\partial x} + v\left[\frac{\partial^2 U}{\partial x^2} + \frac{\partial^2 U}{\partial y^2}\right]$$

$$\frac{\partial}{\partial t}\left[\bar{U} + \hat{u}.e^{i(\alpha x - \omega t)}\right] + \left[\bar{U} + \hat{u}.e^{i(\alpha x - \omega t)}\right].\frac{\partial}{\partial x}\left[\bar{U} + \hat{u}.e^{i(\alpha x - \omega t)}\right]$$

$$+\left[\bar{V} + \hat{v}.e^{i(\alpha x - \omega t)}\right].\frac{\partial}{\partial y}\left[\bar{U} + \hat{u}.e^{i(\alpha x - \omega t)}\right] = -\frac{1}{\rho}\frac{\partial}{\partial x}\left[\bar{P} + \hat{p}.e^{i(\alpha x - \omega t)}\right]$$

$$+v\left\{\frac{\partial^2}{\partial x^2}\left[\bar{U} + \hat{u}.e^{i(\alpha x - \omega t)}\right] + \frac{\partial^2}{\partial y^2}\left[\bar{U} + \hat{u}.e^{i(\alpha x - \omega t)}\right]\right\}$$

$$-i\omega\hat{u}e^{i(\alpha x - \omega t)} + \bar{U}\frac{\partial\bar{U}}{\partial x} + i\alpha\bar{U}\hat{u}.e^{i(\alpha x - \omega t)} + \hat{u}\frac{\partial\bar{U}}{\partial x}.e^{i(\alpha x - \omega t)}$$

$$+i\alpha\hat{u}^2.e^{2i(\alpha x - \omega t)} + \bar{V}\frac{\partial\bar{U}}{\partial y} + \bar{V}\frac{\partial\hat{u}}{\partial y}.e^{i(\alpha x - \omega t)}$$

$$+\hat{v}\frac{\partial\bar{U}}{\partial y}.e^{i(\alpha x - \omega t)} + \hat{v}\frac{\partial\hat{u}}{\partial y}.e^{2i(\alpha x - \omega t)}$$

$$= -\frac{1}{\rho}\frac{\partial\bar{P}}{\partial x} - \frac{1}{\rho}i\alpha\hat{p}.e^{i(\alpha x - \omega t)}$$

$$+v\left[\frac{\partial^2\bar{U}}{\partial x^2} - \alpha^2\hat{u}.e^{i(\alpha x - \omega t)} + \frac{\partial^2\bar{U}}{\partial y^2} + \frac{\partial^2\hat{u}}{\partial y^2}.e^{i(\alpha x - \omega t)}\right]$$

As the stability of the steady flow is studied by linear analysis, which requires small perturbation technique, 5th and 9th term in left hand side and the last term in the right hand side of the equation shown above can be neglected.

Since mean flow has already satisfied that equation, by subtracting mean terms written for mean flow and eliminating exponential terms from the rest, equation shown below can be obtained;

$$-i\omega\hat{u} + i\alpha\overline{U}\hat{u} + \hat{u}\frac{\partial\overline{U}}{\partial x} + \overline{V}\frac{\partial\hat{u}}{\partial y} + \hat{v}\frac{\partial\overline{U}}{\partial y} = -\frac{1}{\rho}i\alpha\hat{p} + v\left(\frac{\partial^2\hat{u}}{\partial y^2} - \alpha^2\hat{u}\right)$$

By writing terms, ω, α, $\hat{u}$, $\hat{v}$, ρ, $\hat{p}$, x and y in non-dimensional form as shown below;

$$\omega^* = \frac{\omega}{1/t} = \frac{\omega h}{V_{inj}} \quad , \quad \alpha^* = \frac{\alpha}{1/h} = \alpha h \quad , \quad \hat{u}^* = \frac{\hat{u}}{V_{inj}} \quad , \quad \hat{v}^* = \frac{\hat{v}}{V_{inj}}$$

$$\overline{U}^* = \frac{\overline{U}}{V_{inj}} \quad , \quad \overline{V}^* = \frac{\overline{V}}{V_{inj}} \quad , \quad \hat{p}^* = \frac{\hat{p}}{\rho V_{inj}{}^2} \quad , \quad x^* = \frac{x}{h} \quad , \quad y^* = \frac{y}{h}$$

$$-i\omega^*\hat{u}^* + i\alpha^*\overline{U}^*\hat{u}^* + \hat{u}^*\frac{\partial\overline{U}^*}{\partial x^*} + \overline{V}^*\frac{\partial\hat{u}^*}{\partial y^*} + \hat{v}^*\frac{\partial\overline{U}^*}{\partial y^*} = -i\alpha^*\hat{p}^* + \frac{1}{Re}\left(\frac{\partial^2\hat{u}^*}{\partial y^{*2}} - \alpha^{*2}\hat{u}^*\right)$$

where;

$$Re = \frac{h.V_{inj}}{v}$$

96

E. Derivation of 2D Non-Dimensional y-Momentum Stability Equation for Local Approach

$$\frac{\partial V}{\partial t} + U\frac{\partial V}{\partial x} + V\frac{\partial V}{\partial y} = -\frac{1}{\rho}\frac{\partial P}{\partial y} + v\left[\frac{\partial^2 V}{\partial x^2} + \frac{\partial^2 V}{\partial y^2}\right]$$

$$\frac{\partial}{\partial t}\left[\bar{V} + \hat{v}.e^{i(\alpha x - \omega t)}\right] + \left[\bar{U} + \hat{u}.e^{i(\alpha x - \omega t)}\right].\frac{\partial}{\partial x}\left[\bar{V} + \hat{v}.e^{i(\alpha x - \omega t)}\right]$$

$$+\left[\bar{V} + \hat{v}.e^{i(\alpha x - \omega t)}\right].\frac{\partial}{\partial y}\left[\bar{V} + \hat{v}.e^{i(\alpha x - \omega t)}\right] = -\frac{1}{\rho}\frac{\partial}{\partial y}\left[\bar{P} + \hat{p}.e^{i(\alpha x - \omega t)}\right]$$

$$+v\left\{\frac{\partial^2}{\partial x^2}\left[\bar{V} + \hat{v}.e^{i(\alpha x - \omega t)}\right] + \frac{\partial^2}{\partial y^2}\left[\bar{V} + \hat{v}.e^{i(\alpha x - \omega t)}\right]\right\}$$

$$-i\omega\hat{v}e^{i(\alpha x - \omega t)} + \bar{U}\frac{\partial\bar{V}}{\partial x} + i\alpha\bar{U}\hat{v}.e^{i(\alpha x - \omega t)}$$

$$+\hat{u}\frac{\partial\bar{V}}{\partial x}.e^{i(\alpha x - \omega t)} + i\alpha\hat{u}\hat{v}.e^{2i(\alpha x - \omega t)} + \bar{V}\frac{\partial\bar{V}}{\partial y} + \bar{V}\frac{\partial\hat{v}}{\partial y}.e^{i(\alpha x - \omega t)}$$

$$+\hat{v}\frac{\partial\bar{V}}{\partial y}.e^{i(\alpha x - \omega t)} + \hat{v}\frac{\partial\hat{v}}{\partial y}.e^{2i(\alpha x - \omega t)} = -\frac{1}{\rho}\frac{\partial\bar{P}}{\partial y} - \frac{1}{\rho}\frac{\partial\hat{p}}{\partial y}.e^{i(\alpha x - \omega t)}$$

$$+v\left[\frac{\partial^2\bar{V}}{\partial x^2} - \alpha^2\hat{v}.e^{i(\alpha x - \omega t)} + \frac{\partial^2\bar{V}}{\partial y^2} + \frac{\partial^2\hat{v}}{\partial y^2}.e^{i(\alpha x - \omega t)}\right]$$

Similarly, as it was done in x-Direction Navier-Stokes equation, 5th and 9th term in left hand side and the last term in the right hand side of the equation shown above can be neglected.

Moreover, as also has been done in x-Direction Navier-Stokes equation, by subtracting terms written for mean flow and eliminating exponential terms from the rest, equation shown below can be obtained;

$$-i\omega\hat{v} + i\alpha\bar{U}\hat{v} + \bar{V}\frac{\partial\hat{v}}{\partial y} + \hat{v}\frac{\partial\bar{V}}{\partial y} = -\frac{1}{\rho}\frac{\partial\hat{p}}{\partial y} + \upsilon\left[-\alpha^2\hat{v} + \frac{\partial^2\hat{v}}{\partial y^2}\right]$$

The term $\partial\bar{V}/\partial x$ is also neglected, since mean flow profiles are assumed to satisfy the contiuity equation as $\bar{U} = xF'(y)$ and $\bar{V} = -F(y)$.

$$\omega^* = \frac{\omega}{1/t} = \frac{\omega h}{V_{inj}} \quad , \quad \alpha^* = \frac{\alpha}{1/h} = \alpha h \quad , \quad \hat{u}^* = \frac{\hat{u}}{V_{inj}} \quad , \quad \hat{v}^* = \frac{\hat{v}}{V_{inj}}$$

$$\bar{U}^* = \frac{\bar{U}}{V_{inj}} \quad , \quad \bar{V}^* = \frac{\bar{V}}{V_{inj}} \quad , \quad \hat{p}^* = \frac{\hat{p}}{\rho V_{inj}{}^2} \quad , \quad x^* = \frac{x}{h} \quad , \quad y^* = \frac{y}{h}$$

$$-i\omega^*\hat{v}^* + i\alpha^*\bar{U}^*\hat{v}^* + \bar{V}^*\frac{\partial\hat{v}^*}{\partial y^*} + \hat{v}^*\frac{\partial\bar{V}^*}{\partial y^*} = -\frac{\partial\hat{p}^*}{\partial y^*} + \frac{1}{Re}\left(\frac{\partial^2\hat{v}^*}{\partial y^{*2}} - \alpha^{*2}\hat{v}^*\right)$$

where;

$$Re = \frac{h.V_{inj}}{\upsilon}$$

F.   Derivation and Reduction of the LNP Approach Formula

The equations governing the general evolution of fluid flow are known as Navier-Stokes equations which represents the conservation of mass and momentum. Using Cartesian tensor notation for an incompressible flow, the equations become,

$$\frac{\partial u_i}{\partial t} = -u_j \frac{\partial u_i}{\partial x_j} - \frac{\partial p}{\partial x_i} + \frac{1}{Re} \nabla^2 u_i \quad , \quad i = 1,2 \; for \; 2D \; flow$$

$$\frac{\partial u_i}{\partial x_i} = 0$$

where each primitive variable is written by using superposition of the mean and perturbating flow variables as,

$$U = \bar{U}(x, y) + u(x, y, t)$$

$$V = \bar{V}(y) + v(x, y, t)$$

$$P = \bar{p}(x, y) + p(x, y, t)$$

Substituting the superposed form into the continuity equation and assuming mean flow is already a solution to that equation, continuity equation for perturbating flow can be obtained as,

$$\frac{\partial u}{\partial x} + \frac{\partial v}{\partial y} = 0 \tag{F.1}$$

Substituting the superposed form into the x-momentum equation and assuming mean flow is already a solution to that equation, after neglecting non-linear terms and products of the perturbating variables with each other, x-momentum equation for perturbating flow can be obtained as,

$$\frac{\partial u}{\partial t} + \bar{U}\frac{\partial u}{\partial x} + u\frac{\partial \bar{U}}{\partial x} + \bar{V}\frac{\partial u}{\partial y} + v\frac{\partial \bar{U}}{\partial y} = -\frac{1}{\rho}\frac{\partial p}{\partial x} + v\left(\frac{\partial^2 u}{\partial x^2} + \frac{\partial^2 u}{\partial y^2}\right) \tag{F.2}$$

Substituting the superposed form into the y-momentum equation and assuming mean flow is already a solution to that equation, after neglecting non-linear terms and products of the perturbating variables with each other, y-momentum equation for perturbating flow can be obtained as,

$$\frac{\partial v}{\partial t} + \bar{U}\frac{\partial v}{\partial x} + \bar{V}\frac{\partial v}{\partial y} + v\frac{\partial \bar{V}}{\partial y} = -\frac{1}{\rho}\frac{\partial p}{\partial y} + v\left(\frac{\partial^2 v}{\partial x^2} + \frac{\partial^2 v}{\partial y^2}\right) \qquad (F.3)$$

Disturbances are assumed to be composed of a number of discrete partial fluctuations,

- Each of which propagates in x-direction only
- Any arbitrary 2D disturbance is assumed to be expanded in Fourier series
- Assuming perturbation is 2D streamfunction

$$\psi(x,y,t) = \varphi(y).e^{i(\alpha x-\omega t)} \qquad (F.4a)$$

$$u = \frac{\partial \psi}{\partial y} = \varphi'(y).e^{i(\alpha x-\omega t)} \qquad (F.4b)$$

$$v = -\frac{\partial \psi}{\partial x} = -i\alpha\varphi(y).e^{i(\alpha x-\omega t)} \qquad (F.4c)$$

After substituing perturbation forms expanded in Fourier series $(F.4)$ into the x-momentum equation for perturbating flow $(F.2)$ and into the y-momentum equation for perturbating flow $(F.3)$, respectively,

$$-i\omega\varphi'.e^{i(\alpha x-\omega t)} + i\alpha\bar{U}\varphi'.e^{i(\alpha x-\omega t)} + \varphi'\frac{\partial \bar{U}}{\partial x}.e^{i(\alpha x-\omega t)} + \bar{V}\varphi''.e^{i(\alpha x-\omega t)} \qquad (F.5)$$

$$-i\alpha\varphi\frac{\partial \bar{U}}{\partial y}.e^{i(\alpha x-\omega t)} + \frac{1}{\rho}\frac{\partial p}{\partial x} = v\left[-\alpha^2\varphi'.e^{i(\alpha x-\omega t)} + \varphi'''.e^{i(\alpha x-\omega t)}\right]$$

100

$$-\alpha\omega\varphi.\,e^{i(\alpha x-\omega t)} + \alpha^2\overline{U}\varphi.\,e^{i(\alpha x-\omega t)} - i\alpha\overline{V}\varphi'.\,e^{i(\alpha x-\omega t)} \qquad (F.6)$$

$$-i\alpha\varphi\frac{\partial\overline{V}}{\partial y}.\,e^{i(\alpha x-\omega t)} + \frac{1}{\rho}\frac{\partial p}{\partial y} = -i\alpha v\left[-\alpha^2\varphi.\,e^{i(\alpha x-\omega t)} + \varphi''.\,e^{i(\alpha x-\omega t)}\right]$$

Differentiating $(F.5)$ with y and $(F.6)$ with x and considering $\overline{\partial V}/\partial x = 0$ as found from earlier sections,

$$-i\omega\varphi''.\,e^{i(\alpha x-\omega t)} + i\alpha\frac{\partial\overline{U}}{\partial y}\varphi'.\,e^{i(\alpha x-\omega t)} + i\alpha\overline{U}\varphi''.\,e^{i(\alpha x-\omega t)} \qquad (F.7)$$

$$+\varphi''\frac{\partial\overline{U}}{\partial x}.\,e^{i(\alpha x-\omega t)} + \varphi'\frac{\partial^2\overline{U}}{\partial x\,\partial y}.\,e^{i(\alpha x-\omega t)} + \frac{\partial\overline{V}}{\partial y}\varphi''.\,e^{i(\alpha x-\omega t)}$$

$$+\overline{V}\varphi'''.\,e^{i(\alpha x-\omega t)} - i\alpha\varphi'\frac{\partial\overline{U}}{\partial y}.\,e^{i(\alpha x-\omega t)} - i\alpha\varphi\frac{\partial^2\overline{U}}{\partial y^2}.\,e^{i(\alpha x-\omega t)}$$

$$+\frac{1}{\rho}\frac{\partial^2 p}{\partial x\,\partial y} = v\left[-\alpha^2\varphi''.\,e^{i(\alpha x-\omega t)} + \varphi^{(IV)}.\,e^{i(\alpha x-\omega t)}\right]$$

$$-i\alpha^2\omega\varphi.\,e^{i(\alpha x-\omega t)} + i\alpha^3\overline{U}\varphi.\,e^{i(\alpha x-\omega t)} + \alpha^2\frac{\partial\overline{U}}{\partial x}\varphi.\,e^{i(\alpha x-\omega t)} \qquad (F.8)$$

$$+\alpha^2\overline{V}\varphi'.\,e^{i(\alpha x-\omega t)} + \alpha^2\varphi\frac{\partial\overline{V}}{\partial y}.\,e^{i(\alpha x-\omega t)} + \frac{1}{\rho}\frac{\partial^2 p}{\partial x\,\partial y}$$

$$= -i\alpha v\left[-i\alpha^3\varphi.\,e^{i(\alpha x-\omega t)} + i\alpha\varphi''.\,e^{i(\alpha x-\omega t)}\right]$$

Equating pressure terms in $(F.7)$ and $(F.8)$ and eliminating exponential expansion terms,

$$-i\omega\varphi'' + i\alpha\frac{\partial\overline{U}}{\partial y}\varphi' + i\alpha\overline{U}\varphi'' + \varphi''\frac{\partial\overline{U}}{\partial x} + \varphi'\frac{\partial^2\overline{U}}{\partial x\,\partial y} + \frac{\partial\overline{V}}{\partial y}\varphi'' + \overline{V}\varphi''' \qquad (F.9)$$

$$-i\alpha\varphi'\frac{\partial\overline{U}}{\partial y} - i\alpha\varphi\frac{\partial^2\overline{U}}{\partial y^2} + i\alpha^2\omega\varphi - i\alpha^3\overline{U}\varphi - \alpha^2\frac{\partial\overline{U}}{\partial x}\varphi - \alpha^2\overline{V}\varphi' - \alpha^2\varphi\frac{\partial\overline{V}}{\partial y}$$

$$= \nu\bigl[-\alpha^2\varphi'' + \varphi^{(IV)} + \alpha^4\varphi - \alpha^2\varphi''\bigr]$$

Taking $\varphi, i\varphi, \varphi', \varphi''$ and $i\varphi''$ common, canceling $i\varphi'$ terms and rearranging,

$$i\varphi''(\alpha\overline{U} - \omega) + i\varphi\left(-\alpha\frac{\partial^2\overline{U}}{\partial y^2} + \alpha^2\omega - \alpha^3\overline{U}\right) - \varphi\alpha^2\left(\frac{\partial\overline{U}}{\partial x} + \frac{\partial\overline{V}}{\partial y}\right) \qquad (F.10)$$

$$+\varphi'\left(\frac{\partial^2\overline{U}}{\partial x\,\partial y} - \alpha^2\overline{V}\right) + \varphi''\left(\frac{\partial\overline{U}}{\partial x} + \frac{\partial\overline{V}}{\partial y}\right) + \overline{V}\varphi''' = \nu\bigl[\varphi^{(IV)} - 2\alpha^2\varphi'' + \alpha^4\varphi\bigr]$$

One can also notice that $\varphi''(\partial\overline{U}/\partial x + \partial\overline{V}/\partial y)$ term and $\varphi\alpha^2(\partial\overline{U}/\partial x + \partial\overline{V}/\partial y)$ are zero due to the fact that mean flow is already satifying continuity equation. Therefore, fourth order perturbation equation for LNP approach becomes,

$$i\varphi''(\alpha\overline{U} - \omega) + i\varphi\left(-\alpha\frac{\partial^2\overline{U}}{\partial y^2} + \alpha^2\omega - \alpha^3\overline{U}\right) \qquad (F.11)$$

$$+\varphi'\left(\frac{\partial^2\overline{U}}{\partial x\,\partial y} - \alpha^2\overline{V}\right) + \overline{V}\varphi''' = \nu\bigl[\varphi^{(IV)} - 2\alpha^2\varphi'' + \alpha^4\varphi\bigr]$$

which slightly differs from the classical Orr-Sommerfeld equation with 2 additional terms due to having such a mean flow profile where the components of the mean flow are $\overline{V} \neq 0$ and $\partial\overline{U}/\partial x \neq 0$,

$$i\varphi''(\alpha\overline{U} - \omega) + i\varphi\left(-\alpha\frac{\partial^2\overline{U}}{\partial y^2} + \alpha^2\omega - \alpha^3\overline{U}\right) \qquad (F.12)$$

$$= \nu\left[\varphi^{(IV)} - 2\alpha^2\varphi'' + \alpha^4\varphi\right]$$

with boundary conditions,

$$\varphi(\pm 1) = \varphi'(\pm 1) = 0 \qquad (F.13)$$

G. Mesh Independence Study for Spatial Hydrodynamic Instability of the Poiseuille Flow

- Results for $N = 40$

Eigenvalues for Poiseuille Flow , $Re_{cr} = 5772.2213$, $\alpha_{cr} = 1.020737$, $\omega_{cr} = 0.2694975$ and $N_{span} = 40$
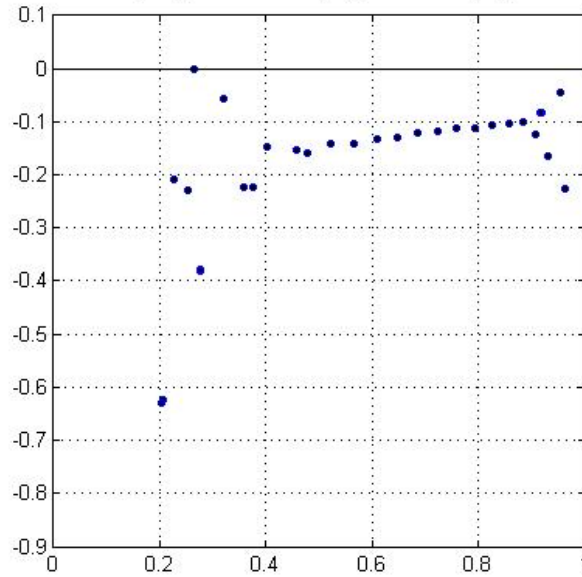
- Results for $N = 60$

Eigenvalues for Poiseuille Flow , $Re_{cr} = 5772.2220$, $\alpha_{cr} = 1.0200504$, $\omega_{cr} = 0.2694081$ and $N_{span} = 60$

105
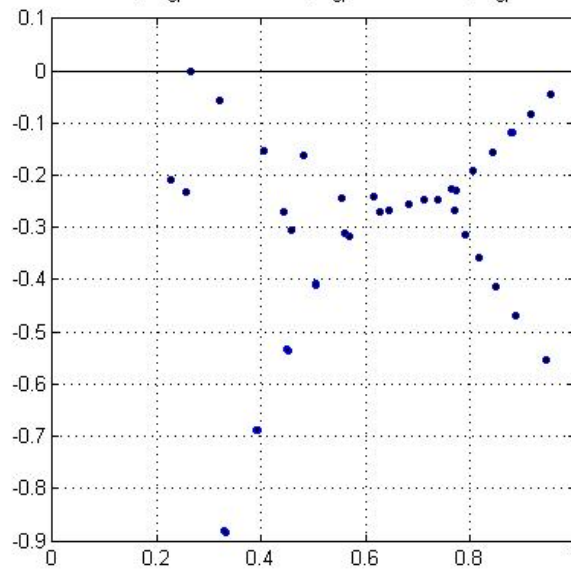
- Results for $N = 80$

Eigenvalues for Poiseuille Flow , Re_{cr} = 5772.2224 , α_{cr} = 1.020623 , ω_{cr} = 0.2694537 and N_{span} = 80
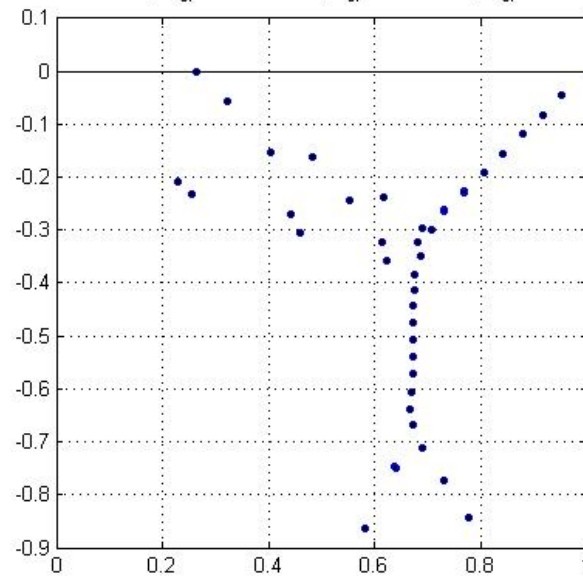
- Results for $N = 100$

Eigenvalues for Poiseuille flow , Re_{cr} = 5772.2221 , α_{cr} = 1.020671 , ω_{cr} = 0.2694756 and N_{span} = 100
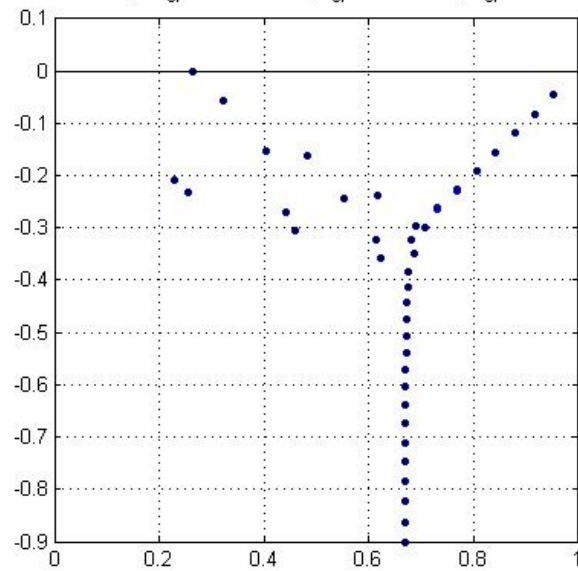
- Results for $N = 120$

Eigenvalues for Poiseuille flow , $Re_{cr} = 5772.2222$, $\alpha_{cr} = 1.020569$, $\omega_{cr} = 0.2694605$ and $N_{span} = 120$
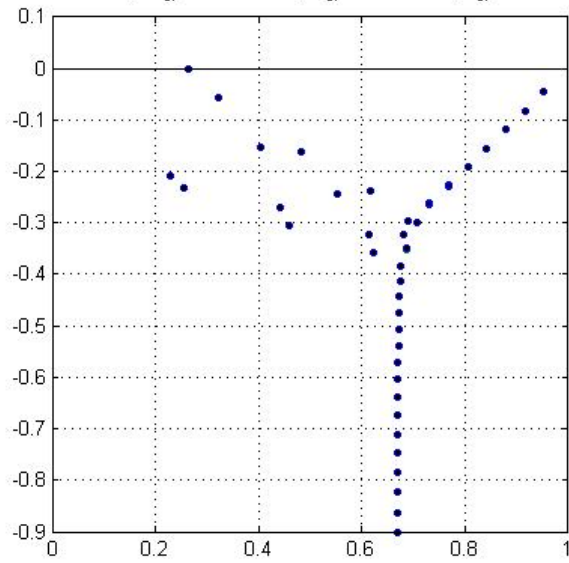
H. Determining the Neutral Curve for Fixed Reynolds Number (LNP Approach)

(α, ω) pair with respect to a given Reynolds number along the whole domain in x-direction combined and neutral curve can be obtained subsequently.

```matlab
% ----------------- LOCAL NON-PARALLEL APPROACH SOLVER -------------------
% ----- Solves the stability equation for local exponential expansion -----
% ------------------- exp(ax - wt) for 2D porous flow --------------------
% -------------- where a = alpha represents the growth rate --------------
% ---------- while w = omega stands for the frequency of the wave ---------
% --------- with BCs ; Phi(-1) = Phi(1) = Phi'(-1) = Phi'(1) = 0 ----------


clc
clear all
close all


% ------------------------- LOADING MEAN FLOW ----------------------------

load('CASE_NAME_MEAN_FLOW.mat');        % Loading mean flow solution

% DM is the matrix holds differentiation matrices used in the calculation
% of mean flow
DM1 = DM(:,:,1);
DM2 = DM(:,:,2);
DM3 = DM(:,:,3);
DM4 = DM(:,:,4);

[ay,ax] = meshgrid(x,y*H/2);

f1_prime = DM1 * f_new;      % f'(y)
f2_prime = DM2 * f_new;      % f''(y)
f3_prime = DM3 * f_new;      % f'''(y)


% v_mean = -f(y) --> Does not change with x
v_mean = - diag(f_new); v_mean = v_mean(2:N,2:N);

% d2u/dxdy = f''(y)--> Does not change with x
d2u_dxdy = diag(f2_prime); d2u_dxdy = d2u_dxdy(2:N,2:N);

I = eye(N-1);

% Chebyshev collocation grid points and differentiation matrix for N = 120
% are generated (N comes from mean flow solution. If N is changed in mean flow
% solution, then Chebyshev collocation grid points and the degree of polynomials
% automatically changed)
[D,y] = cheb(N);
```

109

```
% Reduction of the 4 boundary conditions into 2
S = diag([0; 1 ./(1-y(2:N).^2); 0]);
D3 = (diag(1-y.^2)*DM3 - 6*diag(y)*DM2 - 6*DM1)*S;
D4 = (diag(1-y.^2)*DM4 - 8*diag(y)*DM3 - 12*DM2)*S;

% Since the problem has homogenous B.C's, first and last row/column of the
differentiation matrices can be removed. Also, same procedure is done for the
terms come from mean flow solution



DR1 = DM1(2:N,2:N);
DR2 = DM2(2:N,2:N);
DR3 = D3(2:N,2:N);
DR4 = D4(2:N,2:N);


% At first, delta_alpha is choosen a large value. Thus, stopping criteria is
also large. After the first iteration, the vicinity of the root can be
captured, but the root cannot be obtained accurately. This iteration proceeds
by reducing adelta_alpha and stopping criteria and updating manuelly a_min
and a_max from the results of the previous iteration to obtain the root
(alpha,omega) accurately. It is kind of a bracketing method which restricts
the vicinity of the root until obtaining considerably accurate results


dalpha = 1e-02;
dx = 1000;
Epss = 1e-1;
counter = 0;     % Used for plotting purposes
a_iter = 0;      % Counts the outer iteration for alpha
% a_min and a_max are needed to be entered manuelly

for a = a_min:dalpha:a_max  % Alpha (To make calculation using critical value,
take the imaginary part zero)
    crit = 0;               % Used to determine the point where BL. instability
starts
    EVec = zeros(N-1,N-1);
    EValND = zeros(N-1,N-1);

% Viscous term at the RHS of the LNP (also of Orr-Sommerfeld) approach (Does
not change with x)
    A_vis = (DR4-2*a^2*DR2+a^4*I)/Re;



% The problem is treated as an eigenvalue problem at each x coordinate. After
critical values are found for this coordinate, another coordinate is going
to be enter. Also, for a range of coordinates can be searched. x_min and
x_max are needed to be entered manuelly. "*1000" term comes from mean flow
(delta_x = 0.001)


    for j=x_min*1000 + 1:dx:x_max*1000 + 1
```

```matlab
        if crit == 0
            % u_mean --> u_mean = xf'(y)
            u_mean = diag(x(j) * f1_prime); u_mean = u_mean(2:N,2:N);

            % d2u/dy2 --> d2u/dy2 = xf'''(y)
            d2u_dy2 = diag(x(j) * f3_prime); d2u_dy2 = d2u_dy2(2:N,2:N);

            A = -(A_vis) + (1i*a*u_mean*DR2) - 1i*I*a*(d2u_dy2 + a^2*u_mean) + ...
                DR1*(d2u_dxdy - a^2*v_mean) + v_mean*DR3;
            B = 1i*a*(DR2-I*a^2);

            % Eigenpairs at x(j) --> EVec = Eigenvectors, EVal = Eigenvalues
            [EVec,EValND] = eig(A,B); EVal = diag(EValND);


            for k=1:N-1
                if (imag(EVal(k,1)) > 0 && abs(imag(EVal(k,1)))<Epss && crit == 0)

% If any eigenvalue at x(j) has a positive imaginary part, that x(j) indicates
where the transition begins

                    a_iter = a_iter + 1;
                    crit = crit + 1;
                    a_cr_1stIter(a_iter) = a;          % Critical alpha
                    x_cr_1stIter(a_iter) = (j-1)/1000; % Critical x
                    firstindex_1stIter(a_iter) = k;    % Row index at column
j
                    EVal_cr_1stIter(:,a_iter)  =  EVal;    % Eigenvalues  at
critical x
                    EVec_cr_1stIter(:,:,a_iter)  =  EVec;% Eigenvectors  at
critical x
                    omega_cr_1stIter(a_iter)                              =
                    real(EVal_cr_1stIter(k,a_iter)) * a;
                                                          % Critical frequency
                    imagvalue(a_iter) = abs(imag(EVal(k,1)));

                end

            end

        end

    end

end




% ------------- Post-Process For u' & v' && Mode Seperation -------------%

for k = 1:length(firstindex_1stIter)
```

```matlab
% u_pert = (Phi)'
    u_pert(:,k) = [0;DR1*EVec_cr_1stIter(:,firstindex_1stIter(k),k);0];

% v_pert = -i * a * Phi
    v_pert(:,k)                              =                              [0;-
a_cr_1stIter(k)*1i*EVec_cr_1stIter(:,firstindex_1stIter(k),k);0];


    if ((u_pert(2,k)<0 && u_pert(N,k)>0) || (u_pert(2,k)>0 && u_pert(N,k)<0))

        mode_1stIter(1,k) = 1;      % u' is antisymmetric (Mode = 1)

    else
        mode_1stIter(1,k) = 2;      % u' is symmetric (Mode = 2)

    end

end



c1 = 0;
c2 = 0;

for k=1:length(mode_1stIter)
    if mode_1stIter (1,k) == 1
        c1 = c1 + 1;
        a_cr_mode1_1stIter(1,c1) = a_cr_1stIter(1,k);
        omega_cr_mode1_1stIter(1,c1) = omega_cr_1stIter(1,k);
        x_cr_mode1_1stIter(1,c1) = x_cr_1stIter(1,k);
        imagvalue_mode1(1,c1) = imagvalue(1,k);
        EVal_mode1(:,c1) = EVal_cr_1stIter(:,k);
    else
        c2 = c2 + 1;
        a_cr_mode2_1stIter(1,c2) = a_cr_1stIter(1,k);
        omega_cr_mode2_1stIter(1,c2) = omega_cr_1stIter(1,k);
        x_cr_mode2_1stIter(1,c2) = x_cr_1stIter(1,k);
        imagvalue_mode2(1,c2) = imagvalue(1,k);
        EVal_mode2(:,c2) = EVal_cr_1stIter(:,k);
    end

end




% --------------------- Sorting alpha, x and omega ---------------------

outercount = 0;
for i = min(x_cr_mode1_1stIter):dx:max(x_cr_mode1_1stIter)
    innercount = 0;
    outercount = outercount + 1;
    for j = 1:length(x_cr_mode1_1stIter)

        if (x_cr_mode1_1stIter(1,j) == i)
```

```matlab
            innercount = innercount + 1;
            index = j;
            x_cr_mode1_1stIter_sorted(innercount,outercount)          =
x_cr_mode1_1stIter(1,j);
            a_cr_mode1_1stIter_sorted(innercount,outercount)          =
a_cr_mode1_1stIter(1,j);
            omega_cr_mode1_1stIter_sorted(innercount,outercount)      =
omega_cr_mode1_1stIter(1,j);

        end

    end

    numOfind_mode1_1stIter(1,outercount) = innercount;
end




outercount = 0;
for i = min(x_cr_mode2_1stIter):dx:max(x_cr_mode2_1stIter)
    innercount = 0;
    outercount = outercount + 1;
    for j = 1:length(x_cr_mode2_1stIter)

        if (x_cr_mode2_1stIter(1,j) == i)

            innercount = innercount + 1;
            index = j;
            x_cr_mode2_1stIter_sorted(innercount,outercount)          =
x_cr_mode2_1stIter(1,j);
            a_cr_mode2_1stIter_sorted(innercount,outercount)          =
a_cr_mode2_1stIter(1,j);
            omega_cr_mode2_1stIter_sorted(innercount,outercount)      =
omega_cr_mode2_1stIter(1,j);

        end

    end
    numOfind_mode2_1stIter(1,outercount) = innercount;
end
```

I. Mesh Independency Study for Spatial Hydrodynamic Instability of the Porous Flow (LNP Approach) – Mode-1

x	N = 41 α	N = 41 ω	N = 61 α	N = 61 ω	N = 81 α	N = 81 ω	N = 101 α	N = 101 ω	N = 121 α	N = 121 ω	N = 141 α	N = 141 ω
20	13,57576027	86,10676663	13,63591463	86,45011645	13,61574495	86,38244404	13,63399722	86,4422308	13,63278816	86,43825036	13,63289425	86,43842862
18	12,526202	78,50978497	12,67658201	78,93562004	12,67807255	78,94420269	12,67466609	79,93222863	12,66409975	78,89880364	12,67547707	78,9344675
16	11,70493075	71,41047144	11,64284161	71,17335562	11,64238499	71,17021828	11,6449113	71,17822573	11,64516622	71,17934417	11,64520072	71,17954888
14	10,55587608	63,19103932	10,53587648	63,15270214	10,53537353	63,15103678	10,53399955	63,14765485	10,53390349	63,14768154	10,53398889	63,14790584
12	9,30405492	54,72075577	9,33198493	54,80685402	9,33367211	54,81061241	9,33158054	54,80453223	9,33198907	54,80588374	9,3319229	54,80563697
10	8,05294251	46,18360849	8,02539754	46,10024944	8,02656841	46,10264996	8,02670775	46,10381953	8,02646937	46,1030749	8,02645308	46,10298309
8	6,59787237	36,9581072	6,60064881	36,9565112	6,60093945	36,9573299	6,6006096	36,95598835	6,60046185	36,95552131	6,60045435	36,95548776
6	5,05747422	27,27426565	5,05014444	27,24496018	5,05113542	27,24805644	5,05058593	27,24641058	5,05064353	27,2465648	5,05064419	27,24655969
4	3,8435943	17,94624316	3,84123811	17,94282301	3,84133372	17,9431556	3,84141686	17,94355418	3,84141219	17,94354881	3,84141428	17,94355577
3,31	**3,40937386**	**14,01963469**	3,47536247	14,28630606	3,47506533	14,28509731	3,47442703	14,28247561	3,47438131	14,28228491	3,47441666	14,2824292
3,302	-	-	**3,4338087**	**14,08953158**	**3,43290819**	**14,08581868**	**3,43074994**	**14,07700834**	**3,43057093**	**14,07627226**	**3,4306988**	**14,07679575**
3,302	-	-	**3,39127612**	**13,91518588**	**3,392145**	**13,91875955**	**3,39428585**	**13,9275417**	**3,39446608**	**13,92827836**	**3,39433401**	**13,92773641**
3,31	**3,40227243**	**13,99047321**	3,34449927	13,74923816	3,34476561	13,75034354	3,34538796	13,75290666	3,34543933	13,75311573	3,34539991	13,75295351
4	2,68450187	12,82463746	2,68167426	12,80943772	2,68169497	12,80953763	2,68172641	12,80966404	2,68172777	12,80966684	2,68172227	12,80964029
6	2,00871193	13,17326049	2,00810922	13,17136966	2,00810874	13,1713389	2,00808841	13,17120112	2,00808656	13,17119181	2,00808372	13,17117297
8	1,6880066	13,78152677	1,68853794	13,78774259	1,68852429	13,78765067	1,68853152	13,78776151	1,68853342	13,78777799	1,68853126	13,78775954
10	1,49169315	14,39006443	1,49229202	14,39435734	1,49229929	14,39450028	1,49231027	14,3945469	1,49230962	14,39453284	1,49230774	14,3945133
12	1,35671378	14,96803616	1,35680789	14,9657001	1,35682626	14,96583654	1,35681418	14,96566733	1,35681284	14,96566162	1,35681139	14,96564448
14	1,25672685	15,50690078	1,25636379	15,50053525	1,25635787	15,50033258	1,2563496	15,50033023	1,25635114	15,50035368	1,25634989	15,50033585
16	1,17868242	16,00735642	1,1781958	16,00215669	1,17817282	16,00191284	1,17818426	16,00211694	1,17818514	16,00211379	1,178183652	16,0020921
18	1,1155096	16,4753091	1,11519916	16,47473678	1,11519281	16,47487431	1,11520447	16,47493127	1,11520278	16,47490344	1,11520147	16,47488348
20	1,06308198	16,9177111	1,06307787	16,92210359	1,06309788	16,92251612	1,06309215	16,9223109	1,06309105	16,92231291	1,06309029	16,92297225

J. Mesh Independency Study for Spatial Hydrodynamic Instability of the Porous Flow (LNP Approach) – Mode-2

x	N = 41 α	N = 41 ω	N = 61 α	N = 61 ω	N = 81 α	N = 81 ω	N = 101 α	N = 101 ω	N = 121 α	N = 121 ω	N = 141 α	N = 141 ω
20	-	-	13,61357623	86,37849568	13,63052358	86,42985417	13,63363769	86,4410318	13,63283689	86,43837264	13,63290564	86,43846797
18	12,5635528	78,61945733	12,65525622	78,86935872	12,67715969	78,94086079	12,67496033	78,9330505	12,67543998	78,93435319	12,67548439	78,93449495
16	11,6918504	71,35419089	11,64354281	71,17511007	11,64347487	71,17375986	11,64506319	71,17884877	11,64519826	71,17946835	11,64025065	71,16415838
14	10,54588596	63,16875715	10,51735024	63,09652615	10,51682154	63,09492063	10,53401503	63,14785216	10,53394648	63,14781171	-	-
12	9,31560808	54,7554274	9,31521333	54,75579439	9,31681119	54,75991211	9,33177174	54,80515764	9,33103282	54,8029935	9,33099601	54,80284066
10	8,03786671	46,13775772	8,02579729	46,10119362	8,01153749	46,0579984	8,01173678	46,05890626	8,01199964	46,05967965	8,02570346	46,10072558
8	6,58544369	36,91437255	6,58777612	36,91736204	6,59829472	36,94898912	6,58770744	36,91702288	6,59818689	36,94854924	6,58755234	36,91652975
6	4,99043493	27,06039673	4,98820632	27,05193158	4,98839739	27,05254148	4,98830232	27,05225122	4,98831224	27,05227974	4,9883121	27,05226966
4,898	**3,46754652**	**19,22473549**	**3,44167866**	**19,13144411**	**3,44135647**	**19,13029289**	**3,44077096**	**19,1281768**	**3,44077193**	**19,12817929**	**3,44096292**	**19,12886581**
4,898	**3,36370457**	**18,84852648**	**3,38841524**	**18,93855409**	**3,38857053**	**18,93912951**	**3,38917119**	**18,94131153**	**3,3891923**	**18,94138733**	**3,38898608**	**18,94063541**
6	2,1595553	16,0658439	2,15930044	16,06474949	2,15930276	16,06475927	2,15929957	16,064742	2,1592909	16,06473977	2,15929328	16,0647126
8	1,51098375	15,35773588	1,51087479	15,35697677	1,51087656	15,35698819	1,51087701	15,35698812	1,51087697	15,35698755	1,51087328	15,35696521
10	1,17922033	15,12254597	1,17916207	15,12196846	1,17916331	15,12197893	1,17916409	15,12198276	1,17916411	15,12198258	1,17916142	15,12196243
12	0,9706947	15,00998248	0,9706578	15,00949719	0,97065875	15,00950704	0,97065949	15,00951213	0,97065954	15,00951238	0,97065726	15,0094919
14	0,82615793	14,94639959	0,82613188	14,94596712	0,82613266	14,94597668	0,82613333	14,94598243	0,82613338	14,94598267	0,82613144	14,94596256
16	0,71964177	14,90669813	0,71964112	14,90629892	0,71964177	14,90630813	0,71964237	14,90631422	0,71964242	14,90631457	0,71964073	14,90629458
18	0,63777115	14,88015074	0,63775536	14,87977383	0,63775593	14,87978296	0,63775647	14,87978927	0,63775651	14,87978956	0,63775496	14,87976902
20	0,57277015	14,86148424	0,57275706	14,86112303	0,57275756	14,86113195	0,5727805	14,86113844	0,57275809	14,8611388	0,57275675	14,86111903

K. Spatial Instability Code for Local Approach (LNP)

This code can be used instead of the one given in Appendix.C6 by taking $\alpha_i = 0$ in the "for loop".

```
% ----------------- LOCAL NON-PARALLEL APPROACH SOLVER -------------------
% ----- Solves the stability equation for local exponential expansion -----
% ------------------ exp(ax - wt) for 2D porous flow --------------------
% -------------- where a = alpha represents the growth rate -------------
% ---------- while w = omega stands for the frequency of the wave ---------
% --------- with BCs ; Phi(-1) = Phi(1) = Phi'(-1) = Phi'(1) = 0 ----------


clc
clear all
close all


% ------------------------- LOADING MEAN FLOW ---------------------------

load('CASE_NAME_MEAN_FLOW.mat');        % Loading mean flow solution

% DM is the matrix holds differentiation matrices used in the calculation
% of mean flow
DM1 = DM(:,:,1);
DM2 = DM(:,:,2);
DM3 = DM(:,:,3);
DM4 = DM(:,:,4);

[ay,ax] = meshgrid(x,y*H/2);

f1_prime = DM1 * f_new;      % f'(y)
f2_prime = DM2 * f_new;      % f''(y)
f3_prime = DM3 * f_new;      % f'''(y)


% v_mean = -f(y) --> Does not change with x
v_mean = - diag(f_new); v_mean = v_mean(2:N,2:N);

% d2u/dxdy = f''(y)--> Does not change with x
d2u_dxdy = diag(f2_prime); d2u_dxdy = d2u_dxdy(2:N,2:N);

I = eye(N-1);

% Chebyshev collocation grid points and differentiation matrix for N = 120
% are generated (N comes from mean flow solution. If N is changed in mean flow
% solution, then Chebyshev collocation grid points and the degree of polynomials
% automatically changed)
[D,y] = cheb(N);

% Reduction of the 4 boundary conditions into 2
```

```
S = diag([0; 1 ./(1-y(2:N).^2); 0]);
D3 = (diag(1-y.^2)*DM3 - 6*diag(y)*DM2 - 6*DM1)*S;
D4 = (diag(1-y.^2)*DM4 - 8*diag(y)*DM3 - 12*DM2)*S;

% Since the problem has homogenous B.C's, first and last row/column of the
differentiation matrices can be removed. Also, same procedure is done for the
terms come from mean flow solution



DR1 = DM1(2:N,2:N);
DR2 = DM2(2:N,2:N);
DR3 = D3(2:N,2:N);
DR4 = D4(2:N,2:N);

% At first, delta_alpha is choosen a large value. Thus, stopping criteria is
also large. After the first iteration, the vicinity of the root can be
captured, but the root cannot be obtained accurately. This iteration proceeds
by reducing adelta_alpha and stopping criteria and updating manuelly a_min
and a_max (both real and imaginary part this time) from the results of the
previous iteration to obtain the root (alpha,omega) accurately. It is kind
of a bracketing method which restricts the vicinity of the root until
obtaining considerably accurate results



dalpha = 0.01;
dx = 100;
Epss = 0.1;
counter = 0;     % Used for plotting purposes
a_iter = 0;      % Counts the outer iteration for alpha

for a_real = real(a)_min:dalpha:real(a)_max

    % Alpha (To make calculation using critical value, take the imaginary
part zero)
    for a_imag = imag(a)_min:dalpha:imag(a)_max
        a = a_real + 1i*a_imag;
        crit = 0;        % Used to determine the point where BL. instability
starts

        EVec = zeros(N-1,N-1);
        EValND = zeros(N-1,N-1);

 % Viscous term at the RHS of the LNP (also of Orr-Sommerfeld) approach (Does
not change with x)
        A_vis = (D4-2*a^2*D2+a^4*I)/Re;


% The problem is treated as an eigenvalue problem at each x coordinate. After
critical values are found for this coordinate, another coordinate is going
to be enter. Also, for a range of coordinates can be searched. x_min and
x_max are needed to be entered manuelly. "*1000" term comes from mean flow
(delta_x = 0.001)
```

```matlab
        for j=x_min*1000 + 1:dx:x_max*1000 + 1

            if crit == 0
                % u_mean --> u_mean = xf'(y)
                u_mean = diag(x(j) * f1_prime); u_mean = u_mean(2:N,2:N);

                % d2u/dy2 --> d2u/dy2 = xf'''(y)
                d2u_dy2 = diag(x(j) * f3_prime); d2u_dy2 = d2u_dy2(2:N,2:N);

                A  =  -(A_vis)  +  (1i*a*u_mean*D2)  -  1i*I*a*(d2u_dy2  +
a^2*u_mean) + ...
                        D*(d2u_dxdy - a^2*v_mean) + v_mean*D3;

                B = 1i*a*(D2-I*a^2);

                % Eigenpairs  at  x(j)  -->  EVec  =  Eigenvectors,  EVal  =
        Eigenvalues
                [EVec,EValND] = eig(A,B); EVal = diag(EValND);


% OMEGA is the value which is searched for. That means, for a given Reynolds
number, x-position and temporal growth, spatial growth is sought. The "if"
condition  determines  if  the  dispersion  relation  (Re,alpha,omega,x)  is
satisfied, i.e. if the alpha is in the vicinity of the root.

                for k=1:N-1
                    if (abs(imag(EVal(k,1))  *  a_real  +  real(EVal(k,1))  *
a_imag) < Epss && abs((OMEGA) - (real(EVal(k,1)) * a_real - imag(EVal(k,1))
* a_imag)) < 0.00000001 && crit == 0)   % If any eigenvalue at x(j) has a
positive imaginary part, that x(j) indicates where the transition begins
                        a_iter = a_iter + 1;
                        crit = crit + 1;
                        % Critical alpha
                        a_real_cr_1stIter(a_iter) = a_real;
                        a_imag_cr_1stIjter(a_iter) = a_imag;
                        a_cr_1stIter(a_iter) = a_real + 1i*a_imag;

                        % Row index at column j
                        firstindex_1stIter(a_iter) = k;

                        % Eigenvalues at critical x
                        EVal_cr_1stIter(:,a_iter) = EVal;

                        % Eigenvectors at critical x
                        EVec_cr_1stIter(:,:,a_iter) = EVec;

                        % Critical frequency
                        omega_cr_1stIter(a_iter) = real(EVal(k,1)) * a_real
- imag(EVal(k,1)) * a_imag;
                        value(a_iter)  =  abs(imag(EVal(k,1))  *  a_real  +
real(EVal(k,1)) * a_imag);
                        x_cr(a_iter) = j - 1;
                    end
```

```matlab
                end

            end

        end

    end

end




% ------------- Post-Process For u' & v' && Mode Seperation --------------%


% We get rid of the existance of pressure term. Since it is an eigenvalue
% problem, eigenvectors can be scaled. Therefore, at the end of the calculation
% of alpha for given omega, x and Reynolds number, eigenvectors are scaled
% up/down to satisfy the boundary conditions for pressure (p'(-1) = p'(1) = 0).


EVec_cr_1stIter = EVec_cr_1stIter * SCALE;
EVec_save = EVec_cr_1stIter(:,firstindex_1stIter(1),1);
for k = 1:length(firstindex_1stIter)

    % u_pert = (Phi)'
    u_pert(:,k) = [0;D*EVec_cr_1stIter(:,firstindex_1stIter(k),k);0];

    % v_pert = -i * a * Phi
    v_pert(:,k)                              =                              [0;-
a_cr_1stIter(k)*1i*EVec_cr_1stIter(:,firstindex_1stIter(k),k);0];

    % u_pert' = (Phi)''
    u_pert_y(:,k) = [0;D2*EVec_cr_1stIter(:,firstindex_1stIter(k),k);0];

    % u_pert'' = (Phi)'''
    u_pert_yy(:,k) = [0;D3*EVec_cr_1stIter(:,firstindex_1stIter(k),k);0];

    if ((u_pert(2,k)<0 && u_pert(N,k)>0) || (u_pert(2,k)>0 && u_pert(N,k)<0))

        mode_1stIter(1,k) = 1;      % u' is antisymmetric

    else
        mode_1stIter(1,k) = 2;      % u' is symmetric

    end

end



c1 = 0;
c2 = 0;
```

122

```matlab
for k=1:length(mode_1stIter)
    if mode_1stIter (1,k) == 1
        c1 = c1 + 1;
        a_cr_mode1_1stIter(1,c1) = a_cr_1stIter(1,k);
        omega_cr_mode1_1stIter(1,c1) = omega_cr_1stIter(1,k);
        value_mode1(1,c1) = value(1,k);
        EVal_mode1(:,c1) = EVal_cr_1stIter(:,k);
    else
        c2 = c2 + 1;
        a_cr_mode2_1stIter(1,c2) = a_cr_1stIter(1,k);
        omega_cr_mode2_1stIter(1,c2) = omega_cr_1stIter(1,k);
        value_mode2(1,c2) = value(1,k);
        EVal_mode2(:,c2) = EVal_cr_1stIter(:,k);
    end

end


figure(1)
plot(y,abs(u_pert),'g')
hold on
plot(y,abs(v_pert),'r')

figure(2)
plot(y,real(u_pert),'g')
hold on
plot(y,real(v_pert),'r')



% POST-PROCESS FOR P' USING X-MOMENTUM EQUATION IN LNP APPROACH


% x_index is the position in x-direction where alpha is calculated. du_dy and
% u_mean_pp are the mean flow variables which depend on x-coordinate

u_pert_pp = u_pert(2:N);
v_pert_pp = v_pert(2:N);
u_pert_y_pp = u_pert_y(2:N);
u_pert_yy_pp = u_pert_yy(2:N);
du_dx = f1_prime(2:N);
du_dy = x(1,x_index) * f2_prime; du_dy = du_dy(2:N);
u_mean_pp = x(1,x_index) * f1_prime; u_mean_pp = u_mean_pp(2:N);
v_mean_pp = - f_new; v_mean_pp = v_mean_pp(2:N);


p_pert = [1;((-1i * omega_cr_1stIter * u_pert_pp) + (du_dx .* u_pert_pp) + ...
            (1i * a_cr_1stIter * u_mean_pp .* u_pert_pp) + (v_mean_pp .* u_pert_y_pp) + ...
            (du_dy    .*    v_pert_pp)    -    (1/Re)*(u_pert_yy_pp    - (a_cr_1stIter^2)*u_pert_pp)) / (-1i * a_cr_1stIter);1];

figure(3)
```

```matlab
plot(y,abs(p_pert),'r')



  NStr = num2str(N);
  FileName = strcat(NStr, 'CASE_NAME_LNP');
  fileID = fopen(FileName, 'w');
  fprintf(fileID, '%f\n', f_new);
  fclose(fileID);

  save(FileName, 'EVec_save', 'a_cr_mode2_1stIter');
```

L. Derivation of 2D Non-Dimensional Continuity Stability Equation for Non-Local Approach

$$\frac{\partial U}{\partial x} + \frac{\partial V}{\partial y} = 0$$

$$\frac{\partial}{\partial x}\left[\bar{U} + \hat{u}.e^{i\left[\int_{x_0}^{x}\alpha dX - \omega t\right]}\right] + \frac{\partial}{\partial y}\left[\bar{V} + \hat{v}.e^{i\left[\int_{x_0}^{x}\alpha dX - \omega t\right]}\right] = 0$$

$$\frac{\partial \bar{U}}{\partial x} + \frac{\partial \hat{u}}{\partial x}.e^{i\left[\int_{x_0}^{x}\alpha dX - \omega t\right]} + i\alpha\hat{u}.e^{i\left[\int_{x_0}^{x}\alpha dX - \omega t\right]} + \frac{\partial \bar{V}}{\partial y} + \frac{\partial \hat{v}}{\partial y}.e^{i\left[\int_{x_0}^{x}\alpha dX - \omega t\right]} = 0$$

By assuming the mean flow has already satisfied this equation, continuity equation can be reduced into a form that only includes perturbating flow as shown below.

$$\frac{\partial \hat{u}}{\partial y}.e^{i\left[\int_{x_0}^{x}\alpha dX - \omega t\right]} + i\alpha\hat{u}.e^{i\left[\int_{x_0}^{x}\alpha dX - \omega t\right]} + \frac{\partial \hat{v}}{\partial y}.e^{i\left[\int_{x_0}^{x}\alpha dX - \omega t\right]} = 0$$

$$\frac{\partial \hat{u}}{\partial y} + i\alpha\hat{u} + \frac{\partial \hat{v}}{\partial y} = 0$$

By writing terms α, $\hat{u}$, $\hat{v}$ and y in non-dimensional form;

$$\alpha^* = \frac{\alpha}{1/h} = \alpha h \quad , \quad \hat{u}^* = \frac{\hat{u}}{V_{inj}} \quad , \quad \hat{v}^* = \frac{\hat{v}}{V_{inj}} \quad , \quad y^* = \frac{y}{h} \quad , \quad x^* = \frac{x}{h}$$

$$\frac{\partial \hat{u}^*}{\partial x^*} + i\alpha^*\hat{u}^* + \frac{\partial \hat{v}^*}{\partial y^*} = 0$$

M. Derivation of 2D Non-Dimensional x-Momentum Stability Equation for Non-Local Approach

$$\frac{\partial U}{\partial t} + U\frac{\partial U}{\partial x} + V\frac{\partial U}{\partial y} = -\frac{1}{\rho}\frac{\partial P}{\partial x} + v\left[\frac{\partial^2 U}{\partial x^2} + \frac{\partial^2 U}{\partial y^2}\right]$$

$$\frac{\partial}{\partial t}\left[\overline{U} + \hat{u}.e^{i\left[\int_{x_0}^x \alpha dX - \omega t\right]}\right] + \left[\overline{U} + \hat{u}.e^{i\left[\int_{x_0}^x \alpha dX - \omega t\right]}\right].\frac{\partial}{\partial x}\left[\overline{U} + \hat{u}.e^{i\left[\int_{x_0}^x \alpha dX - \omega t\right]}\right]$$

$$+ \left[\overline{V} + \hat{v}.e^{i\left[\int_{x_0}^x \alpha dX - \omega t\right]}\right].\frac{\partial}{\partial y}\left[\overline{U} + \hat{u}.e^{i\left[\int_{x_0}^x \alpha dX - \omega t\right]}\right]$$

$$= -\frac{1}{\rho}\frac{\partial}{\partial x}\left[\overline{P} + \hat{p}.e^{i\left[\int_{x_0}^x \alpha dX - \omega t\right]}\right]$$

$$+ v\left\{\frac{\partial^2}{\partial x^2}\left[\overline{U} + \hat{u}.e^{i\left[\int_{x_0}^x \alpha dX - \omega t\right]}\right] + \frac{\partial^2}{\partial y^2}\left[\overline{U} + \hat{u}.e^{i\left[\int_{x_0}^x \alpha dX - \omega t\right]}\right]\right\}$$

$$-i\omega\hat{u}.e^{i\left[\int_{x_0}^x \alpha dX - \omega t\right]} + \overline{U}\frac{\partial \overline{U}}{\partial x} + \overline{U}\frac{\partial \hat{u}}{\partial x}.e^{i\left[\int_{x_0}^x \alpha dX - \omega t\right]} + i\alpha\overline{U}\hat{u}.e^{i\left[\int_{x_0}^x \alpha dX - \omega t\right]}$$

$$+\hat{u}\frac{\partial \hat{u}}{\partial x}.e^{2i\left[\int_{x_0}^x \alpha dX - \omega t\right]} + i\alpha\hat{u}^2.e^{2i\left[\int_{x_0}^x \alpha dX - \omega t\right]}$$

$$+\hat{u}\frac{\partial \overline{U}}{\partial x}.e^{i\left[\int_{x_0}^x \alpha dX - \omega t\right]} + \overline{V}\frac{\partial \overline{U}}{\partial y} + \overline{V}\frac{\partial \hat{u}}{\partial y}.e^{i\left[\int_{x_0}^x \alpha dX - \omega t\right]}$$

$$+\hat{v}\frac{\partial \overline{U}}{\partial y}.e^{i\left[\int_{x_0}^x \alpha dX - \omega t\right]} + \hat{v}\frac{\partial \hat{u}}{\partial y}.e^{2i\left[\int_{x_0}^x \alpha dX - \omega t\right]}$$

$$= -\frac{1}{\rho}\frac{\partial \overline{P}}{\partial x} - \frac{1}{\rho}\frac{\partial \hat{p}}{\partial x}.e^{i\left[\int_{x_0}^x \alpha dX - \omega t\right]} - \frac{1}{\rho}i\alpha\hat{p}.e^{i\left[\int_{x_0}^x \alpha dX - \omega t\right]}$$

$$+v\left[\frac{\partial^2 \overline{U}}{\partial x^2} + \frac{\partial^2 \hat{u}}{\partial x^2}.e^{i\left[\int_{x_0}^x \alpha dX - \omega t\right]} + 2i\alpha\frac{\partial \hat{u}}{\partial x}.e^{i\left[\int_{x_0}^x \alpha dX - \omega t\right]}\right]$$

$$+i\hat{u}\frac{\partial \alpha}{\partial x}.e^{i\left[\int_{x_0}^x \alpha dX - \omega t\right]} - \alpha^2\hat{u}.e^{i\left[\int_{x_0}^x \alpha dX - \omega t\right]} + \frac{\partial^2 \overline{U}}{\partial y^2} + \frac{\partial^2 \hat{u}}{\partial y^2}.e^{i\left[\int_{x_0}^x \alpha dX - \omega t\right]}$$

As the stability of the steady flow is studied by linear analysis, which requires small perturbation technique, 4th and 8th term in right hand side of the equation shown above can be neglected.

By separating exponential terms from the main equation, equation shown below can be obtained after some elimination process;

$$-i\omega\hat{u} + \bar{U}\frac{\partial \hat{u}}{\partial x} + i\alpha\bar{U}\hat{u} + \hat{u}\frac{\partial \bar{U}}{\partial x} + \bar{V}\frac{\partial \hat{u}}{\partial y} + \hat{v}\frac{\partial \bar{U}}{\partial y}$$

$$= -\frac{1}{\rho}\frac{\partial \hat{p}}{\partial x} - \frac{1}{\rho}i\alpha\hat{p} + v\left(2i\alpha\frac{\partial \hat{u}}{\partial x} + i\hat{u}\frac{\partial \alpha}{\partial x} - \alpha^2\hat{u} + \frac{\partial^2 \hat{u}}{\partial y^2}\right)$$

By writing terms, $\omega, \alpha, \hat{u}, \hat{v}, \rho, \hat{p}, x$ and y in non-dimensional form as shown below;

$$\omega^* = \frac{\omega}{1/t} = \frac{\omega h}{V_{inj}} \quad , \quad \alpha^* = \frac{\alpha}{1/h} = \alpha h \quad , \quad \hat{u}^* = \frac{\hat{u}}{V_{inj}} \quad , \quad \hat{v}^* = \frac{\hat{v}}{V_{inj}}$$

$$\bar{U}^* = \frac{\bar{U}}{V_{inj}} \quad , \quad \bar{V}^* = \frac{\bar{V}}{V_{inj}} \quad , \quad \hat{p}^* = \frac{\hat{p}}{\rho V_{inj}^2} \quad , \quad x^* = \frac{x}{h} \quad , \quad y^* = \frac{y}{h}$$

$$-i\omega^*\hat{u}^* + \bar{U}^*\frac{\partial \hat{u}^*}{\partial x^*} + i\alpha^*\bar{U}^*\hat{u}^* + \hat{u}^*\frac{\partial \bar{U}^*}{\partial x^*} + \bar{V}^*\frac{\partial \hat{u}^*}{\partial y^*} + \hat{v}^*\frac{\partial \bar{U}^*}{\partial y^*}$$

where;

$$Re = \frac{h.V_{inj}}{v}$$

N. Derivation of 2D Non-Dimensional y-Momentum Stability Equation for Non-Local Approach

$$\frac{\partial V}{\partial t} + U\frac{\partial V}{\partial x} + V\frac{\partial V}{\partial y} = -\frac{1}{\rho}\frac{\partial P}{\partial y} + v\left[\frac{\partial^2 V}{\partial x^2} + \frac{\partial^2 V}{\partial y^2}\right]$$

$$\frac{\partial}{\partial t}\left[\bar{V} + \hat{v}.e^{i\left[\int_{x_0}^{x}\alpha dX - \omega t\right]}\right] + \left[\bar{U} + \hat{u}.e^{i\left[\int_{x_0}^{x}\alpha dX - \omega t\right]}\right].\frac{\partial}{\partial x}\left[\bar{V} + \hat{v}.e^{i\left[\int_{x_0}^{x}\alpha dX - \omega t\right]}\right]$$

$$+\left[\bar{V} + \hat{v}.e^{i\left[\int_{x_0}^{x}\alpha dX - \omega t\right]}\right].\frac{\partial}{\partial y}\left[\bar{V} + \hat{v}.e^{i\left[\int_{x_0}^{x}\alpha dX - \omega t\right]}\right]$$

$$= -\frac{1}{\rho}\frac{\partial}{\partial x}\left[\bar{P} + \hat{p}.e^{i\left[\int_{x_0}^{x}\alpha dX - \omega t\right]}\right]$$

$$+v\left\{\frac{\partial^2}{\partial x^2}\left[\bar{V} + \hat{v}.e^{i\left[\int_{x_0}^{x}\alpha dX - \omega t\right]}\right] + \frac{\partial^2}{\partial y^2}\left[\bar{V} + \hat{v}.e^{i\left[\int_{x_0}^{x}\alpha dX - \omega t\right]}\right]\right\}$$

$$-i\omega\hat{v}.e^{i\left[\int_{x_0}^{x}\alpha dX - \omega t\right]} + \bar{U}\frac{\partial\bar{V}}{\partial x} + \bar{U}\frac{\partial\hat{v}}{\partial x}.e^{i\left[\int_{x_0}^{x}\alpha dX - \omega t\right]} + i\alpha\bar{U}\hat{v}.e^{i\left[\int_{x_0}^{x}\alpha dX - \omega t\right]}$$

$$+\hat{u}\frac{\partial\hat{v}}{\partial x}.e^{2i\left[\int_{x_0}^{x}\alpha dX - \omega t\right]} + i\alpha\hat{u}\hat{v}.e^{2i\left[\int_{x_0}^{x}\alpha dX - \omega t\right]}$$

$$+\bar{V}\frac{\partial\bar{V}}{\partial y} + \bar{V}\frac{\partial\hat{v}}{\partial y}.e^{i\left[\int_{x_0}^{x}\alpha dX - \omega t\right]} + \hat{v}\frac{\partial\bar{V}}{\partial y}.e^{i\left[\int_{x_0}^{x}\alpha dX - \omega t\right]}$$

$$+\hat{v}\frac{\partial\hat{v}}{\partial y}.e^{2i\left[\int_{x_0}^{x}\alpha dX - \omega t\right]} = -\frac{1}{\rho}\frac{\partial\bar{P}}{\partial y} - \frac{1}{\rho}\frac{\partial\hat{p}}{\partial y}.e^{i\left[\int_{x_0}^{x}\alpha dX - \omega t\right]}$$

$$+v\left[\frac{\partial^2\bar{V}}{\partial x^2} + \frac{\partial^2\hat{v}}{\partial x^2}.e^{i\left[\int_{x_0}^{x}\alpha dX - \omega t\right]} + 2i\alpha\frac{\partial\hat{v}}{\partial x}.e^{i\left[\int_{x_0}^{x}\alpha dX - \omega t\right]}\right.$$

$$+i\hat{v}\frac{\partial\alpha}{\partial x}.e^{i\left[\int_{x_0}^{x}\alpha dX - \omega t\right]} - \alpha^2\hat{v}.e^{i\left[\int_{x_0}^{x}\alpha dX - \omega t\right]} + \frac{\partial^2\bar{V}}{\partial y^2} + \left.\frac{\partial^2\hat{v}}{\partial y^2}.e^{i\left[\int_{x_0}^{x}\alpha dX - \omega t\right]}\right]$$

Similarly, as it was done in x-Direction Navier-Stokes equation, by separating exponential terms from the main equation, equation shown below can be obtained after some elimination process;

$$-i\omega\hat{v} + \bar{U}\frac{\partial\hat{v}}{\partial x} + i\alpha\bar{U}\hat{v} + \bar{V}\frac{\partial\hat{v}}{\partial y} + \hat{v}\frac{\partial\bar{V}}{\partial y}$$

$$= -\frac{1}{\rho}\frac{\partial\hat{p}}{\partial y} + v\left[2i\alpha\frac{\partial\hat{v}}{\partial x} + i\hat{v}\frac{\partial\alpha}{\partial x} - \alpha^2\hat{v} + \frac{\partial^2\hat{v}}{\partial y^2}\right]$$

$$\omega^* = \frac{\omega}{1/t} = \frac{\omega h}{V_{inj}} \quad , \quad \alpha^* = \frac{\alpha}{1/h} = \alpha h \quad , \quad \hat{u}^* = \frac{\hat{u}}{V_{inj}} \quad , \quad \hat{v}^* = \frac{\hat{v}}{V_{inj}}$$

$$\bar{U}^* = \frac{\bar{U}}{V_{inj}} \quad , \quad \bar{V}^* = \frac{\bar{V}}{V_{inj}} \quad , \quad \hat{p}^* = \rho V_{inj}{}^2\hat{p} , \quad x^* = \frac{x}{h} \quad , \quad y^* = \frac{y}{h}$$

$$\frac{1}{Re} = \frac{h.V_{inj}}{v}$$

$$-i\omega^*\hat{v}^* + \bar{U}^*\frac{\partial\hat{v}^*}{\partial x^*} + i\alpha^*\bar{U}^*\hat{v}^* + \bar{V}^*\frac{\partial\hat{v}^*}{\partial y^*} + \hat{v}^*\frac{\partial\bar{V}^*}{\partial y^*}$$

$$= -\frac{\partial\hat{p}^*}{\partial y^*} + \frac{1}{Re}\left(2i\alpha^*\frac{\partial\hat{v}^*}{\partial x^*} + i\hat{v}^*\frac{\partial\alpha^*}{\partial x^*} - \alpha^{*2}\hat{v}^* + \frac{\partial^2\hat{v}^*}{\partial y^{*2}}\right)$$

O. Derivation and Reduction of the PSE Approach Formula

The equations governing the general evolution of fluid flow are known as Navier-Stokes equations which represents the conservation of mass and momentum. Using Cartesian tensor notation for an incompressible flow, the equations become,

$$\frac{\partial u_i}{\partial t} = -u_j \frac{\partial u_i}{\partial x_j} - \frac{\partial p}{\partial x_i} + \frac{1}{Re} \nabla^2 u_i \quad , \quad i = 1,2 \; for \; 2D \; flow$$

$$\frac{\partial u_i}{\partial x_i} = 0$$

where each primitive variable is written by using superposition of the mean and perturbating flow variables as,

$$U = \bar{U}(x,y) + u(x,y,t)$$

$$V = \bar{V}(y) + v(x,y,t)$$

$$P = \bar{p}(x,y) + p(x,y,t)$$

Substituting the superposed form into the continuity equation and assuming mean flow is already a solution to that equation, continuity equation for perturbating flow can be obtained as,

$$\frac{\partial u}{\partial x} + \frac{\partial v}{\partial y} = 0 \tag{$O.1$}$$

Substituting the superposed form into the x-momentum equation and assuming mean flow is already a solution to that equation, after neglecting non-linear terms and products of the perturbating variables with each other, x-momentum equation for perturbating flow can be obtained as,

$$\frac{\partial u}{\partial t} + \bar{U}\frac{\partial u}{\partial x} + u\frac{\partial \bar{U}}{\partial x} + \bar{V}\frac{\partial u}{\partial y} + v\frac{\partial \bar{U}}{\partial y} = -\frac{1}{\rho}\frac{\partial p}{\partial x} + v\left(\frac{\partial^2 u}{\partial x^2} + \frac{\partial^2 u}{\partial y^2}\right) \tag{$O.2$}$$

Substituting the superposed form into the y-momentum equation and assuming mean flow is already a solution to that equation, after neglecting non-linear terms and products of the perturbating variables with each other, y-momentum equation for perturbating flow can be obtained as,

$$\frac{\partial v}{\partial t} + \bar{U}\frac{\partial v}{\partial x} + \bar{V}\frac{\partial v}{\partial y} + v\frac{\partial \bar{V}}{\partial y} = -\frac{1}{\rho}\frac{\partial p}{\partial y} + \nu\left(\frac{\partial^2 v}{\partial x^2} + \frac{\partial^2 v}{\partial y^2}\right) \qquad (O.3)$$

Disturbances are assumed to be composed of a number of discrete partial fluctuations,

- Each of which propagates in x-direction only
- Any arbitrary 2D disturbance is assumed to be expanded in Fourier series
- Assuming perturbation is 2D streamfunction
- Growth rate and wavenumber is the function of streamwise direction
- The velocity profiles, amplitude function, growth rate and wavenumber weakly depend on streamwise direction. Therefore, 2nd order derivatives of α and φ with respect to streamwise direction, $\partial^2/\partial x^2$, and the products of first order derivatives of those variables with respect to streamwise direction, $\partial/\partial x$, are sufficiently small to be negligible.

$$\psi(x, y, t) = \varphi(x, y). e^{i\left(\int_{x_0}^{x} \alpha(X)dX - \omega t\right)} \qquad (O.4a)$$

$$u = \frac{\partial \psi}{\partial y} = \frac{\partial \varphi}{\partial y}. e^{i\left(\int_{x_0}^{x} \alpha(X)dX - \omega t\right)} \qquad (O.4b)$$

$$v = -\frac{\partial \psi}{\partial x} = -\frac{\partial \varphi}{\partial x}. e^{i\left(\int_{x_0}^{x} \alpha(X)dX - \omega t\right)} - i\alpha\varphi. e^{i\left(\int_{x_0}^{x} \alpha(X)dX - \omega t\right)} \qquad (O.4c)$$

After substituing perturbation forms expanded in Fourier series $(O.4)$ into the x-momentum equation for perturbating flow (0.2) and into the y-momentum equation for perturbating flow (0.3), respectively,

$$-i\omega \frac{\partial \varphi}{\partial y} \cdot e^{i\left(\int_{x_0}^{x} \alpha(X)dX - \omega t\right)} + \overline{U}\frac{\partial^2 \varphi}{\partial x \partial y}e^{i\left(\int_{x_0}^{x} \alpha(X)dX - \omega t\right)} \tag{0.5}$$

$$+i\alpha\overline{U} \frac{\partial \varphi}{\partial y} \cdot e^{i\left(\int_{x_0}^{x} \alpha(X)dX - \omega t\right)} + \frac{\partial \varphi}{\partial y}\frac{\partial \overline{U}}{\partial x} \cdot e^{i\left(\int_{x_0}^{x} \alpha(X)dX - \omega t\right)} + \overline{V}\frac{\partial^2 \varphi}{\partial y^2} \cdot e^{i\left(\int_{x_0}^{x} \alpha(X)dX - \omega t\right)}$$

$$-\frac{\partial \varphi}{\partial x}\frac{\partial \overline{U}}{\partial y} \cdot e^{i\left(\int_{x_0}^{x} \alpha(X)dX - \omega t\right)} - i\alpha\varphi \frac{\partial \overline{U}}{\partial y} \cdot e^{i\left(\int_{x_0}^{x} \alpha(X)dX - \omega t\right)} + \frac{1}{\rho}\frac{\partial p}{\partial x}$$

$$= \nu \left[2i\alpha \frac{\partial^2 \varphi}{\partial x \partial y}e^{i\left(\int_{x_0}^{x} \alpha(X)dX - \omega t\right)} + i\alpha'\frac{\partial \varphi}{\partial y} \cdot e^{i\left(\int_{x_0}^{x} \alpha(X)dX - \omega t\right)} \right.$$

$$\left. -\alpha^2 \frac{\partial \varphi}{\partial y} \cdot e^{i\left(\int_{x_0}^{x} \alpha(X)dX - \omega t\right)} + \frac{\partial^3 \varphi}{\partial y^3} \cdot e^{i\left(\int_{x_0}^{x} \alpha(X)dX - \omega t\right)} \right]$$

$$i\omega \frac{\partial \varphi}{\partial x} \cdot e^{i\left(\int_{x_0}^{x} \alpha(X)dX - \omega t\right)} - \alpha\omega\varphi \cdot e^{i\left(\int_{x_0}^{x} \alpha(X)dX - \omega t\right)} \tag{0.6}$$

$$-2i\alpha\overline{U} \frac{\partial \varphi}{\partial x} \cdot e^{i\left(\int_{x_0}^{x} \alpha(X)dX - \omega t\right)} - i\alpha'\overline{U}\varphi \cdot e^{i\left(\int_{x_0}^{x} \alpha(X)dX - \omega t\right)}$$

$$+\alpha^2 \overline{U}\varphi \cdot e^{i\left(\int_{x_0}^{x} \alpha(X)dX - \omega t\right)} - \overline{V}\frac{\partial^2 \varphi}{\partial x \partial y} \cdot e^{i\left(\int_{x_0}^{x} \alpha(X)dX - \omega t\right)} - i\alpha\overline{V}\frac{\partial \varphi}{\partial y} \cdot e^{i\left(\int_{x_0}^{x} \alpha(X)dX - \omega t\right)}$$

$$-\frac{\partial \overline{V}}{\partial y}\frac{\partial \varphi}{\partial x} \cdot e^{i\left(\int_{x_0}^{x} \alpha(X)dX - \omega t\right)} - i\alpha\varphi \frac{\partial \overline{V}}{\partial y} \cdot e^{i\left(\int_{x_0}^{x} \alpha(X)dX - \omega t\right)} + \frac{1}{\rho}\frac{\partial p}{\partial y} =$$

$$\nu \left[-3\alpha^2 \frac{\partial \varphi}{\partial x} \cdot e^{i\left(\int_{x_0}^{x} \alpha(X)dX - \omega t\right)} - 3\varphi\alpha\alpha' \cdot e^{i\left(\int_{x_0}^{x} \alpha(X)dX - \omega t\right)} - i\varphi\alpha^3 \cdot e^{i\left(\int_{x_0}^{x} \alpha(X)dX - \omega t\right)} \right.$$

$$\left. +\frac{\partial^3 \varphi}{\partial x \partial y^2} \cdot e^{i\left(\int_{x_0}^{x} \alpha(X)dX - \omega t\right)} + i\alpha \frac{\partial^2 \varphi}{\partial y^2} \cdot e^{i\left(\int_{x_0}^{x} \alpha(X)dX - \omega t\right)} \right]$$

Differentiating (0.5) with y and (0.6) with x and considering $\partial \overline{V}/\partial x = 0$ as found from earlier sections,

$$-i\omega\frac{\partial^2\varphi}{\partial y^2}.e^{i\left(\int_{x_0}^x \alpha(X)dX-\omega t\right)} + \frac{\partial\overline{U}}{\partial y}\frac{\partial^2\varphi}{\partial x\partial y}.e^{i\left(\int_{x_0}^x \alpha(X)dX-\omega t\right)} \qquad (0.7)$$

$$+\overline{U}\frac{\partial^3\varphi}{\partial x\partial y^2}.e^{i\left(\int_{x_0}^x \alpha(X)dX-\omega t\right)} + i\alpha\frac{\partial\overline{U}}{\partial y}\frac{\partial\varphi}{\partial y}.e^{i\left(\int_{x_0}^x \alpha(X)dX-\omega t\right)}$$

$$+i\alpha\overline{U}\frac{\partial^2\varphi}{\partial y^2}.e^{i\left(\int_{x_0}^x \alpha(X)dX-\omega t\right)} + \frac{\partial\varphi}{\partial y}\frac{\partial^2\overline{U}}{\partial x\,\partial y}.e^{i\left(\int_{x_0}^x \alpha(X)dX-\omega t\right)}$$

$$+\frac{\partial\overline{U}}{\partial x}\frac{\partial^2\varphi}{\partial y^2}.e^{i\left(\int_{x_0}^x \alpha(X)dX-\omega t\right)} + \frac{\partial\overline{V}}{\partial y}\frac{\partial^2\varphi}{\partial y^2}.e^{i\left(\int_{x_0}^x \alpha(X)dX-\omega t\right)}$$

$$+\overline{V}\frac{\partial^3\varphi}{\partial y^3}.e^{i\left(\int_{x_0}^x \alpha(X)dX-\omega t\right)} - \frac{\partial^2\overline{U}}{\partial y^2}\frac{\partial\varphi}{\partial x}.e^{i\left(\int_{x_0}^x \alpha(X)dX-\omega t\right)}$$

$$-\frac{\partial\overline{U}}{\partial y}\frac{\partial^2\varphi}{\partial x\partial y}.e^{i\left(\int_{x_0}^x \alpha(X)dX-\omega t\right)} - i\alpha\frac{\partial\overline{U}}{\partial y}\frac{\partial\varphi}{\partial y}.e^{i\left(\int_{x_0}^x \alpha(X)dX-\omega t\right)}$$

$$-i\alpha\varphi\frac{\partial^2\overline{U}}{\partial y^2}.e^{i\left(\int_{x_0}^x \alpha(X)dX-\omega t\right)} - \nu\left[2i\alpha\frac{\partial^3\varphi}{\partial x\partial y^2}.e^{i\left(\int_{x_0}^x \alpha(X)dX-\omega t\right)}\right.$$

$$+i\alpha'\frac{\partial^2\varphi}{\partial y^2}.e^{i\left(\int_{x_0}^x \alpha(X)dX-\omega t\right)} - \alpha^2\frac{\partial^2\varphi}{\partial y^2}.e^{i\left(\int_{x_0}^x \alpha(X)dX-\omega t\right)}$$

$$\left.-\frac{\partial^4\varphi}{\partial y^4}.e^{i\left(\int_{x_0}^x \alpha(X)dX-\omega t\right)}\right] = \frac{1}{\rho}\frac{\partial^2 p}{\partial x\partial y}$$

$$-2\alpha\omega\frac{\partial\varphi}{\partial x}.e^{i\left(\int_{x_0}^x \alpha(X)dX-\omega t\right)} - \alpha'\omega\varphi.e^{i\left(\int_{x_0}^x \alpha(X)dX-\omega t\right)} \qquad (0.8)$$

$$-i\omega\alpha^2\varphi.e^{i\left(\int_{x_0}^x \alpha(X)dX-\omega t\right)} - 2i\alpha\frac{\partial\overline{U}}{\partial x}\frac{\partial\varphi}{\partial x}.e^{i\left(\int_{x_0}^x \alpha(X)dX-\omega t\right)}$$

$$+2\alpha^2\overline{U}\frac{\partial\varphi}{\partial x}.e^{i\left(\int_{x_0}^x \alpha(X)dX-\omega t\right)} - i\frac{\partial\overline{U}}{\partial x}\varphi\alpha'.e^{i\left(\int_{x_0}^x \alpha(X)dX-\omega t\right)}$$

$$+3\bar{U}\varphi\alpha\alpha'.e^{i\left(\int_{x_0}^{x}\alpha(X)dX-\omega t\right)}+\frac{\partial\varphi}{\partial x}\bar{U}\alpha^2.e^{i\left(\int_{x_0}^{x}\alpha(X)dX-\omega t\right)}$$

$$+i\bar{U}\varphi\alpha^3.e^{i\left(\int_{x_0}^{x}\alpha(X)dX-\omega t\right)}+\frac{\partial\bar{U}}{\partial x}\varphi\alpha^2.e^{i\left(\int_{x_0}^{x}\alpha(X)dX-\omega t\right)}$$

$$-2i\bar{V}\alpha\frac{\partial^2\varphi}{\partial x\partial y}.e^{i\left(\int_{x_0}^{x}\alpha(X)dX-\omega t\right)}-i\alpha'\bar{V}\frac{\partial\varphi}{\partial y}.e^{i\left(\int_{x_0}^{x}\alpha(X)dX-\omega t\right)}$$

$$+\alpha^2\bar{V}\frac{\partial\varphi}{\partial y}.e^{i\left(\int_{x_0}^{x}\alpha(X)dX-\omega t\right)}-2i\alpha\frac{\partial\bar{V}}{\partial y}\frac{\partial\varphi}{\partial x}.e^{i\left(\int_{x_0}^{x}\alpha(X)dX-\omega t\right)}$$

$$-i\varphi\alpha'\frac{\partial\bar{V}}{\partial y}.e^{i\left(\int_{x_0}^{x}\alpha(X)dX-\omega t\right)}+\varphi\alpha^2\frac{\partial\bar{V}}{\partial y}.e^{i\left(\int_{x_0}^{x}\alpha(X)dX-\omega t\right)}$$

$$+\nu\left[-3i\alpha^3\frac{\partial\varphi}{\partial x}.e^{i\left(\int_{x_0}^{x}\alpha(X)dX-\omega t\right)}-6i\varphi\alpha^2\alpha'.e^{i\left(\int_{x_0}^{x}\alpha(X)dX-\omega t\right)}\right.$$

$$-i\alpha^3\frac{\partial\varphi}{\partial x}.e^{i\left(\int_{x_0}^{x}\alpha(X)dX-\omega t\right)}+\varphi\alpha^4.e^{i\left(\int_{x_0}^{x}\alpha(X)dX-\omega t\right)}$$

$$+2i\alpha\frac{\partial^3\varphi}{\partial x\partial y^2}.e^{i\left(\int_{x_0}^{x}\alpha(X)dX-\omega t\right)}+i\alpha'\frac{\partial^2\varphi}{\partial y^2}.e^{i\left(\int_{x_0}^{x}\alpha(X)dX-\omega t\right)}$$

$$\left.-\alpha^2\frac{\partial^2\varphi}{\partial y^2}.e^{i\left(\int_{x_0}^{x}\alpha(X)dX-\omega t\right)}\right]$$

Equating pressure terms in (0.7) and (0.8) and eliminating exponential expansion terms and dropping $(\partial\bar{U}/\partial x+\partial\bar{V}/\partial y)$ terms due to the fact that mean flow has already satisfied the continuity equation, fourth order perturbation equation for PSE approach can be obtained as shown below,

$$\left\{\left[-i\omega\frac{\partial^2\varphi}{\partial y^2}+i\alpha\overline{U}\frac{\partial^2\varphi}{\partial y^2}+\frac{\partial\varphi}{\partial y}\frac{\partial^2\overline{U}}{\partial x\,\partial y}+\overline{V}\frac{\partial^3\varphi}{\partial y^3}-i\alpha\varphi\frac{\partial^2\overline{U}}{\partial y^2}\right.\right. \tag{O.9}$$

$$\left.\left.+i\omega\alpha^2\varphi-i\overline{U}\varphi\alpha^3-\alpha^2\overline{V}\frac{\partial\varphi}{\partial y}\right]-\nu\left[-2\alpha^2\frac{\partial^2\varphi}{\partial y^2}+\frac{\partial^4\varphi}{\partial y^4}+\varphi\alpha^4\right]\right\}$$

$$+\left\{\left[\overline{U}\frac{\partial^3\varphi}{\partial x\partial y^2}-\frac{\partial^2\overline{U}}{\partial y^2}\frac{\partial\varphi}{\partial x}+2\alpha\omega\frac{\partial\varphi}{\partial x}\right.\right.$$

$$\left.\left.-3\alpha^2\overline{U}\frac{\partial\varphi}{\partial x}+2i\overline{V}\alpha\frac{\partial^2\varphi}{\partial x\partial y}\right]-\nu\left[4i\alpha\frac{\partial^3\varphi}{\partial x\partial y^2}-4i\alpha^3\frac{\partial\varphi}{\partial x}\right]\right\}$$

$$+\left\{\left[\omega\alpha'\varphi-3\overline{U}\varphi\alpha\alpha'+i\alpha'\overline{V}\frac{\partial\varphi}{\partial y}\right]-\nu\left[i\alpha'\frac{\partial^2\varphi}{\partial y^2}-6i\varphi\alpha^2\alpha'+i\alpha'\frac{\partial^2\varphi}{\partial y^2}\right]\right\}$$

with boundary conditions,

$$\varphi(\pm 1)=\varphi'(\pm 1)=0 \tag{O.10}$$

P. Parabolized Stability Equation Code

```matlab
% ----------- PARABOLIZED STABILITY EQUATION APPROACH SOLVER --------------
% ---- Solves the stability equation for growing exponential expansion ----
% -------------- exp(int(a(x) dx) - wt) for 2D porous flow --------------
% ------------- where a(x) = alpha represents the growth rate -------------
% ---------- while w = omega stands for the frequency of the wave --------
% --------- with BCs ; Phi(-1) = Phi(1) = Phi'(-1) = Phi'(1) = 0 ----------


clc
clear all
close all


% ------------------------ LOADING MEAN FLOW ------------------------

load('CASE_NAME_MEAN_FLOW.mat');
load('CASE_NAME_LNP.mat');

options = optimset('MaxFunEvals', 1e10, 'TolFun', 1e-15, 'MaxIter', 1000);

a_init = a_cr_mode2_1stIter;
Phi_init = EVec_save;

% DM is the matrix holds differentiation matrices used in the calculation
% of mean flow
DM1 = DM(:,:,1);
DM2 = DM(:,:,2);
DM3 = DM(:,:,3);
DM4 = DM(:,:,4);

[ay,ax] = meshgrid(x,y*H/2);

f1_prime = DM1 * f_new;      % f'(y)
f2_prime = DM2 * f_new;      % f''(y)
f3_prime = DM3 * f_new;      % f'''(y)


% v_mean = -f(y) --> Does not change with x
v_mean = - diag(f_new); v_mean = v_mean(2:N,2:N);

% d2u/dxdy = f''(y)--> Does not change with x
d2u_dxdy = diag(f2_prime); d2u_dxdy = d2u_dxdy(2:N,2:N);

I = eye(N-1);

% Chebyshev collocation grid points and differentiation matrix for N = 120
% are generated (N comes from mean flow solution. If N is changed in mean flow
% solution, then Chebyshev collocation grid points and the degree of polynomials
% automatically changed)
[D,y] = cheb(N);
```

```matlab
% Reduction of the 4 boundary conditions into 2
S = diag([0; 1 ./(1-y(2:N).^2); 0]);
D3 = (diag(1-y.^2)*DM3 - 6*diag(y)*DM2 - 6*DM1)*S;
D4 = (diag(1-y.^2)*DM4 - 8*diag(y)*DM3 - 12*DM2)*S;

% Since the problem has homogenous B.C's, first and last row/column of the
% differentiation matrices can be removed. Also, same procedure is done for the
% terms come from mean flow solution



DR1 = DM1(2:N,2:N);
DR2 = DM2(2:N,2:N);
DR3 = D3(2:N,2:N);
DR4 = D4(2:N,2:N);
% x_last is the non-dimensional length of the domain which is needed to be
% manuelly introduced

x0 = 5.6;  % The starting position of x (Neighbourhood of marginally stable
% region)
x_n = zeros(((x_last - x0)/deltax) + 1,1);
x_n(1,1) = x0;

dx = x(1,2) - x(1,1);
deltax = dx * 200;

a = zeros(((x_last - x0)/deltax) + 1,1);
a(1,1) = a_init;

Phi = zeros(N-1,((x_last - x0)/deltax) + 1);
Phi(:,1) = Phi_init;

Vinj = 1.70;

Omega = (690*2*pi*0.01)/Vinj;  % Non-dimensional frequency of the wave

outer_iter = 1;
yy = y(2:N,1);

relax_i = 1e-03; % Relaxation for imag(a)
relax_r = 1e-02; % Relaxation for real(a)
relaxp = 1;      % Relaxation for Phi

% If the alpha(j+1) is wanted to be guessed, the slope for both real and
% imaginary part of alpha can be used (Not Necessary)
da_real = -0.84;
da_imag = -0.36854;

n = zeros(((x_last - x0)/deltax) + 1,1);
n(1,1) = 0;

u_pert_init = max(abs(DR1 * Phi(:,outer_iter)));
n = zeros(((x_last - x0)/deltax) + 1,1);
u_pert(1,1) = u_pert_init;
```

```matlab
for j = x0*1000 + 1 + deltax:200:x_last * 1000 + 1

    outer_iter = outer_iter + 1;
    inner_iter = 0;

    nominator = 100 + 100i;

     % u_mean(j+1) --> u_mean = x(j+1) f'(y)
     u_mean = diag(x(1,j) * f1_prime); u_mean = u_mean(2:N,2:N);

     % d2u/dy2(j+1) --> d2u/dy2 = x(j+1) f'''(y)
     d2u_dy2 = diag(x(1,j) * f3_prime); d2u_dy2 = d2u_dy2(2:N,2:N);


    % Initial guess for the next x position  (Phi is not needed to be
guessed)
    if outer_iter <= 2
        a_old =  (real(a(outer_iter -  1,1))  +  da_real*deltax)  +
1i*(imag(a(outer_iter - 1,1)) + da_imag*deltax) ;
        a_old = a(outer_iter - 1,1);
        Phi_old = Phi(:,outer_iter - 1);
    else
        a_old = 2 * a(outer_iter - 1,1) - a(outer_iter - 2,1);
        Phi_old = 2 * Phi(:,outer_iter - 1) - Phi(:,outer_iter - 2);
    End

    icount = 0;



% The stopping criteria is to have zero for the nominator of the normalization
condition. It can be seen if nominator becomes zero (with some tolerance),
alpha will not change in inner iteration, i.e. alpha converges.

    while (((abs(imag(nominator)) > 1e-10 || abs(real(nominator)) > 1e-10))
&& (inner_iter < 10000))


        inner_iter = inner_iter + 1;

        % L0 = Orr-Sommerfeld operatör
        % L1 = LNP Contribution
        % L01 = L0 + L1 = LNP Operator (Initial Guess)

        L01 = (-1i * Omega * DR2) + (1i * a_old * u_mean * DR2) + ...
            (d2u_dxdy * DR1) + (v_mean * DR3) - (1i * a_old * d2u_dy2 * I)
+ ...
            (1i * Omega * a_old^2 * I) - (1i * a_old^3 * u_mean * I) - ...
            (a_old^2 * v_mean * DR1) - ((1/Re) * (DR4 - 2 * a_old^2 * DR2 +
a_old^4 * I));

        L2 = (u_mean * DR2) - (d2u_dy2 * I) + (2 * a_old * Omega * I) - ...
            (3 * a_old^2 * u_mean * I)  + (2i * v_mean * a_old * DR1) - ...
            ((4i * a_old /Re) * (DR2 - a_old^2 * I));
```

139

```matlab
        L3 = (Omega * I) - (3 * a_old * u_mean * I)  + (1i * v_mean * DR1) - ...
            ((2i/Re) * (DR2 - 3 * a_old^2 * I));

        % LHS of the system
        Mat = deltax * L01 + L2 + (a_old - a(outer_iter - 1,1)) * L3;

        % By taking the inverse of the matrix (L2 is the RHS of the system)

         MtoM = inv(Mat) * L2;
         Phi_new = MtoM * Phi(:,outer_iter - 1);

            % One can also take the inverse of the matrix using QR
            decomposition. However, it is tried and it gives bad results
            (according to the residual of the resulting solution)

%         R = qr(Mat);
%          Phi_new = R\(R'\(Mat'*(L2 * Phi(:,outer_iter - 1))));


        Phi_old = (relaxp * Phi_new) + ((1-relaxp) * Phi_old);
        nominator = trapz(yy,conj(Phi_old) .* (Phi_old - Phi(:,outer_iter - 1)));
        denominator = trapz(yy,(abs(Phi_old)).^2);

        a_new = a_old - (2i/deltax) * (nominator/denominator);

        a_old = (relax_r * real(a_new)) + ((1-relax_r) * real(a_old)) + ...
                1i * ((relax_i * imag(a_new)) + ((1-relax_i) * imag(a_old)));



            % At each 50th inner iteration, residual, real(alpha)  and
            imag(alpha) is plotted to see the convergence.

        if mod(inner_iter,50) == 0;
            icount = icount + 1;
            ii(icount,1) = icount * 50;

            res = (Mat * Phi_new) - (L2 * Phi(:,outer_iter - 1));
            l2(icount,1) = norm(res,2);

            figure(1)
            plot(ii,l2)
            hold all

            apr(icount,1) = real(a_old);

            figure(2)
            plot(ii,apr,'r')
            hold all

            api(icount,1) = imag(a_old);
```

140

```matlab
            figure(3)
            plot(ii,api,'r')
            hold all

        end

    end


    clear ii l2 apr api
    clf(figure(1)); clf(figure(2)); clf(figure(3));

    Phi(:,outer_iter) = Phi_new;
    a(outer_iter,1) = a_old;
    x_n(outer_iter,1) = j/1000;

    % Calculating "n factor"

    n(outer_iter,1) = trapz(x_n(1:outer_iter,1),- imag(a(1:outer_iter,1)));

        % A0 (the initial amplitude of the disturbance) is missing in that
        formulation. It depends of the test results.

    u_pert(outer_iter,1) = exp(n(outer_iter,1));


end

figure(4)
plot(x_n,u_pert)
```